2019-10-18

Protein phosphatase 2A-B56 regulates mitosis by interacting with LS/TPI/V motif containing proteins

Chaudhuri, Sibapriya

UNIVERSITY OF CALGARY

Protein phosphatase 2A-B56 regulates mitosis by interacting with LS/TPI/V motif containing proteins

by

Sibapriya Chaudhuri

A THESIS

SUBMITTED TO THE FACULTY OF GRADUATE STUDIES

IN PARTIAL FULFILMENT OF THE REQUIREMENTS FOR THE

DEGREE OF DOCTOR OF PHILOSOPHY

GRADUATE PROGRAM IN BIOLOGICAL SCIENCES

CALGARY, ALBERTA

OCTOBER, 2019

Abstract

Reversible protein phosphorylation is an important post translational modification that controls diverse signaling pathways including the eukaryotic cell cycle signaling. Protein phosphatase 2A (PP2A) is a highly conserved protein phosphatase that removes phosphate groups from serine/threonine residues on proteins. PP2A is a trimeric enzyme consisting of a catalytic or C subunit, a scaffolding or A subunit and a regulatory or B subunit. In humans, B56 is one of the four families of B subunits. PP2A-B56 is an important mitotic protein phosphatase that is essential for proper execution of several mitotic events such as alignment and segregation of sister chromatids. The primary objective of this study was to understand the mechanisms that controls interaction between PP2A-B56 and its mitotic interactors. This study shows that PP2A-B56 interacts with important mitotic regulators through a LS/TPI/V motif. The LS/TPI/V proteins are widespread in the human proteome and are conserved across eukaryotes. The LS/TPI/V proteins take part in multiple signaling pathways including the eukaryotic cell cycle. The interaction between PP2A-B56 and the LS/TPI/V proteins occur in an isoform dependent and phosphorylation dependent manner. Among the five isoforms of B56, B56 gamma 3 and B56 delta have a preference for binding to dephosphorylated LS/TPI/V peptides. The LS/TPI/V motif gets phosphorylated as the cell enters prophase and gets dephosphorylated at mitotic exit. This phosphorylation event is controlled by Aurora Kinase B. B56 delta has a preference for binding to LS/TPI/V proteins when the motif is dephosphorylated. This preference is contributed by the C terminal tail of B56 delta.

Keywords: phosphatase, mitosis, cell cycle, PP2A-B56, protein-protein interaction

Acknowledgements

I would like to thank everyone who helped me during my tenure at graduate school, with the science and outside of science. I would like to thank my PhD supervisor, Dr. Greg Moorhead for his support throughout my years of graduate school. It is from him that I learnt the art of research and not just the art of research. With utmost patience, he listened to all my unformed ideas, guided me to ask the right questions, and then supported and encouraged me in all my scientific adventures. Not just research, it is because of his constant support that I could undertake extensive TAing responsibilities which turned out to be one of the most fulfilling experiences of my graduate degree. How he teaches and mentors his undergraduate course students was always an example to learn from.

I would like to thank the members of my graduate committee, Dr. Vanina Zaremberg and Dr. Kenneth Ng for their support over the years and for the many discussions and committee meetings.

I would like to thank all the past and present members of the Moorhead lab for their support. I would like to thank Dr. Amr Kataya for his excellent ideas and for all the discussions and brainstorming sessions. I would like to thank the undergraduate students, Shan Jin Wang, Viviana Heather and Tejinder Gill who worked on this project. I would like to thank Isha Nasa for sharing her scientific insights about my project over the years, Brooke Rackel and Ahmad for the coffee and the "coffee" breaks and the laughs, Jayde Johnson and Christopher White Gloria for always having my back and looking out for me. I would like to thank members of the Zarmeberg lab, particularly Suria Ganesan and Maxwell, members of the Prenner lab, particularly Weam, Kevin and Mark, Dr. Turner

and members of the Turner lab, particularly Sean Booth and Elina, Dr. Marcus Samuel and members of the Samuel lab, particularly Abhi, Sabine and Jamshed, for sharing reagents, instruments and for brainstorming science with me. I would like to thank Dr. Muench for showing me how to use the microscope, Dr. Justin MacCallum and Dr. Prenner for helping with troubleshooting ITC experiments. I would like to thank Dr. Elke Lohmeier Vogel and Dr. Constance Finney for helping me develop good teaching practices. My best moments in Calgary were spent in the company of friends who I met in graduate school. It is graduate school that taught me the beauty of diversity and that sometimes best friends have nothing in common. I would like to thank Liane Babes, my flat mate of 4 years, for being there for me. I would like to thank Cristina Solis, Shweta Sah, Suria Ganesan, Richard Xiang, Jessie Chrisholm, Anupama Ariyaratne, Pratyush Gupta, Ana Paula Monteiro, Rucha Deo, Cory and Mae for the fun times and for standing by me when life got a bit dark and twisted. I would like to thank all those I missed in my acknowledgements and I am sure I missed many.

I would like to thank my parents, grandmother, my sister and her family for their support. I would particularly like to thank my mother and dedicate this thesis to her.

Table of Contents

List of Tables

List of Figures and Illustrations

List of Symbols, Abbreviations and Nomenclature

Symbol	Definition
APC/C	Anaphase Promoting Complex/Cyclosome
ARPP19	cAMP-Regulated Phosphoprotein 19
ATCC	American Type Culture Collection
ATP	Adenosine Triphosphate
AURKA	Aurora Kinase A
AURKB	Aurora Kinase B
BSA	Bovine Serum Albumin
BUBR1	Mitotic spindle checkpoint protein BubR1
CDC20	Cell cycle division protein 20
CDC25	Cell division cycle 25
CDCA2	Cell division cycle associated 2
CDK	Cyclin dependent kinase
CENP-E	Centromere protein E
CEP120	Centrosomal protein of 120kDa
CEP192	Centrosomal protein of 192kDa
DAPI	4′,6-diamidino-2-phenylindole
DMEM	Dulbecco's Modified Eagle Medium
DNA	Deoxyribonucleic acid
DSN1	Kinetochore associated protein
DSP	Dual specificity phosphatase
DTT	Dithiothreitol
E	Glutamic acid
ECL	Enhanced Chemiluminescence
EDTA	Ethylene diamine tetra acetic acid
EM	Electron microscope
ENSA	Endosulfine alpha
FBS	Fetal bovine serum
FZR	Fizzy related protein
G1	Growth phase 1
G2	Growth phase 2
GFP	Green fluorescent protein
GO	Gene ontology
GWL	Greatwall kinase
HAD	Haloacid dehalogenase
HEAT	Huntingtin/elongation factor/A-subunit/TOR
IDOHA	Inhibitor 2 docking on hydrophobic and acidic grooves

IFA	Immunofluorescence assay
IP	Immunoprecipitation experiment
KEGG	Kyoto Encyclopedia of Genes and Genomes
KLH	Keyhole limpet hemocyanin
KMN	KNL-1/Mis12 complex/Ndc80 complex
LB	Luria Broth
MAD2	Mitotic spindle assembly checkpoint protein
MCC	Mitotic checkpoint complex
mRNA	Messenger ribonucleic acid
mTOR	Mammalian target of rapamycin
MYPHONE	Myosin phosphatase N-terminal element
MYPT1	Myosin phosphatase targeting subunit 1
NAF	Sodium Floride
Nek	NimA related kinase
PAGE	Polyacrylamide gel electrophoresis
PBS	Phosphate buffer saline
PCM	Pericentriolar material
PCR	Polymerase chain reaction
PDB	Protein Data Bank
PKA	Protein kinase A
PKB	Protein kinase B
PLK1	Polo like kinase 1
PMSF	Phenyl methyl sufonyl fluoride
PP1	Protein phosphatase one
PP2A	Protein phosphatase 2A
PP2Ac	Protein phosphatase 2A catalytic subunit
PPM	Metallo protein phosphatase
PPP	Phospho protein phosphatase
PTEN	Phosphatase and tension homolog
PTP	Protein tyrosine phosphatase
RB	Retinoblastoma protein
SAC	Spindle Assembly Checkpoint
Ser (S)	Serine
SpiDoc	Spinophilin docking site for the C-terminal groove
TCA	Trichloro acetic acid
Thr (T)	Threonine
Tyr (Y)	Tyrosine
Uniprot	Universal Protein Resource
UV	Ultraviolet

Epigraph

Realist is just another name for a quitter – Captain Haddock, The Adventures of Tintin.

Related publications

- Nasa, I., L. Trinkle-Mulcahy, P. Douglas, **S. Chaudhuri**, S. P. Lees-Miller, K. S. Lee, and G. B. Moorhead. "Recruitment of Pp1 to the Centrosomal Scaffold Protein Cep192." Biochem Biophys Res Commun 484, no. 4 (2017)
- Labandera, A. M., Vahab, A. R., **Chaudhuri, S.**, Kerk, D. & Moorhead, G. B. The mitotic PP2A regulator ENSA/ARPP-19 is remarkably conserved across plants and most eukaryotes. *Biochemical and biophysical research communications* **458**, 739-744, (2015)

Chapter 1 Introduction

1.1: Reversible protein phosphorylation is a process mediated by protein kinases and protein phosphatases

Reversible protein phosphorylation is a covalent protein modification which involves addition of phosphate group(s) to one or more amino acid residues by protein kinases and removal of these phosphate groups by protein phosphatases. Protein kinases and protein phosphatases thus work in close co-ordination to regulate the overall phosphorylation status of phosphoproteins. In most cases, protein kinases transfer the terminal phosphoryl group from adenosine tri-phosphate (ATP) to the protein[1]. A protein can be phosphorylated on single or multiple amino acid residues at the same time by the same or different protein kinases. Serine (S), threonine (T) and tyrosine (Y) are the most commonly phosphorylated amino acid residues. Basic amino acids such as histidine, arginine and lysine have also been reported to be phosphorylated. Protein phosphatases remove phosphate groups from phosphoproteins through hydrolysis.

In 1992, the Nobel Prize in Medicine was awarded to E. Fischer and E. Krebs for their studies on reversible protein phosphorylation as a "biological regulatory mechanism". Their findings showed how reversible protein phosphorylation controls glycogen metabolism in muscle extracts[1-3]. Since then, extensive studies have established reversible protein phosphorylation as a common post-translational modification controlling most cellular processes and signal transduction pathways including cell growth, proliferation, motility, apoptosis, metabolism, immune response and neuronal activity[4-7]. Recent high throughput, phosphoproteomic studies using label free quantitation strategies demonstrated that more than 75% of the human proteome is

phosphorylated at a given point of time, with 99% of the phosphorylation occurring on S/T residues and less than 1% occurring on Y residues[8]. In certain cellular events like mitosis and in response to growth factor signaling (such as activated epidermal growth factor receptor), the overall level of protein phosphorylation increases several fold[8]. Phosphorylation status of a protein can affect its conformation, activity, subcellular localization, degradation and binding affinity for its interacting partners[9]. Many disease conditions, including cancer, are causes or effects of aberrant protein phosphorylation[8,10]. It is thus not surprising that protein kinases are currently the pharmaceutical industry's second largest group of drug targets[11,12]. Historically, protein phosphatases have been stigmatized as "undruggable" because of failed compound screens, and the previously prevalent notion that these enzymes have little regulation and act non-specifically on substrates[13]. A limited number of solved X-ray crystallography or NMR structures and broad specificity of protein phosphatase inhibitors have further hindered development of therapeutic compounds. However, recent advancement in the protein phosphatase field suggest that protein phosphatases perhaps should not be classified as undruggable, but rather considered insufficiently explored as drug targets[13].

1.2: Protein kinases

Genomic analysis studies suggest that the human genome codes for 518 protein kinases, out of which 478 are typical kinases and 40 are atypical kinases[14]. The 478 typical kinases have evolved from a common ancestor and share an evolutionarily conserved approximately 300 amino acid long kinase domain [14]. The first eukaryotic protein kinase to be crystallized was protein kinase A (PKA) which has the basic domain

architecture and structure observed in all typical kinases crystallized henceforth. The structure of PKA is used here (Figure 1.1) as an example to understand the underlying catalytic mechanism of eukaryotic protein kinases[15]. The kinase domain typically consists of a N lobe and a C lobe, joined by a flexible hinge region which is responsible for stabilizing the interaction with Mg-ATP (Figure 1.1A)[16]. The N lobe has five antiparallel beta sheets and two alpha helices whereas the C lobe is mainly alpha helical (Figure 1.1 C,D). The Mg-ATP is largely buried between the two lobes and shielded from exposure to the solvent as seen in the space filling model of the enzyme (Figure 1.1B)[17]. Scattered throughout the kinase domain are twelve specific highly conserved sequence motifs that mediate the catalytic and scaffolding functions of the kinase. Of particular importance are the glycine rich loop and the P+1 loop. The glycine rich loop is a GxGxxG motif located between β1 and β2 sheets and co-ordinates the phosphates in ATP (Figure 1.1B)[16]. The P+1 loop accommodates the P+1 residue of the substrate docked to the peptide binding groove[16]. Protein kinases are often regulated through phosphorylation of a key residue (usually T but can also be S/Y) on a region within the kinase domain called the activation loop or T loop or activation segment[18]. The activation loop is a short stretch of amino acids surrounded by highly conserved flanking DFG and APE motifs and is found to be highly conserved across species[14]. The activation loop, once phosphorylated, changes conformation resulting in correct orientation of the substrate binding and catalytic sites and thereby converting an inactive enzyme to its active state[18]. In some cases, the activation loop in dephosphorylated state can block the access of the substrate to the active site. Kinases that need activation by phosphorylation usually have a cluster of

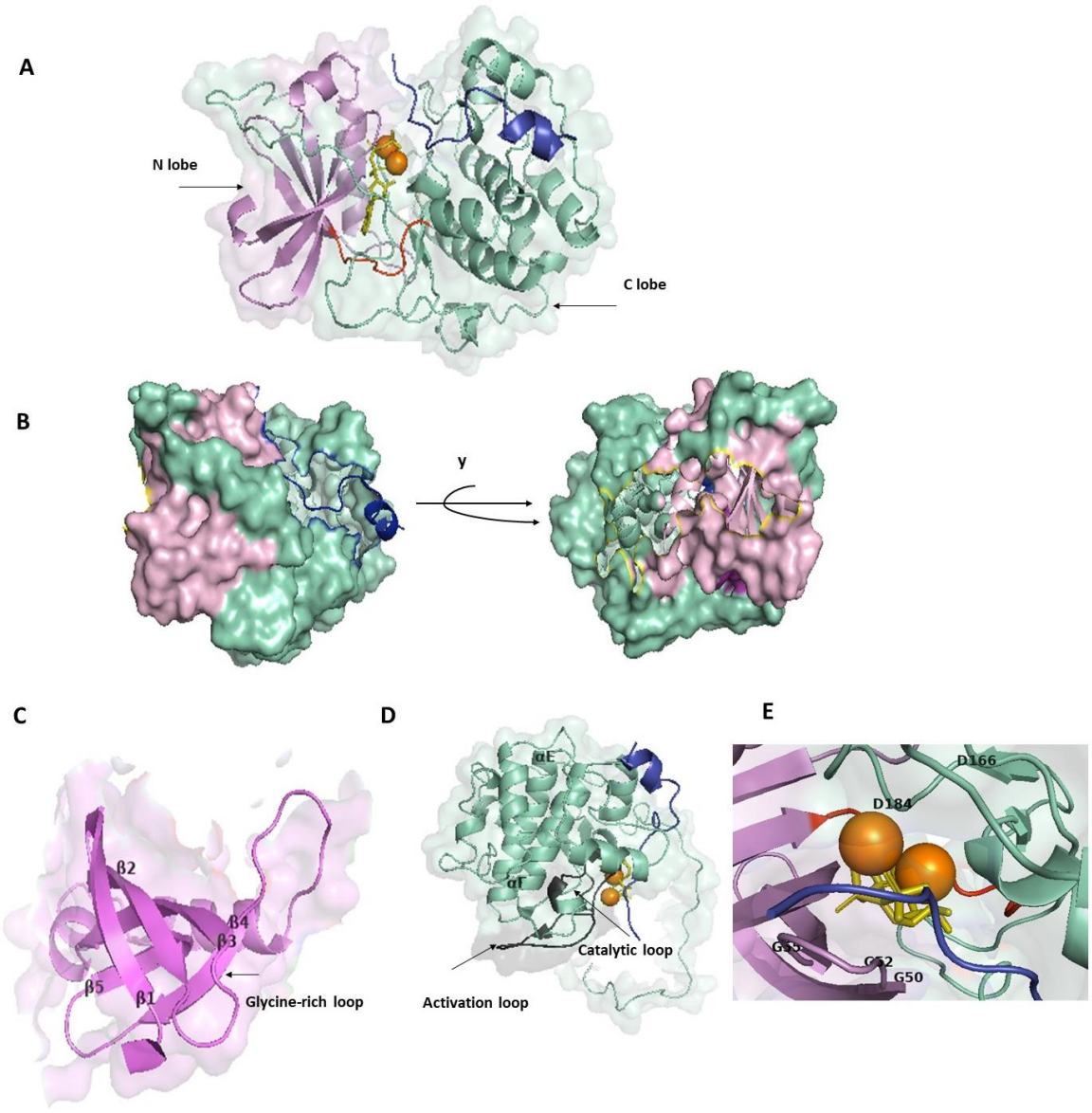

Figure 1.1: Conserved core architecture of eukaryotic protein kinases. The crystal structure of Protein Kinase A (PKA) (PDB ID: 1atp) crystallized with Mn-ATP and a peptide inhibitor reconstructed using Pymol. (A) The N lobe is represented in purple, the hinge region is in red, the C lobe is in cyan-green. Mn-ATP is in orange and the twenty amino-acid long inhibitor peptide derived from Protein Kinase Inhibitor (PKI) co-crystallized is in blue. (B) Space filling model of PKA showing the N lobe and the C lobe. The Mn-ATP is buried within the lobes. (C) The N lobe primarily consists of five beta sheets and one alpha helix. (D) The C lobe is primarily alpha helical and contains the activation loop and the catalytic loop. The activation loop is shown in grey. (E) Zoomed in view showing docking of Mn-ATP to the active site.

positive residues in their catalytic motif which is neutralized by the phosphorylated residue in the activation loop[18]. Close to the activation loop is the catalytic loop which contains the active site of the enzyme (Figure 1.1D).

1.3: Protein phosphatases

1.3.1: Diversity and classification of protein phosphatases.

Even though protein kinases and protein phosphatases jointly regulate reversible protein phosphorylation, protein phosphatases are under-represented in numbers in comparison[9,19]. The human genome codes for only 147 protein phosphatases with only 40 catalytic subunits dephosphorylating S/T residues[9,20,21]. This apparent under-representation in number questions the substrate specificity of protein phosphatases. Protein phosphatases often function as multimeric enzymes which are assembled from a limited number of catalytic subunits interacting with many different regulatory subunits[22]. This vast array of interacting regulatory subunits not only contribute to the diversity of the phosphatase population, but also confer substrate specificity, dictate subcellular compartmentalization and modulate activity of these phosphatases[22]. Chen et al. has recently attempted to define the human phosphatome using a computational approach[19]. Using genomic data on protein phosphatases across eukaryotes, they predicted that the human phosphatome consists of 264 phosphatases out of which 189 are experimentally characterized and predicted protein phosphatases[19]. They also identified 79 genes that code for phosphatase pseudogenes which have been minimal residual activity[19]. Unlike protein kinases, protein phosphatases are diverse in their structure as well as their catalytic mechanisms. Traditionally, protein phosphatases are classified into three main

super-families based on their primary sequence, structure, mode of catalysis and substrate specificity and their sensitivity to phosphatase inhibitors[9] (Table 1.1). The first superfamily includes S/T phosphatases belonging to the Phospho-Protein Phosphatase (PPP) family and Protein Phosphatase Metal dependent (PPM) family[9] (Table 1.1). Phosphatases dephosphorylating S/T residues mainly belong to this superfamily, with a few exceptions belonging to the PTP family and the Asp-based family. All members of the PPP family (including PP1, PP2A, PP2B and PP4-PP7) have a structurally related catalytic core that is conserved across eukaryotes. PPP activity was initially classified biochemically as type 1 (PP1) and type 2 (PP2). Type 2 was further classified based on their dependency for metal cations into PP2A which requires no metal ions, PP2B (calcineurin) which is Ca^{+2} stimulated, and PP2C (belonging to the PPM family) which requires Mg^{+2}. PP4 -PP7 were identified much later through genomic studies using degenerate PCR[9]. PP1, PP2A and PP2B share a catalytic domain of 280 amino acids but have otherwise divergent sequence and structures[9]. Because of the shared catalytic domain structure, members of the PPP family are specifically inhibited by a diverse group of naturally occurring toxins such as microcystin and okadaic acid, produced by cyanobacteria and marine dinoflagellates respectively[23]. Microcystins are monocyclic heptapeptides that inhibit both PP1 and PP2A and have a IC_{50} of 0.1 nM for both enzymes[23]. Okadaic acid, a 20-carbon polyether fatty acid is also a potent inhibitor of both PP1 (IC_{50} of 20 nM) and PP2A (IC_{50} of 0.1 nM)[24]. PPP family members, particularly PP1 and PP2A, function as multimeric enzymes formed by association of a single specific phosphatase catalytic subunit with one or more of many regulatory

Table 1.1: Classification of protein phosphatases

Adapted from Moorhead et al. (2007). Protein phosphatases are classified into three main superfamilies – S/T phosphatases, PTPs and Asp based phosphatases.

Superfamily	*Family*	*Class*	*No. of human genes*
Ser/ Thr phosphatases			
	PPP family	PP1	3
		PP2A	2
		PP4	1
		PP5	1
		PP6	1
		PP2B	3
		PP7	2
	PPM family	PP2C	18
PTP (CX5R)			
	Class I PTPs (classic)	Receptor PTP	21
		Non-receptor PTP	17
	Class I PTPs (DSPs)	MAPKP	11
		Slingshots	3
		PRLs	3
		Atypical DSP	19
		CDC14	4
		PTEN	5
		Myotubularins	16
	Class II PTPs	CDC25s	3
	Class III PTPs	LMWPTP	1
Asp-based catalysis (DXDXT/V)			
	FCP/SCP family	FCP1	1
		SCP	3
		FCP/SCP-like**	4
	HAD family		3

subunits. PPM family members including PP2C and pyruvate dehydrogenase phosphatase have dependency on Mg^{+2} cations. In contrast to PPP members which are multimeric, PPM members do not contain regulatory subunits and are not inhibited by microcystin or okadaic acid[25]. Instead, they are characterized by the presence of eleven conserved motifs containing at least nine highly conserved amino acids including four aspartic acid residues that co-ordinate the metal ions. These conserved motifs help in substrate recognition and/or specificity[26]. Metal ions play an important role in the catalytic action of both PPP and PPM members by activating a water molecule for the dephosphorylation reaction.

1.3.2: Active site specificity of PPPs and their catalytic mechanism.

Biochemical studies and solution of the crystal structures of the catalytic subunits of PP1, PP2A and PP5 suggest that the PPPs have a common mechanism of catalysis analogous to other metalloenzymes. Currently PP5 is the only PPP that has been crystallized in complex with a substrate (phospho-mimetic peptide of Cdc37) and is discussed here along with PP1 as representative PPPs (Figure 1.2). The catalytic domain of PP5 shares 35-45% sequence identity with PP1, PP2A, PP4 and PP6 and differs mainly in having an extended N terminal region[27]. Two metal ions bind to the active site of the enzyme and coordinate the phosphate group of the substrate (Figure 1.2). A metal-ligated water molecule is activated to a hydroxide and makes a nucleophilic attack on the substrate phosphate. The metal ions mediating the coordination of the phosphate group are usually in their divalent cationic state. The catalytic subunits of the PPP family however, lack a specific peptide binding cleft in the active site[28] (Figure 1.2A, B,C).

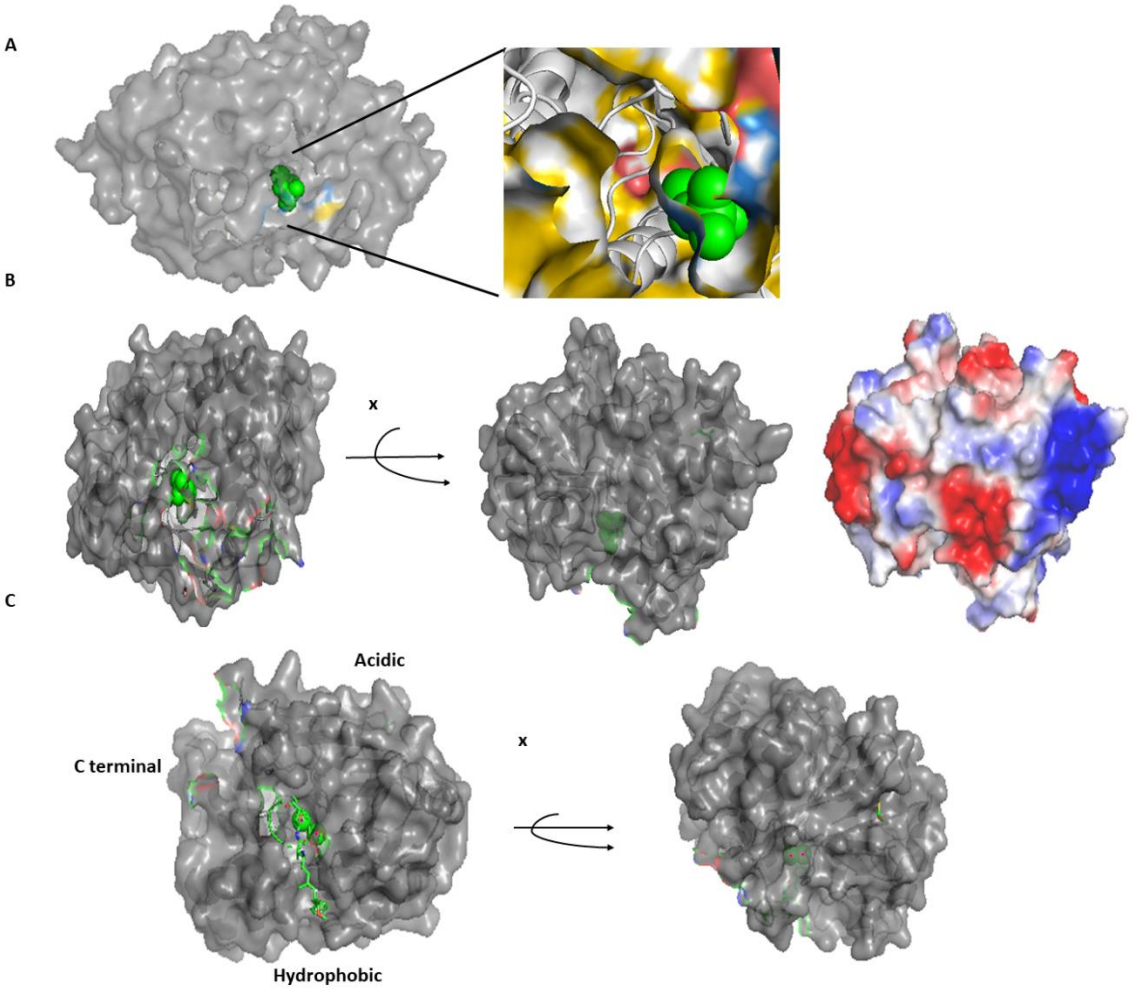

Figure 1.2: Structural aspects of PPP catalytic subunits. All models in this figure are reconstructed using Pymol. (A) Space filling model of PP5 catalytic subunit (PDB ID 1s95) as a representative of PPP. In green are 2 Mn^{+2} ions and a water molecule. The active site is colored. The hydrophobic residues are in yellow, residues with positive side chains are in blue and the residues with negative residues are in red. The inset shows the zoomed in version of the active site. (B) Space filling model of PP5 catalytic subunit, highlighting the open molecular surface. The electrostatic potential of the surface is also mapped with red showing negative potential and blue showing positive potential. (C) Space filling model of PP1 catalytic subunit (PDB ID 1fjm). The active site with the divalent cations is in green. Like PP5, PP1 also has a very open molecular surface with prominent acidic, hydrophobic and C terminal grooves for binding substrates.

Instead they have a shallow catalytic cleft and relatively open surface that accommodate a diverse range of phosphorylated proteins. In PP1, these regions radiate from the catalytic center in a Y shape – C terminal, hydrophobic groove or acidic substrate binding grooves[28,29] (Figure 1.2C). PP5-Cdc37 structure suggest that a diverse range of amino acid [30]residues and side chains can be accommodated on the substrate and still leave substrate conformation intact, thereby not affecting the dephosphorylation reaction[27]. Sequence alignment of substrates from various PPPs suggest that the catalytic subunit do not recognize specific amino acid sequences, beyond the actual phosphorylated residue[25]. This explains how PPPs can counteract the action of multiple kinases. However, under physiological conditions *in vivo*, the lack of substrate specificity of the catalytic subunits is compensated through their interaction with regulatory subunits. PP1 catalytic subunit and the regulatory B subunits of PP2A can recognize short linear interaction motifs (SLiMs) on their binding partners or substrates[31]. SLiMs are short stretches of protein sequences, about 4-12 amino acids long, usually located in an intrinsically disordered region of protein and mediates protein-protein interactions. SLiMs can be degenerate, with two or three amino acid residues being the key determinants of binding affinities. A hydrophobic groove in PP1, 20Å away from its catalytic site can recognize the RVxF motif (when expanded K/R-K/R/V/I-F/I/M/S/T/Y/D/P-F/W) on many of its interacting partners[31,32]. Binding through this motif provides anchorage and does not change the conformation of the enzyme or the catalytic activity of the phosphatase[33]. RVxF motif containing interacting partners of PP1 often help in PP1 localization to subcellular compartments or to specific proteins, particularly during specific cellular events, like

mitosis. Ninety percent of PP1 docking proteins bind PP1 through the RVxF motif[34]. In addition to RVxF, PP1 has been reported to recognize at least ten other SLiMs[32]. Docking of these SLiMs on an average occupies 400 Å on the surface of PP1[34]. Binding of PP1 to an interactor through a primary motif can lead to an increase in the local concentration of PP1. This can lead to binding through a secondary motif which by itself does have a strong enough affinity to form a stable interaction[34]. One of other well characterized PP1 binding motif is SILK which is centered around 4 amino acids S/I/L/K and facilitates anchorage. Binding through SLiMs such as the myosin phosphatase N terminal element (MyPhoNE), the spinophilin docking site for the C-terminal groove (SpiDoc), ankykrin repeat capping C terminus of PP1 (AnkCap) facilitates substrate selection. PP1 can also recognize SLiMs on its inhibitors and substrates. For example, the inhibitory protein, Inhibitor-2 (I2) interacts with PP1 through RVxF, SILK and the Inhibitor 2 docking on hydrophobic and acidic grooves (IDoHA) motif. While the first two interactions provide anchorage, docking of the IDoHA motif blocks the catalytic site thereby contributing to inhibition of the phosphatase catalytic activity[35]. At a given point in time and space, PP1 interacting proteins can dock on PP1 though one or more of these motifs which bind separate grooves on the PP1 catalytic subunit and can act synergistically or antagonistically to determine which interactor PP1 binds to. PP2A-B56 recognizes LxxIxE motif on its interacting protein partners as suggested by a recent proteomic study (detailed discussion in section 1.6.2)[36].

Phospho-Tyrosine Phosphatases (PTP) including classical tyrosine specific phosphatases as well as dual specificity phosphatases (DSP) comprise the third group[9]

(Table 1.1). The PTP superfamily members have a characteristic CX_5R catalytic signature and are generally monomeric enzymes[9,37]. Unlike PPP and PPM members, PTPs catalyze a dephosphorylation reaction by using a cysteinyl-phosphate enzyme intermediate[26]. Based on gene sequence and structure, PTP members can be further classified into Class I PTPs consisting of classical receptor and non-receptor PTPs and non-classical dual-specificity PTPs, Class II PTPs are solely the Cdc25s and Class III PTPs consisting of low-molecular weight PTPs[9]. In addition to phosphorylated tyrosine, PTPs can sometimes dephosphorylate phosphorylated S/T, mRNA and phosphoinositides[9,38]. The DSPs broadly include the atypical DSPs, the PTENs, the myotubularins and the MAP Kinase Phosphatases[39]. The fourth group of protein phosphatases is defined by their catalytic signature (DXDXT/V) and includes aspartate-based protein phosphatases (Table 1.1). Asp-based protein phosphatases have a catalytic signature of DXDXT/V and uses Asp mediated nucleophilic attack for dephosphorylating the targets[9]. The founding member of this family is FCP1 (TFIIF (transcription initiation factor IIF)-associating component of CTD (C-terminal domain phosphatase) which dephosphorylates the CTD of the largest subunit of RNA polymerase II[9]. A few members of the haloacid dehalogenase (HAD) superfamily have been shown to use a similar catalytic mechanism to dephosphorylate multiple substrates, including S/Y residues[9].

1.4: Protein phosphatase 2A is a trimeric enzyme with multiple functions

Protein phosphatase 2A (PP2A) plays a key role in many cellular processes including cell cycle, DNA replication, transcription, translation, cell proliferation, cytoskeleton dynamics and cell mobility and stress response[40]. PP2A is a heterotrimeric

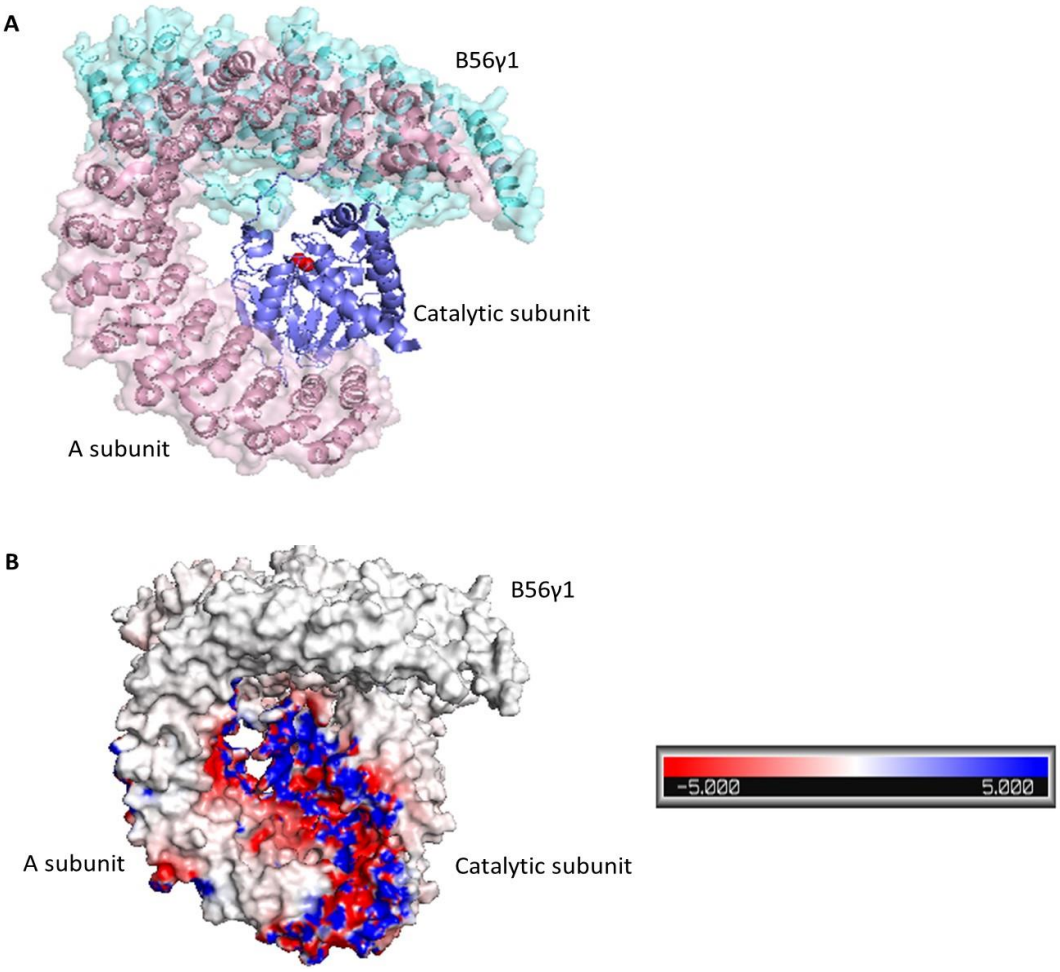

Figure 1.3: Structure of PP2A holoenzyme. PDB structure 2NPP was reconstructed using PyMol. (A) The PP2A holoenzyme is trimeric, consisting of the A subunit represented here in pink, catalytic subunit shown in blue and B56γ1 subunit in cyan green. The Mg^{+2} ions associating with the active site of the catalytic subunit are shown here in red. (B) Electrostatic surface potential of the PP2A holoenzyme generated using APBS plug-in in Pymol. The bar on the right shows the key to the color code.

enzyme consisting of a catalytic subunit (C subunit), and a scaffolding subunit (A subunit) forming the core enzyme which associates with a regulatory subunit (family of B subunits) to form the holo-enzyme (Figure 1.3A)[41]. The crystal structure of the holoenzyme with full length PP2A-Aα, PP2Acα and near full length B56γ1 was simultaneously solved by two independent research groups Cho et al. (2007) and Xu et al., (2007) and reveals intricate details about the enzyme mechanism and regulation[41,42].

1.4.1: Catalytic subunit or C subunit.

The catalytic subunit, otherwise known as PP2Ac, has two different isoforms in humans, known as α and β. The isoforms, though coded by different genes in humans, share about 97% identity in their amino acid sequence[43] (Figure 1.4). Both isoforms are ubiquitously expressed but PP2Acα is more prevalent than PP2Acβ in mammalian cells. In mice, the two isoforms have been shown to be non-redundant in function. Knockout of PP2Acα in mice leads to death on the sixth embryonic day even in the presence of active PP2Acβ[44]. The expression of PP2Ac has been suggested to be tightly controlled through an autoregulatory translational and post-translational mechanism and not at the transcriptional level[40]. This autoregulation contributes to maintaining constant levels of PP2Ac in the cell[45]. The C terminal tail of PP2Ac, having the sequence 304-TPDYEL-309, is extremely conserved not only among PP2Ac across eukaryotes but is also found in catalytic subunits of the other PP2A like phosphatases, PP4 and PP6. In PP2Ac, this motif can undergo phosphorylation on T304 and Y307 and methylation on L309[46]. Phosphorylation of Y307 by a broad range of receptor tyrosine kinases inhibits the catalytic activity of the phosphatase[45]. Though primarily a S/T phosphatase, PP2A can

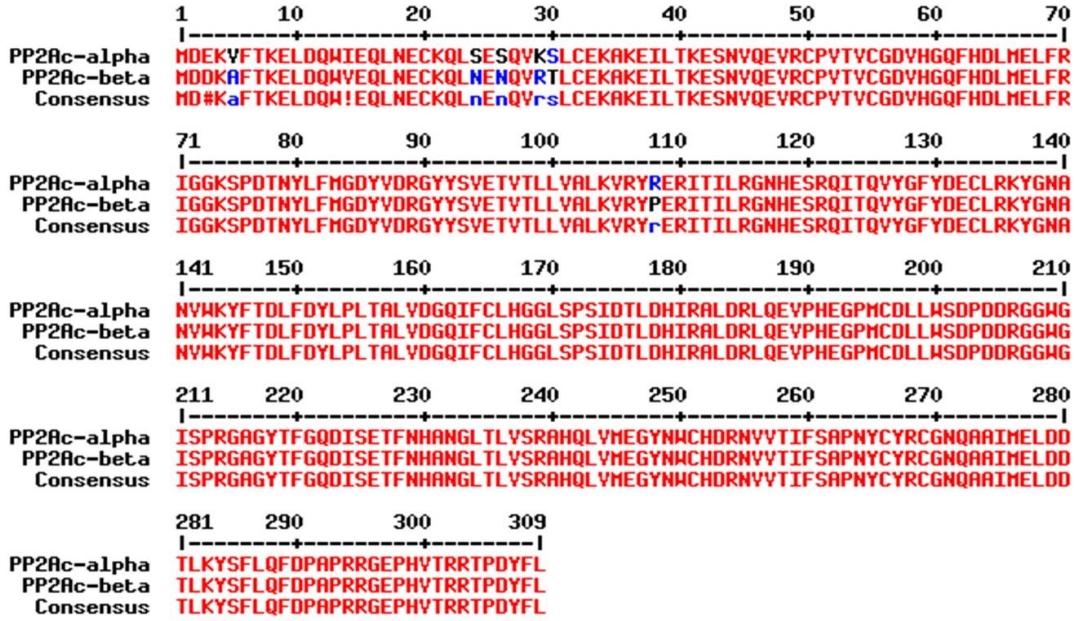

Figure 1.4: The two isoforms of human PP2Ac have 97% amino acid sequence identity: Amino acid sequences of the two isoforms of human PP2Ac were aligned using MultAlin software. These proteins share 97% identity at the level of amino acid sequences. Highly consensus sequence is represented in red, low consensus sequence is represented in blue.

auto dephosphorylate phosphorylated tyrosine residues when activated by PTPA (*p*hospho*t*yrosyl *p*hosphatase *a*ctivator)[45]. Methylation at L-309 promotes the assembly of the heterotrimeric holoenzyme and is specifically required by some regulatory subunits and not others to form the trimer[47,48]. Some controversies exist regarding the importance of the methylation and phosphorylation of the C- terminal residues in cancer tissues, primarily because the antibodies developed to detect these post-translational modifications have shown limited specificity[49].

1.4.2: Scaffolding subunit or A subunit.

The scaffolding subunit or A subunit is a 65kDa protein and has two isoforms, PP2A-Aα and PP2A-Aβ, encoded by two separate genes PPP2R1A and PPP2R1B[50]. In mammalian cells, PP2A Aα is more abundant than PP2A-Aβ. Structurally, the scaffolding subunit consists of 15 tandem HEAT (Huntingtin/elongation factor/A-subunit/TOR) repeats organized into an elongated horse- shoe shaped structure (Figure 1.3A). Each HEAT repeat consists of a pair of anti-parallel alpha helices[41]. The catalytic subunit recognizes and associates with HEAT repeats 11-15 of the A-subunit and this leads to rearrangement of the packing of the HEAT repeats[41]. The active site of the catalytic subunit faces away from the scaffold and remains available for interacting with substrates (Figure 1.3A). The regulatory subunit B56γ1 binds to both PP2A-A subunit through the ridge of HEAT repeat 2-8 on PP2A-Aα and thus lie on the same side as the catalytic subunit in a three-dimensional space (Figure 1.3A). B56γ1, even though doesn't share primary amino acid sequence homology with PP2A-Aα, has a closely related three-dimensional structure. B56γ1 has eight HEAT repeats and associates with the scaffold

through HEAT repeats 4-5[41]. The catalytic subunit and B56γ1 interact at two main points (Figure 1.3A). First the HEAT repeats 6-8 on B56γ1 form hydrogen bonds with α5 region of PP2Acα and secondly the hydrophobic carboxy terminal of PP2Acα is embedded in a groove at the interface between PP2A-Aα and B56γ1. Van der Waals forces, reinforced by hydrogen bonds, maintain this interaction.

1.4.3: Regulatory subunits or B subunits.

The regulatory B subunits identified so far belong to four unrelated gene families. They are B or B55 or PR55 family, B' otherwise known as B56 or PR61 family, B'' or PR72 family and B''' or PR93/PR110 family[51]. Interestingly, these gene families do not share sequence homology but bind to the same region or overlapping region of the core enzyme[41]. However, association of a specific regulatory subunit can alter the holoenzyme's affinity for a substrate several fold[41]. Tau for example, is a substrate of PP2A-B55. Using purified recombinant proteins and reconstituted heterotrimeric holoenzymes, Xu et al. (2008) show that PP2A-B55α has much higher ability to dephosphorylate Tau than PP2A-B56γ1, even though the overall crystal structures of the hetero-trimers are very similar[41]. Different B subunits may have slightly redundant function but still have specific physiological roles due to their specific localization in the cell or tissue specific expression[51].

In mammalian cells, the B55 subunit is encoded by four different genes – PR55α, PR55β, PR55γ and PR55δ[40]. The different isoforms share a high level of sequence similarity but are believed to be expressed in a tissue dependent manner and localize to different subcellular compartments. PP2A-B55 has been shown to be important for

mediating cell signaling, cytoskeleton and Golgi dynamics, as well as regulating cell cycle, particularly mitotic exit, and functioning as tumor suppressor. To date only a few studies have attempted to catalogue a comprehensive list of substrates and/or interactors of B55. Recent proteomic studies have characterized interactomes of B55α and B55β in Xenopus egg extracts[52]. Cataloguing these interactors based on their functions show that most interactors of B55 are involved in metabolism, followed by mitochondrial function, protein trafficking and mitotic regulation[52]. This study also suggests that B55α and B55β mostly have overlapping interactors.

The B56 family of regulatory subunits includes B56α, B56β, B56γ, B56δ and B56ε, and are all being encoded by different genes[53]. In humans, B56β has two isoforms β1 and β2. B56γ has three splice variants γ1, γ2 and γ3[53]. B56γ3 is the longest variant among the three isoforms and consists of an additional C terminal extension of about 60 amino acids (Figure 1.5). As suggested by the multiple alignment (using MultAlin[54] software) in Figure 1.5, the isoforms share a conserved central region (80% conserved) while the N terminal and the C terminal regions are more divergent, suggesting that the termini may aid in isoform specific functions, such as substrate recognition and subcellular localization (Figure 1.5). The predicted molecular weights of the B56 isoforms are listed in Table 1.2.

1.5: The cell cycle is a tightly regulated process:

More than a century ago, Rudolf Virchow proclaimed his famous cell theory, "Omnis Cellula e Cellula" which means that every cell is born from a pre-existing cell[55]. Since then, many researchers around the world have tried to understand the complexities

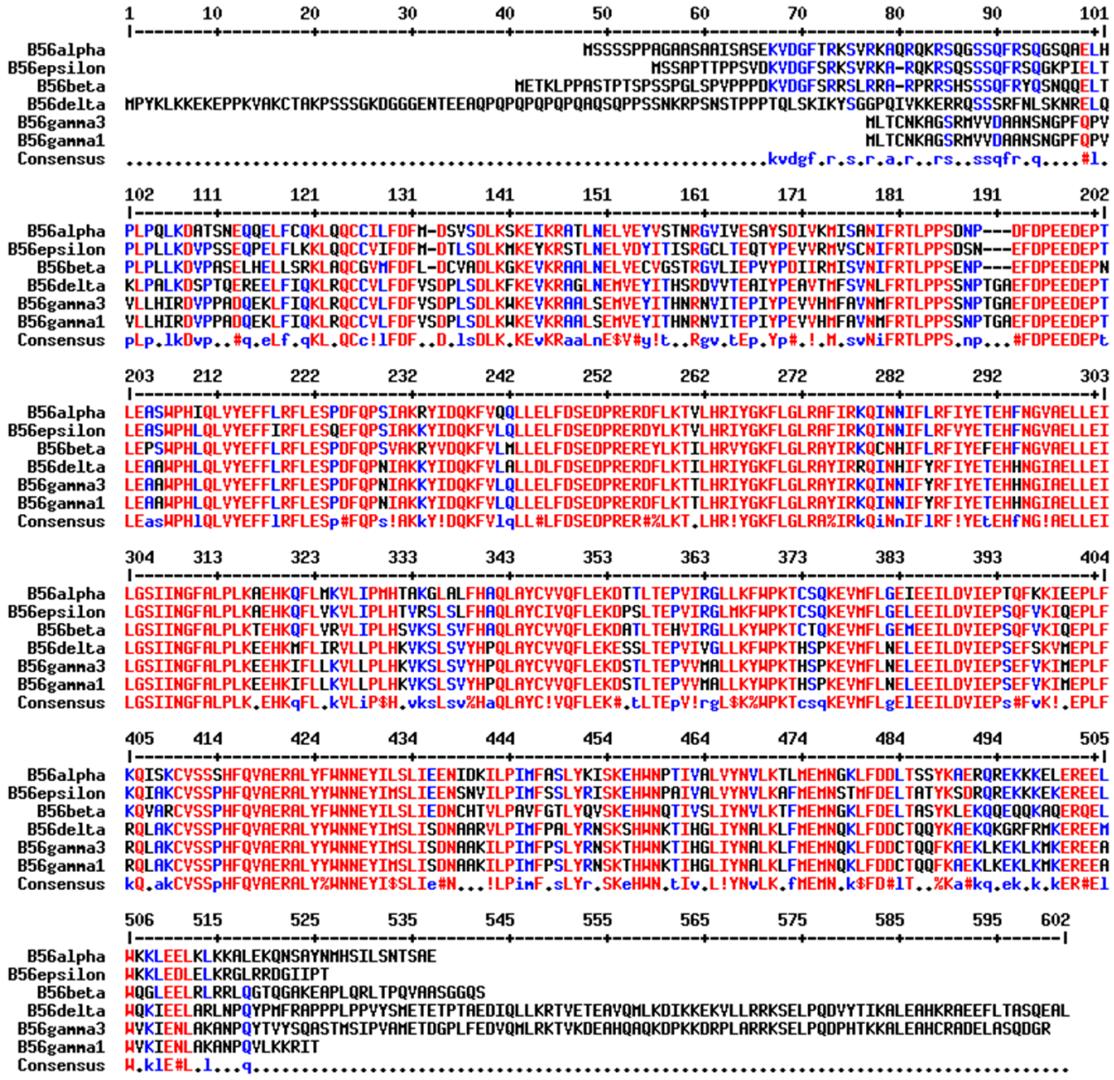

Figure 1.5: B56 isoforms are highly conserved: Sequence alignment of the different human isoforms of B56, generated using MultAlin software. These proteins share a conserved core of approximately 400 amino acids with greater than 80% sequence identity. Some isoforms have an additional N terminal and/or C terminal region. Highly consensus sequence is represented in red, low consensus sequence is represented in blue.

Table 1.2: Predicted molecular weights of human B56 proteins

In humans, there are 5 B56 isoforms. The predicted molecular weights of these proteins are listed below.

B56 isoform	*Uniprot ID*	*Gene name*	*Predicted molecular weight (in kDa)*
B56 alpha	Q15172	PPP2R5A	56.2
B56 beta	Q15173	PPP2R5B	57.3
B56 gamma1	Q13362	PPP2R5C	52.6
B56 gamma3	Q13362	PPP2R5C	61.1
B56 delta	Q14738	PPP2R5D	69.9
B56 epsilon	Q16537	PPP2R5E	54.6

of cell division, regulation of cell cycle and how genetic information is accurately and faithfully transmitted from one cell generation to the next. The cell cycle is a tightly regulated series of events carried out with extreme precision and fidelity and is divided into two main phases -interphase (consisting of G1, S, G2) and mitosis (M phase consisting of prophase, prometaphase, metaphase, telophase and cytokinesis) (Figure 1.6A)[56,57]. During transition from one phase to the other, the cell undergoes extensive reorganization of cellular architecture. Sequential activation and inactivation of various cyclin-dependent kinases (CDK) and their association with the corresponding cyclin protein, contribute to the smooth transition between these phases (Figure 1.5A). G1 phase begins upon completion of mitosis (Figure 1.5A). During G1, the cell grows bigger in size and synthesizes proteins and other components necessary for DNA replication[56]. In early G1 phase, the cell is responsive to growth factor stimulation and other environmental conditions[56]. During unfavorable conditions, cells can exit the cell cycle in G1 and remain in a quiescent state called G0[57]. Terminally differentiated and non-dividing cells usually exist in G0 phase[58]. G1 is followed by S phase where DNA duplication takes place (Figure 1.5A). In G2 phase, following the S phase, the cell synthesizes proteins essential for mitosis including microtubules[57]. G2 is followed by the mitotic phase (Figure 1.5A). During prophase of mitosis, chromosome condensation and centrosome separation takes place and the mitotic spindle starts to assemble[59]. In prometaphase, the nuclear envelope breaks down, sister chromatids attach to the mitotic spindle and migrate to the centre of the cell[59]. In metaphase, sister chromatids become bi-oriented by attaching to microtubules from opposite ends through the kinetochore, large

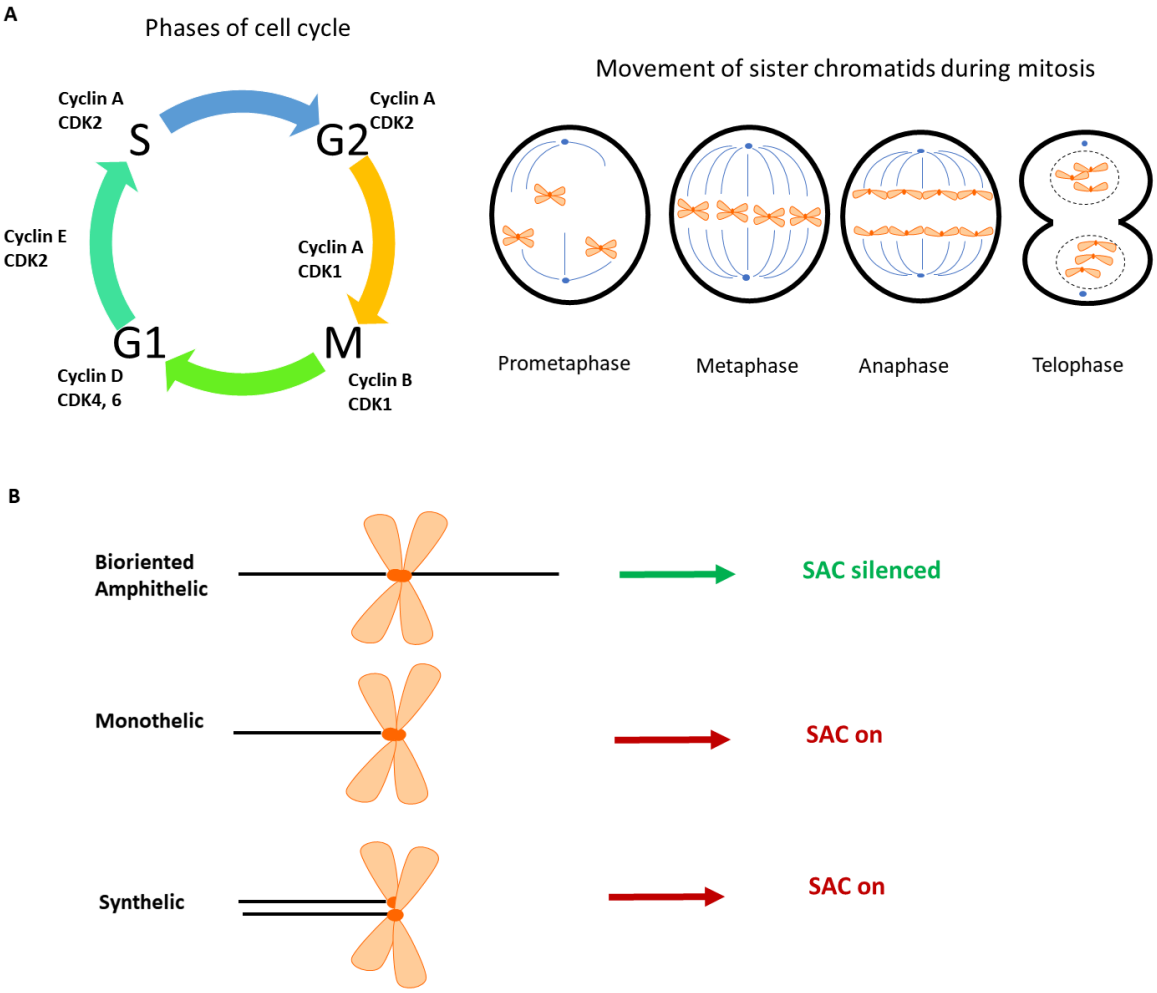

Figure 1.6: Stages of cell cycle and conditions for SAC silencing: (A) Left panel shows different stages of the cell cycle. Interphase is divided into G1, S and G2. Interphase is followed by mitosis. CDK and cyclins regulate cell cycle. The levels of different cyclins fluctuate throughout the cell cycle. Right panel shows different stages of mitosis and movement of chromosomes during these phases. (B) Possible orientations of sister chromatids during metaphase. Only bi-oriented amphithelic sister chromatids lead to silencing of SAC. Figure not drawn to scale.

protein complex that assemble on centromeric DNA. Centromeres are enriched in histone H3 variant CENP-A[60]. CENP-A is the platform for recruiting kinetochore proteins collectively known as the constitutive centromere-associated network (CCAN). These proteins form the "inner kinetochore". The "outer kinetochore" complex otherwise known as the kinetochore microtubule network (KMN) consisting of several kinetochore-microtubule binding proteins (KNL1, MIS12 and NDC80 complex) is recruited to CCAN during mitosis[61]. The mode of attachment of bioriented sister chromatids to microtubules is called amphitelic[62] (Figure 1.6B). Various other attachment states such as syntelic and monotelic attachments are also possible[62] (Figure 1.6B). However, only amphitelic bi-oriented sister chromatids can be equally segregated during anaphase[63] (Figure 1.6B). To check for this, the cell has a safety mechanism called the spindle assembly checkpoint (SAC) that prevents unattached or incorrectly attached sister chromatids from moving onto anaphase, thereby protecting the daughter cells from aneuploidy, alterations in chromosome copy number and tumorigenesis[64]. On a local level, an error correction mechanism exists that allows stabilization of bioriented amphitelic sister chromatids and removal of erroneous attachments. This operates based on the ability of kinetochore-centromere complex to detect tension or lack of tension between kinetochore and microtubules. SAC operates on a more global level and monitors the attachment of spindle microtubules to kinetochores and checks for occupancy of microtubule as well as inter-kinetochore tension[65]. SAC is highly sensitive and the onset of anaphase can be blocked by the presence of a single unattached kinetochore[63]. In addition to erroneous sister chromatids attachment, SAC can be activated by several other conditions including

but not limited to spindle geometry and microtubule tip dynamics[66,67]. SAC negatively regulates the ability of CDC20 to activate the E3 ubiquitin ligase, anaphase promoting complex/cyclosome (APC/C) and thereby prevents the polyubiquitylation and degradation of cyclinB and securin (explained in details in section 1.6.1)[62]. Mitotic checkpoint complex (MCC) consisting of Mad2, BubR1, Bub3 and CDC20, is the main effector of SAC[64]. How MCC inhibits APC/C activity is still poorly understood. However, components of MCC has been shown to bind to CDC20 directly. BubR1 and Mad2 both have distinct binding sites on CDC20[68]. Binding of Mad2 to CDC20 is required prior to BubR1-CDC20 interaction[69]. The ability of CDC20 to bind to its interactors is also regulated by phosphorylation. Binding of CDC20 to other components of MCC, prevents it from being associated with APC/C[68,70]. Studies show that incorporation of CDC20 in the MCC can also increase APC/C-dependent autoubiquitylation and degradation of CDC20[64]. On silencing of SAC, MCC is found to dissociate from APC/C[64]. In addition to the MCC, the KMN network is also involved in checkpoint signaling[62]. At metaphase-anaphase transition, cohesion between sister chromatids is lost. Sister chromatids are held together from their formation in S phase till metaphase by the cohesin complex (consisting of Smc1/3, Rad21 and SA)[71]. Cohesin complex loads on to DNA during G1 phase and entraps a single chromatid[72]. The loading of cohesin to DNA is facilitated by the NIPBL-MAU heterodimer and the unloading reaction later in anaphase is promoted by Pds5-WAPL[72,73]. After DNA replication in S phase, the complex gains additional cohesiveness through acetylation of two key lysine residues of Smc3 which promotes recruitment of Sororin by Pds5 and hence

destabilization of any Pds5-WAPL complex[73]. Cohesin topologically binds sister chromatids together through intergenic regions on chromatid arms and through centromeric region[74]. During prophase and prometaphase, most of the cohesion on the chromatid arms is lost through a phosphorylation-dependent and proteolysis-independent manner. Centromeric cohesion is lost during metaphase-anaphase transition mainly through proteolysis[74]. On silencing of SAC, securin is degraded through APC/C^{CDC20} mediated polyubiquitylation. Securin is an inhibitor of the protease, separase. Activated separase now cleaves Rad21 in the centromeric cohesin complex, thereby segregating the sister chromatids[74]. In anaphase, sister chromatids move to opposite spindle poles. In telophase, nuclear components are repackaged into identical daughter nuclei. Mitosis is closely followed by cytokinesis which essentially divides the cell cytoplasm and results in formation of two new daughter cells. In multicellular organisms, mitosis is crucial for growth and tissue renewal and is tightly regulated. Since transcription and translation are suppressed during mitosis[75-77], regulation through post-translational modifications, particularly reversible protein phosphorylation and proteolysis is very important.

1.6: Mitosis is regulated by reversible protein phosphorylation

1.6.1: Regulation of mitosis by mitotic protein kinases.

Regulation of mitosis by reversible protein phosphorylation is achieved through co-ordinated activities of mitotic protein kinases and mitotic protein phosphatases. As the cell enters mitosis, there is a marked increase in the level of protein phosphorylation[8]. The major mitotic kinases are CDK1, Aurora kinase (AURK) A/B, Polo-like kinase 1 (Plk1), Greatwall kinase (Gwl), Haspin and NIMA (not in mitosis A) related kinases[78-81].

During cell cycle, there are dynamic changes in the activities of these kinases (Figure 1.7) as well as their localization. The phosphorylation events leading to cellular reorganizations during interphase to mitosis transitions are mainly orchestrated by CDK1-cyclinB activity[82]. CDK1 is activated during G2/M transition by dephosphorylation of key residues T14 and Y15 located in the ATP-binding pocket of the kinase[83]. This is achieved by the dual-specificity phosphatase Cdc25C whose activity at this point is higher than that of the opposing kinases Wee1 and Myt1 which keep CDK1 inactivated through phosphorylation of the same residues[84-86]. CDK1 also gets phosphorylated on T161 of its T loop by cyclin activating kinase (CAK, also known as CDK7) and this stabilizes its interaction with cyclins[87]. Once activated, CDK1-cyclinB directly or indirectly regulates most mitotic phosphorylation events until all chromosomes are aligned at the metaphasic plate. Studies in yeast cells, Xenopus egg extracts and human cells have revealed numerous substrates of CDK1-cyclinB including those driving nuclear envelope breakdown, centrosome separation, chromosome condensation, mitotic spindle assembly and Golgi fragmentation[88,89]. The CDK1-cyclinB full substrate consensus sequence, as revealed by several substrate-trapping studies is S/T-P-X-K/R, where X is any amino acid residue. However, in several cases, a minimal motif of S/T-P is found to be sufficient[90]. AURKA and Plk1 are both localized to centrosomes and spindle poles during G2/M phases and both play a role in centrosome maturation and spindle assembly[91]. AURKA/B usually recognize and phosphorylate the sequence R/K-R/K-X-S/T-Θ where X is any amino acid residue and Θ is a hydrophobic amino acid[92]. The amino acid sequences recognized and phosphorylated by AURKB,

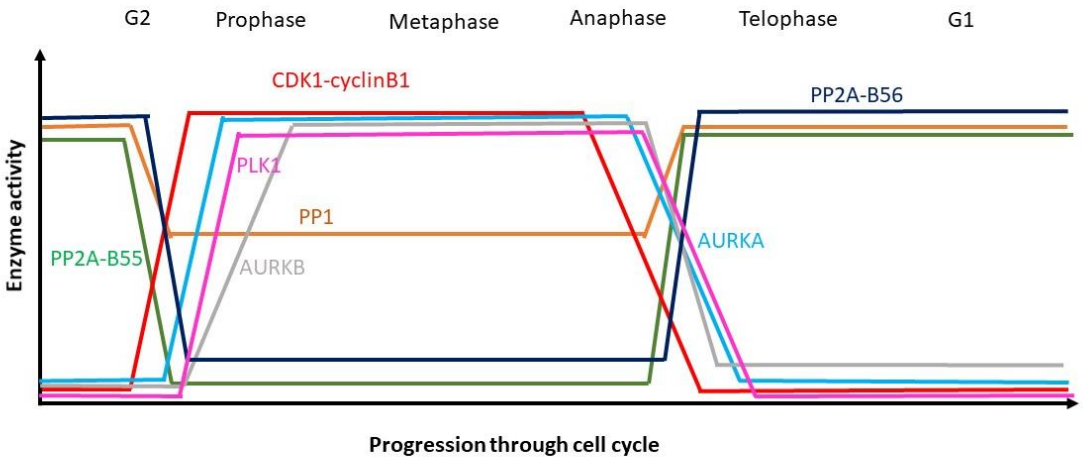

Figure 1.7: Activities of kinases and phosphatases changes over cell cycle. The activities of mitotic protein kinases and mitotic protein phosphatases are found to fluctuate during the cell cycle. Typically, as the cells enter mitosis, the mitotic protein kinase activities are enhanced. CDK1-cyclinB1 activity is shown in red, Plk1 activity in pink, AURKA activity in cyan and AURKB activity in gray. As the cell exit mitosis, the mitotic phosphatases have higher activity. PP1 activity is shown in brown, PP2A-B55 activity is shown in green and PP2A-B56 activity is shown in navy blue. Figure adapted from Nasa et al., 2018[81]. Figure not drawn to scale.

AURKA and PKA are very similar. Specificity is achieved through spatial and temporal regulation of these kinases. During mitosis, AURKB and AURKA localize to different cellular locations in the cell and are activated in a time-dependent fashion. However, existence of some substrate redundancy between AURKA and AURKB has been reported[93]. During mitosis AURKA gets activated by auto-phosphorylating T288 residue in its T loop[94]. During the cell cycle, AURKA associates with its coactivators Bora, Cep192 and TPX in a temporarily and spatially regulated manner. In interphase cells, Bora is present in the nucleus[95]. In late G2, Bora is phosphorylated by CDK1-cyclinB and localizes to the cytoplasm where it associates with AURKA[96]. Recent studies show that CDK1-cyclinA could be phosphorylating Bora in late G2 when CDK1-cyclinB is still inactive[97]. *In vitro* assays suggest that Bora increases the kinase activity of AURKA by several fold[95]. AURKA-Bora activates Plk1. Phosphorylated Bora docks on to C-terminal polo box domain (PBD) of Plk1 and releases it from its intramolecular interaction with the N terminal catalytic domain, which now moves away from blocking the T-loop and thereby making the T-loop more accessible to AURKA. AURKA then phosphorylates Plk1 on T210 on its T loop and activates it[98]. Once cells are in mitosis, Plk1 phosphorylates Bora and triggers Bora's degradation process[99]. It is not yet clear how Plk1 continues to be phosphorylated on T210 after degradation of Bora, but studies suggest that residual AURKA-Bora or AURKB may be responsible[100]. Decreased Bora levels allow AURKA to bind to its other co-activators, Cep192 and TPX2 at the centrosomes and microtubules respectively. Binding of TPX2 to AURKA can activate it through allosteric activation even in absence of its T-loop (T288) phosphorylation.

However, once TPX2 is bound to AURKA, it can also promote the autophosphorylation of its T-loop[79]. TPX2 binding also prevents PP1 and PP6 from dephosphorylating the T-loop of AURKA[79]. AURKA-TPX2 plays an important role in spindle assembly and in microtubule nucleation[79]. AURKA-Cep192 plays an important role in centrosome maturation and is also know to recruit Plk1 to the centrosomes[79].

AURKB shares 70% sequence similarity with AURKA in its catalytic domain, but differs considerably in the length and sequence of its N terminal[101]. However, AURKB has a very different cell localization pattern, function and substrates. AURKB activity is maximal during mitosis[101]. AURKB along with inner centromere protein (INCENP), borealin and survivin forms the chromosomal passenger complex (CPC). As a part of CPC, AURKB first associates with inner centromere/kinetochore until anaphase, then localizes to the midzone of the central spindle during anaphase and finally is found to concentrate at the midbody of cells undergoing cytokinesis[101]. AURKB is activated through multiple steps. AURKB first binds to the IN box of INCENP and gets partially activated[102]. AURKB then phosphorylates a TSS motif on the C-terminal of INCENP, which further enhances the activity of the kinase in a positive feedback loop[102]. However, for full activation of AURKB, T232 on its T-loop must be auto-phosphorylated. The autophosphorylation is likely to happen in trans as it is enhanced by a higher concentration of CPC at the centromere[103]. There is some evidence showing that AURKB must be phosphorylated on S331 to be able to phosphorylate INCENP on its TSS motif. However, S331 phosphorylation is not required for autophosphorylation of T232 on the T loop[104]. Chk1 could be one of the kinases that phosphorylate S331 on

AURKB[104]. It has also been speculated that phosphorylation of borealin by Mps1 regulates AURKB activity, but this is still a matter of debate[105-107]. AURKB has many roles in mitosis. In G2, AURKB phosphorylates histone H3 on S10 and S28 residues and this has been proposed to be responsible for chromatin condensation[108]. Along with Plk1, phosphorylation by AURKB is responsible for removal of the cohesin complex from chromosome arms during prophase and prometaphase through the prophase pathway[109]. Removal of cohesion from the arms but its retention at the centromere is essential for biorientation of sister chromatids. During metaphase-anaphase transition, AURKB plays an important role in regulating both error correction and SAC. Inhibition of AURKB leads to stabilization of erroneous attachments of sister chromatids which are dissolved on re-activation of AURKB[110,111]. During the process of error correction, to eliminate and detach incorrectly attached microtubules, key proteins in the KMN network are phosphorylated resulting in changes in their binding affinity. AURKB can phosphorylate numerous substrates on the kinetochore-microtubule interface, including members of the KMN to prevent microtubule binding. The best studied is the multi-site phosphorylation of Ndc80, a member of the KMN complex, on its N terminal by AURKB. It is proposed that this multi-site phosphorylation leads to accumulation of negative charges that disrupts the interactions between Ndc80 and the acidic C terminal tails of microtubules[112]. However, phosphorylation of Ndc80 has been shown to be insufficient to inactivate the microtubule binding ability of KMN *in vitro*[113]. To inactivate microtubule binding, AURKB has been reported to phosphorylate additional members of the KMN complex simultaneously including Dsn1 (a protein belonging to the Mis12 complex of

the KMN) and the N terminal microtubule binding domain of KNL1[113]. In addition to members of the KMN network, AURKB also phosphorylates microtubule binding proteins and microtubule depolymerizing kinesins to regulate kinetochore-microtubule dynamics. Studies propose that AURKB can differentiate between different types of kinetochore-microtubule attachment and destabilize the erroneous ones. To achieve this, it has been speculated that AURKB senses the tension at the kinetochore-microtubule interface. Bipolar attachments generate sufficient tension resulting in an increase in centromere-kinetochore distance and/or structural changes in kinetochore and thereby leads to inhibition of AURKB activity at the kinetochore-microtubule interface[112].

APC/C is a multi-subunit (15 subunits including its co-activator) complex and is a substrate of CDK1-cyclinB[114]. Once phosphorylated by CDK1-cyclinB, APC/C can bind to its co-activator CDC20[114]. Satisfaction of SAC leads to rise in activity of APC/C^{CDC20} which now targets several mitotic regulators including cyclinB and securin for degradation thereby promoting the initiation of mitotic exit[115]. Degradation of cyclinB leads to termination of CDK1-cyclinB phosphorylation events. In later anaphase, decreased CDK1 activity allows APC/C to bind to its second co-activator CDH1 (CDC20 homologue 1) which now targets different molecules for ubiquitination and degradation including CDC20[115]. Other mitotic kinases such as AURKA and Plk1 are destined for degradation in telophase and cytokinesis. APC/C^{CDH1} regulates exit from mitosis and events in G1[115]. APC/C is inactivated before entry into S phase. Substrates of APC/C are primarily recognized by the co-activators (CDC20 and CDH1) through short amino acid motifs such as D-box (recognized by both CDC20 and CDH1) and KEN box (only

CDH1). Three-dimensional reconstruction of this multi-subunit complex to a resolution of 7.4Å by Chang et al. show that APC/C adopts a triangular shape delineated by a lattice-like shell. The base of the triangle is predominantly occupied by APC4 and APC5 and partially by APC1. Out of the 15 subunits, only APC2 and APC11 have been shown to have roles in catalysis and only APC10 and the co-activator have been shown to have roles in substrate recognition[116]. APC1 is the largest of all the subunits (predicted mass 216 kDa) consisting of a proteasome-cyclosome (PC) domain, a mid-helical domain and a N-terminal WD-40 domain and is believed to act as a scaffold[117]. High throughput phospho-proteomic studies have shown that APC1 gets phosphorylated on multiple residues during mitosis[8]. However, further studies need to be done to assess if APC1 and the other APC/C subunits have a more active role in controlling cell cycle events. Protein degradation and decline in mitotic protein kinase activities is not sufficient for cells to exit mitosis. To reinstall the phosphorylation levels characteristic of interphase cells, controlled and sequential dephosphorylation by mitotic protein phosphatases is essential.

1.6.2: Regulation of mitosis by mitotic protein phosphatases.

Mitotic protein phosphatases exhibit control at different levels. They can directly dephosphorylate phosphoproteins (substrates of protein kinases) or they can directly or indirectly regulate protein kinases. One common mechanism of directly regulating protein kinase activities is through modulating the phosphorylation of the kinase T-loop. For example, PP1 in complex with its various regulatory subunits can dephosphorylate the T-loop of AURKB, Plk1, Mps1 and Gwl[118-121]. PP6 has been reported to dephosphorylate the T-loop of AURKA[122]. The surge in protein phosphorylation levels

that drives a cell into mitosis is not just achieved through activation of protein kinases but also through inhibiting the activities of protein phosphatases. Studies show that when interphase cells are treated with okadaic acid at a concentration that inhibits both PP1 and PP2A, they enter into a pseudo-mitotic state, characterized by chromosome condensation, microtubule aster formation, centrosome separation and higher CDK1-cyclinB activity[123,124].

The key mitotic protein phosphatases are PP1, PP6 and PP2A. Biochemical and genetic studies have shown that during mitosis, PP1 can antagonize the activities of CDK1-cyclinB, AURKB, Mps1 and Plk1. In humans there are three isoforms of PP1 (PP1α. PP1β and PP1γ) which differ mainly in the sequences of their C terminal region[125]. As discussed in section 1.3, PP1 can recognize and bind to specific SLiMs on its interactors, the best described being the RVxF motif[33]. About 90% of PP1 interacting proteins contain an RVxF motif which acts primarily as an anchor to recruit PP1. During mitosis many of its interactors bind PP1 through the RVxF motif and target it to specific locations in the cell in a temporally regulated manner. For example, Repoman and Ki67 target PP1 to chromatin at the beginning of anaphase. Repoman-PP1 has been reported to dephosphorylate H3S10 at anaphase-telophase transition and this has been proposed to contribute to the process of chromatin reorganization[126]. Repoman-PP1 also interacts with importinβ and participates in the nuclear membrane re-assembly process[126]. In addition to being a targeting subunit, Repoman is also a substrate of PP1. Mutating Repoman's PP1 binding domain is sufficient to abolish recruitment of PP1 to the chromatin[127]. Knl1, Mypt1, and Kifl8A are some of the other interactors that bind PP1 through the RVxF

motif during mitosis and contribute to controlling dephosphorylation of chromatin associated factors[128]. The residue x in the RVxF motif is often a S/T which thereby makes it a substrate for phosphorylation by AURKB[129]. When phosphorylated by AURKB on the RVSF motif, these proteins show limited or no association with PP1[129]. Knl1 phosphorylation at the kinetochore-microtubule interface by AURKB is important for correct biorientation of sister chromatids and error correction as discussed in section 1.6.1. Binding of PP1 to Knl1 is stalled by its phosphorylation of the RVSF motif, thereby preventing recruitment of PP1 to the kinetochores until the SAC has been silenced[130]. In addition to sharing substrates, PP1 also regulates the pool of active AURKB. In complex with Sds22, PP1 can dephosphorylate T232 on the T loop of AURKB[119,131]. In mammalian cells, suppression of PP1 activity has been reported to rescue cells from AURKB depletion phenotypes suggesting that AURKB and PP1 antagonize each other[132]. PNUTS (phosphatase 1 nuclear subunit) binds to PP1 through RVSF as well as φφ motif and an arginine residue and is involved in inhibitory regulation of PP1. PNUTs also directly binds to AURKB and other members of CPC and KMN. It is speculated that by activating AURKB, PNUTS can indirectly antagonize PP1 activities[133]. Even though PP1 and AURKB antagonize each other, it is unlikely that PP1 has a role in sister chromatid biorientation. PP1 localizes to the kinetochore only after sister chromatids have bioriented[134]. Preventing PP1 recruitment to kinetochore-microtubule interface has been reported to not impair chromosome alignment[119,134]. In addition to antagonization by AURKB, the mitotic activities of PP1 are modulated through several other mechanisms. PP1 and CDK1-cyclinB also antagonize each other

during mitosis. CDK1-cyclinB phosphorylates T320 on the C terminal tail of PP1[135,136]. This phosphorylation has an inhibitory effect on the phosphatase activity of PP1. A decrease in active CDK1-cyclinB levels during metaphase-anaphase transition triggers PP1 to auto-dephosphorylate and activate itself[137]. Phosphoproteomic analysis of HeLa cells treated with nocodazole, demonstrate that the occupancy of phosphorylation of T320 site on PP1 is about 60%, suggesting that not all PP1 is inactive during mitosis[138]. In addition to directly phosphorylating PP1 catalytic subunit, CDK1-cyclinB also phosphorylates several regulatory subunits of PP1, such as Repoman, and prevents their binding to PP1[139]. Phosphorylation of Inhibitor 1 (I1) by PKA and Inhibitor 2 (I2) by CDK1-cyclinB influence their binding to PP1 and thereby inhibition of PP1 activity during mitosis[81].

Several mass spectrometry studies suggest that PP2A-B55 targets S/TP residues, often with basic residues upstream and downstream. It is proposed that the basic residues facilitate binding to the acidic surface of PP2A-B55, similar to interactions between TAU and B55[41]. Since a SP/TP site is often phosphorylated by CDK1-cyclinB, it is speculated that PP2A-B55 and CDK1-cyclinB antagonize each other through shared substrates. Recent studies have demonstrated that PP2A-B55 is the major phosphatase antagonizing CDK1-cyclinB. Entry of a cell into mitosis is fueled by simultaneous activation of CDK1-cyclinB and inhibition of PP2A-B55 (see Figure 1.7). In late G2 phase, active CDK1-cyclinB phosphorylates Gwl on its T-loop and activates it[140]. Activated Gwl phosphorylates two heat-stable proteins ENSA (α-Endosulfine) and ARPP19 (cyclic adenosine monophosphate regulated protein 19), both of which are remarkably conserved

across eukaryotes[141-143]. ENSA and Arpp19 share a SLiM, FDSGDY, which when phosphorylated by Gwl binds to the active site of PP2A-B55[143,144]. Phosphorylated ENSA and ARPP19 behave as substrates of PP2A-B55 which get slowly dephosphorylated by the phosphatase[145]. In presence of active Gwl, this is a dynamic interaction. When Gwl activity decreases, PP2A-B55 activates itself by dephosphorylating ENSA and ARPP19, which now have a different binding affinity and are not associated with PP2A-B55[140]. This mechanism of controlling PP2A-B55 activity promotes mitotic phosphorylation state in two ways. Inhibition of PP2A-B55 leads to direct stabilization and maintenance of many phosphorylated targets of CDK1-cyclinB, as both the enzymes share substrates. Secondly, Gwl indirectly regulates CDK1-cyclinB activity by directly regulating Cdc25C[140]. When Gwl is immunodepleted, Cdc25C is inactive and cannot dephosphorylate CDK1[140]. For reactivation of PP2A-B55, Gwl must be inactivated. This is achieved by dephosphorylation of Gwl by PP1 in anaphase[140,146,147]. PP1 dephosphorylates several sites on Gwl including the highly conserved S883 in its T-loop[146]. PP2A-B55, once activated, also contributes to dephosphorylation of hyper-phosphorylated Gwl. CDK1-cyclinB can also directly inhibit PP2A by phosphorylating a TP site on the C terminal of its catalytic domain[128]. The exact mechanism by which the phosphorylation of this site is regulated is yet to be elucidated. PP2A-B55 is also involved in reassembly of Golgi complex and nuclear envelope reassembly during mitotic exit[148]. In an RNAi screen for mitotic phosphatases, which when knocked down delay mitotic exit, PP2A-B55α was scored as a hit[149]. The study proposed that PP2A-B55α acts synergistically with Importinβ1 to control mitotic exit[149].

The role of PP2A in mitosis is less studied. Like ENSA and ARPP19, Bod1 is a heat-stable small protein which when phosphorylated by CDK1-cyclinB acts as a specific inhibitor of PP2A-B56[150]. Bod1 like PP2A-B56 is associated with the kinetochore[150]. Loss of Bod1 from the kinetochore results in hyper-activation of PP2A-B56 resulting in large scale dephosphorylation at the kinetochore-microtubule interface and premature loss of sister chromatid cohesion[150]. Like ENSA and ARPP19, Bod1 also has a conserved motif through which it binds PP2A-B56[150]. In stable cell lines expressing GFP tagged B56 subunits (all isoforms) the localization of B56 was found to be highest at the centromere in prometaphase and was decreased (α, ε) or undetectable by metaphase (β, γ, δ)[151]. Nocodazole treatment suggested that localization of most of the B56 isoforms (α,β,δ,ε) is sensitive to microtubule attachment[151]. Depletion of B56 isoforms by RNAi resulted in unstable kinetochore-microtubule attachments which were reversed when treated with AURKB inhibitors[44]. Recent mass spectrometric studies have demonstrated that PP2A-B56 recognizes the SLiM LxxIxE or when expanded L/C/V/M/I/F-S/T-P-I/L/V/M-X[36]. Crystallography studies show key amino acid residues between heat repeat 3-5 on B56 are involved in binding this SLiM[152] (Figure 1.8). BubR1, an important SAC protein interacts with PP2A-B56 through this SLiM and recruits it to the metaphase plate. In BubR1, the motif is LSPIxE and phosphorylation of SP enhances B56α binding as shown by ITC experiments[153]. Repoman also has the LSPIxE motif and binds to B56γ in nocodazole arrested or taxol treated cells, but not in interphase cells[154]. B56 however, can also bind to interactors without the LxxIxE motif. An example being the Shugoshin proteins (Sgo1 and Sgo2). Shugoshin proteins protect centromeric cohesion through

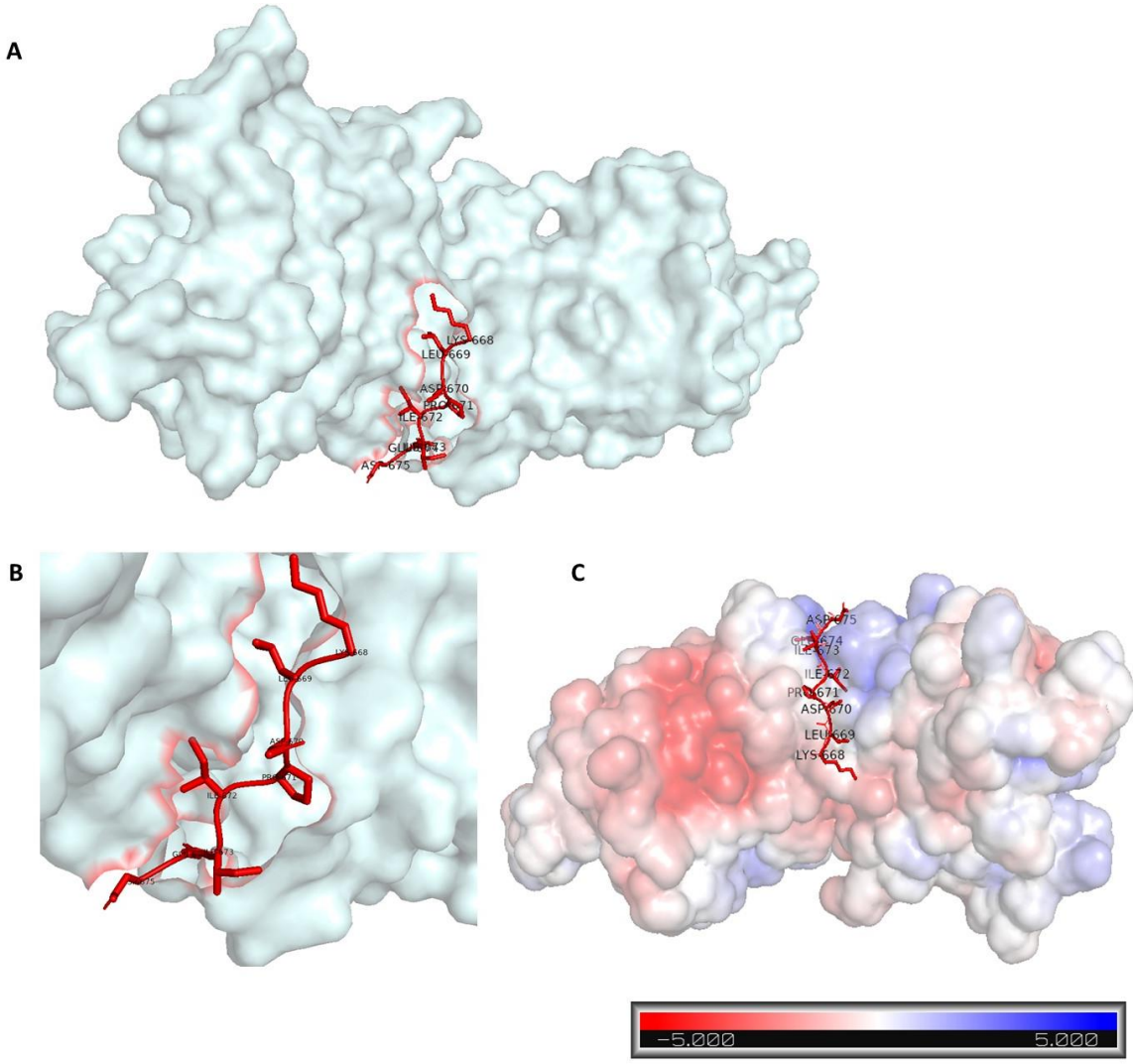

Figure 1.8: Interaction of B56γ1 with a peptide containing LxxIxE residues. PDB structure 5jja was reconstructed in Pymol. B56 proteins contain several heat repeats. (A) The LxxIxE peptide (derived from BubR1) shown in red which makes contact with B56 gamma1shown in cyan. The amino acid residues in heat repeat 3 and 4 of B56 gamma1 are mainly responsible for interacting with LxxIxE peptide. (B) Zoomed in view of the peptide. (C) The LxxIxE peptide is laid on top of the electrostatic surface representation of B56 gamma1, created with APBS plug-in in Pymol. The heatmap on the bottom shows the key to the color code.

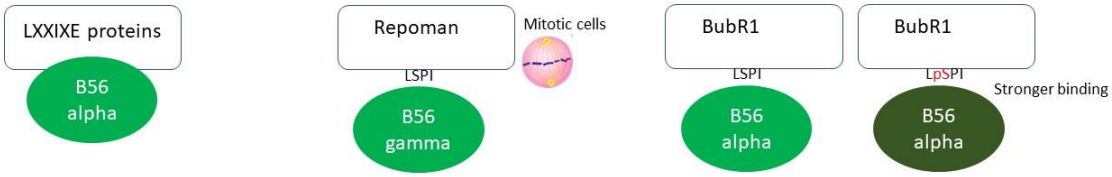

Figure 1.9: Summary of the current knowledge of interaction between B56 and LS/TPI/V proteins. Left panel summarizes the key findings from the study by Hertz et al., 2016. Using a proteomic approach this study shows that B56 proteins binds to interactors containing the LxxIxE motif. Using a substitution scanning mutagenesis assay, this study showed that E is essential in position 6 of this motif for binding of the two proteins. Middle panel summarizes the key findings from the study by Prevost et al., 2013. Using an immunoprecipitation assay, this study showed that Repoman interacts with B56 gamma in mitotic cells. Using site directed mutagenesis and biochemical studies, they showed that a motif spanning four amino acids LSPI is essential for this binding. Right panel summarizes the key findings from the study done by Kruse et al., 2013. Using a yeast two hybrid system, this study showed that BubR1 interacted with all B56 isoforms. Using isothermal calorimetry, they showed that recombinant purified B56 alpha had higher affinity of binding to phosphorylated LSPI peptides than dephosphorylated ones.

recruitment of the B56 phosphatase[155]. Sgo1 does not contain an LxxIxE motif and has been shown to interact with B56 through a distinct region as demonstrated by crystallography studies[156]. The current knowledge about the various interactions between B56 proteins and LS/TPI/V proteins is summarized in Figure 1.9.

1.7: Hypothesis

We hypothesize that binding of PP2A-B56 to its interacting proteins containing an LS/TPI/V motif is regulated in a cell-cycle dependent manner and is critical for the progression of cell cycle. I will address this hypothesis with the following specific aims.

1.7.1: Specific aim 1.

Identify additional potential interacting protein partners of PP2A-B56 containing the LS/TPI/V motif that play a role in mitotic regulation. Using in-silico, biochemical and proteomic approaches, I intend to identify interactors of PP2A-B56.

1.7.2: Specific aim 2.

Investigate if association of PP2A-B56 with these novel interacting partners is dependent on the phosphorylation status of LS/TPI/V motif. Using biochemical, biophysical and cell biology tools, I intend to investigate how phosphorylation of LS/TPI/V motif regulates its interaction with B56 proteins.

1.7.3: Specific aim 3.

Study the functional significance of these novel interactions, particularly their role in mitotic progression.

Chapter 2: Methods

2.1: Cell lines used

2.1.1: HeLa.

HeLa (human epithelial adenocarcinoma cell line derived from cervical cancer, ATCC CCL2)[157,158] were grown in 100 X 20 mm tissue culture plates (Corning) in DMEM (Thermo Fisher Scientific) supplemented with 10% FBS (Invitrogen), 2 mM L-glutamine (Corning), 100 IU/mL penicillin and 100 µg/mL streptomycin (Thermo Fisher Scientific). The cells were maintained at 37ºC in a humidified atmosphere of 5% CO_2. Cells were sub-cultured in the ratio of 1:4. Growth media was discarded and the attached cell layer was washed with phosphate buffered saline (PBS) (137 mM NaCl, 2.7 mM KCl, 8 mM Na_2HPO_4, 2 mM KH_2PO_4) and incubated in presence of 0.25% (w/v) Trypsin, 0.53 mM EDTA, at 37ºC for 5 minutes to detach the cell layer. Serum containing growth media was added to stop trypsinization. Cells were collected by centrifugation at 1000 rpm for 10 minutes, washed and seeded into new plates for subculturing. For long term storage and future use, the cells were trypsinized, washed in pre-warmed growth media, counted using a hemocytometer and resuspended at a cell density of 3 X 10^7 cells/mL in freezing solution consisting of 90% FBS and 10% DMSO (Sigma) and stored at -80ºC. To test for viability, cell suspensions were stained with 0.4% of trypan blue solution. Live, viable cells remained unstained and were counted using a hemocytometer. The cells were used for further experiments only if at least 90% of the population was viable.

2.1.2: HEK293T.

HEK293T is epithelial cell line (ATCC CRL-3216) derived from human embryonic kidney[159]. HEK293T cells were used for all transfections. The cells were cultured in 100 X 20 mm tissue culture plates in DMEM supplemented with 10% FBS, 2 mM L-glutamine, 100 IU/mL penicillin and 100 µg/mL streptomycin. The cells were maintained at 37^{o}C in a humidified atmosphere of 5% CO_2 and subculture in the ratio of 1:6. Cells were frozen at a concentration of 3 X 10^7 cells/mL in freezing solution and stored at -80^{o}C.

2.2: Antibodies and peptides

2.2.1: Peptides.

All peptides used in this study are listed in Table 2.1. Peptides were purchased from GL Biochem (Shanghai) Ltd, China. All peptides were HPLC purified and were obtained at 95-98% purity. A small percentage of trifluoroacetic acid (TFA) was present in the purified peptides as an impurity. Wherever indicated peptides were dialyzed extensively against PBS before use to remove TFA.

2.2.2: In-house generated phospho-specific antibodies.

Phospho-specific antibodies were raised in house in rabbits against Repoman S597, APC1 S555, Cep120 T368, iASPP S567 and DSN1 S30. The peptides used for raising these antibodies are listed in Table 2.1

2.2.3: Commercially obtained primary antibodies.

All commercially purchased antibodies used in this study are listed in Table 2.2.

Table 2.1: Peptides used in this study

Peptides used in this study are listed below. Amino acids in red following the letter p represents a phosphorylated residue.

Protein Name	*Peptide Sequence*	
	Unmodified	*Modified*
Repoman	KPLLSPIPEK	KPLLpSPIPEK
APC1	KVLLSPVPELRK	KVLLpSPVPELRK
Cep120	KKKVLTPIKEK	KKKVLpTPIKEK
Cep120 mutant	KKKVLSPIKEK	KKKVLpSPIKEK
DSN1	KHQLESSLSPVEVFAK	KHQLESSLpSPVEVFAK
Greatwall kinase	KKDLELALSPIHNSSK	KKDLELALpSPIHNSSK
FZR1	KPYSLSPVSNK	KPYSLpSPVSNK
RB	KADMYLSPVRSPK	KADMYLpSPVRSPK
iASPP	KEPELSPITEK	KEPELpSPITEK
YLPM1	GKKRVRWADLE	GKKRARAADLE
RIF1	KRRVSFADK	KRRVpSFADK
MPP10	KESLKRVTFAL	KESLKRVpTFAL

Table 2.2: List of commercial antibodies used in this study

Commercial antibodies were purchased from various companies. The dilutions at which they were used are listed.

Antibody target	*Source*	*Dilution used*	*References (PMID)*
APC1	Bethyl laboratories	1/1000	28404789
Aurora A phospho T288	Abcam	1/500	26078008
B56 beta	Thermo Fisher Scientific	1/500	28404789
B56 delta	Bethyl laboratories	1/1000	22893788
B56 gamma	Santa Cruz	1/500	23362328
Cep120	LifeSpan Bioscience Inc	1/1000	N/A
Cyclin B	Santa Cruz	1/1000	29764992
Cyclin E	Abcam	1/500	29764992
DSN1	Abcam	1/1000	N/A
HA	Sigma-Aldrich	1/1000	21593317
Histone 3 Serine 10	Upstate Biotechnologies	1/1000	29764992
iASPP	Abcam	1/1000	29731851
MPM2	Millipore	1/500	29764992
PLK1 phospho T210	Abcam	1/1000	29764992
PP2A catalytic subunit	Abcam	1/1000	23362328
PP2A-A subunit	Abcam	1/1000	23362328
Repoman	Abcam	1/1000	23362328
Tubulin	Sigma-Aldrich	1/2000	29764992

2.2.4: Commercial secondary antibodies.

Horseradish peroxide (HRP) conjugated goat anti mouse IgG (H and L) and HRP conjugated goat anti rabbit IgG (H and L) were purchased from Thermo Fisher Scientific and were used at 1:5000 dilution for western blotting. Alexa Flour conjugated secondary antibodies used for microscopy were purchased from Thermo Fisher Scientific and were used at 1:500 dilution for microscopy.

2.3: SDS PAGE and Western Blotting

2.3.1: Protein quantification.

The Bradford assay was used to estimate the amount of protein present in a sample. A standard curve was generated by plotting the absorbance of varying amounts of a known concentration of Bovine Serum Albumin (BSA). To measure the unknown concentration of a protein sample, 1-10 µL of the sample was added to 1 mL of Bradford reagent (10% v/v phosphoric acid (stock 85%), 5% v/v methanol. 0.05 mg/mL of Coomassie Blue G250) in a cuvette, vortexed to mix, absorbance was read at 595 nm and extrapolated to the standard curve. All readings were measured in triplicate. An equal volume of sample buffer in 1 mL of Bradford reagent was used as a blank.

2.3.2: SDS PAGE.

To separate proteins, present in a sample, SDS PAGE was used. Resolving gel of various acrylamide concentrations was prepared based on the size of the proteins to be separated. A 10% resolving gel (10% acrylamide, 25 mM Tris (pH 8.8), 0.02% SDS, 0.02% ammonium persulfate and 2 µL of *N*,*N*,*N′*,*N′*-tetramethylelthylenediamine TEMED (per 10 mL of gel solution)) was used for resolving most proteins ranging in

molecular weight from 30 kDa to 120 kDa. 4% stacking gel (4% acrylamide, 25 mM Tris-Cl (pH 6.8), 0.02% SDS, 0.02% ammonium persulfate and 2 µL of TEMED (per 10 mL of stacking gel solution)) was used in all cases. Gels were resolved (stacking gel 100 V, resolving gel 150V) in running buffer (25 mM Tris, 250 mM glycine, 0.1% SDS, pH 8.3). To visualize proteins resolved on SDS-PAGE, the gels were first fixed in destaining solution (40% (v/v) methanol, 10% (v/v) glacial acetic acid) for 10 minutes, washed three times in double distilled water (ddH_20), and then incubated in colloidal Coomassie blue staining solution (0.12% (w/v) colloidal Coomassie blue G-250, 10% (w/v) ammonium sulfate,10% (v/v) phosphoric acid, 20% (v/v) methanol) for one hour. Following staining, gels were destained by washing three times with ddH_20.

2.3.3: Western blotting.

Proteins resolved on SDS PAGE were transferred on to a nitrocellulose membrane (0.45 µm pore size, Bio-Rad) using a wet tank transfer set-up (Bio-Rad). The transfer stack was assembled such that the gel was oriented towards the cathode and the nitrocellulose membrane towards the anode. Transfer was carried out in transfer buffer (25 mM Tris, 192 mM glycine; 20% (v/v) methanol) for 1.5 hours at 100 Volts. Following transfer, membranes were transiently stained used Ponceau stain (0.1% w/v Ponceau stain, 5% v/v methanol) and the molecular weight standards were marked using a pencil. Membranes were destained by rinsing in ddH_20 and blocked in blocking solution (5% (w/v) fat-free milk in TBST (25 mM Tris (pH 7.5), 500 mM NaCl, 0.1% Tween 20) for 1 hour. For blots involving identification of the presence of phosphorylation, a 20% (w/v) fat-free milk in TBST solution containing phosphatase

inhibitors (50 mM NaF, 20 mM Na pyrophosphate) was used as blocking buffer. Blocking was followed by incubation with primary antibody in blocking solution for 2-4 hours, followed by three washes with TBS (25 mM Tris (pH 7.5), 500 mM NaCl) and incubation with secondary antibody in 5% fat-free milk in TBST for 1 hour. The membrane was then washed 3 times in TBST. The protein present was detected using reagents for enhanced chemiluminescence (Perkin Elmer Western Lightning Plus ECL). The antibody dilutions used are listed in Table 2.2.

2.4: Peptide coupling

2.4.1: Coupling of phosphorylated peptides to carrier proteins.

Phosphorylated peptides were conjugated to carrier proteins such as Bovine Serum Albumin (BSA) (Bioshop) and Keyhole Limpet Hemocyanin (KLH) (Pierce) using glutaraldehyde mediated coupling. The peptides were synthesized with an N terminus lysine residue (Table 2.1). Glutaraldehyde covalently conjugates the carrier proteins to the N terminus of the peptides using the free amine group on lysine. 12 mg of each peptide was dissolved in PBS to make a 10 mg/mL solution. The pH was checked and if acidic, was adjusted to pH 7. Six mg of peptide was coupled to 6 mg of BSA or to 6 mg of KLH in presence of 0.2% glutaraldehyde and phosphatase inhibitors (50 mM NaF, 20 mM Na pyrophosphate). The total volume of the coupling mixture was set to 2 mL. The reaction mixture was incubated end over end at room temperature for 4 hours following which it was quenched with 100 mM Tris-Cl (pH 7.5). The conjugated peptides were then dialyzed against PBS overnight at 4^{o}C.

2.4.2: Coupling to peptides to Sepharose matrix.

Synthetic peptides (Table 2.1), both phosphorylated and non-phosphorylated versions, were coupled to activated cyanogen bromide (CNBr) Sepharose (GE Healthcare) using amine group mediated covalent conjugation through a terminal lysine residue. Five mg of peptide was coupled to 2 mL of swollen matrix. The reaction was carried out in coupling buffer (0.1 M $NaHCO_3$, 0.5 M NaCl, pH 8.3) at 4^{o}C for 4 hours. Protein phosphatase inhibitors (50 mM NaF, 20 mM Na pyrophosphate) were included in the reaction for conjugation of phosphorylated peptides. After the coupling step, the reaction was quenched by incubating end over end in presence of 100 mM Tris-Cl (final concentration), pH 8 at 4^{o}C for 1 hour. Uncoupled ligands were removed by washing with buffers of alternating pH (0.1 M acetic acid/sodium acetate at pH 4.0 and 0.1 M Tris-Cl, 0.5 M NaCl at pH 8) for three cycles. For short-term storage, peptide coupled matrix was stored in 10 mM Tris-Cl (pH 7.5) in presence of protein phosphatase inhibitors (50 mM NaF, 20 mM Na pyrophosphate) at 4^{o}C. For long term storage, the peptide coupled matrix was stored in 20% (v/v) ethanol at 4^{o}C.

2.5: Generation and purification of phospho-specific antibodies

For generation of phospho-specific antibodies, phosphorylated peptides were conjugated to carrier proteins as described in section 2.4.1. The resulting peptide-protein conjugate was used for immunization of New Zealand white, female rabbits. Animals were housed and cared for according to the standardized protocols established by the animal care committee at the University of Calgary. Before immunization, the rabbits were pre-screened to ensure that their sera had minimal pre-existing reactivity against

HeLa cell extracts as described previously[160]. Briefly 1 mL of sera were collected from the rabbit and used at a dilution of 1:2500 to perform a western blot analysis against asynchronous and mitotic HeLa cell lysates. Animals showing minimal or no pre-existing response were selected for immunization. The animals were immunized by one priming injection followed by three booster doses, with 21 days interval between two consecutive injections. All injections were given subcutaneously. Freund's complete adjuvant was used for the priming injection. For booster doses, Freund's incomplete adjuvant was used. The animals were bled 12 days following each booster dose and the crude sera were tested for reactivity against phospho peptides by dot blots as described in section 2.6. Following the third booster dose, the response of the crude sera to the phospho-peptides were tested and the terminal bleed was obtained based on the presence of some reactivity. After collection, the blood was allowed to clot and then centrifuged at 1000 rpm at 4^{o}C for 10 minutes to separate the clot from the serum. For long-term use, the sera were stored in -80^{o}C in small aliquots. The antibodies that specifically recognize the phospho epitopes constitute a small portion of the total antibodies present in the rabbit sera and were purified by affinity chromatography using a phospho peptide conjugated CNBr Sepharose column. A column volume of 1 mL was used to purify 4 mL of sera. The phospho peptide was covalently conjugated to CNBr Sepharose as described in section 2.4.2. Rabbit sera were dialyzed overnight against PBS and then diluted with 10 mM Tris (pH 7.5) at a ratio of 1:2. Protein phosphatase inhibitors (50 mM NaF, 20 mM Na pyrophosphate) were included in the solution to minimize dephosphorylation of the peptides. Diluted serum was nutated with the phospho peptide coupled matrix for 4 hours

at 4^{o}C and then loaded on to pre-chilled gravity flow chromatography column (Bio-Rad). The flow-through was collected and tested later for sensitivity. The column was washed with 20 column volumes (CV) of buffer 1 (10 mM Tris (pH 7.5), 100 mM NaCl, 50 mM NaF, 20 mM Na pyrophosphate) followed by 20 CV of buffer 2 (10 mM Tris (pH 7.5), 50 mM NaF, 20 mM Na pyrophosphate). The bound antibody was eluted from the column using 100 mM glycine (pH 2). The eluting antibody was collected in 1 mL fractions. To prevent denaturation at low pH, the antibody was collected in eppendorf tubes containing appropriate volume of 1 M Tris at pH 8.8 so that the resultant solution is neutral. The antibody was then dialyzed against PBS overnight and then concentrated using a 10K cut-off centrifugal filter units (EMD Millipore). The antibody concentration was measured using Bradford assay. Antibodies were stored in small aliquots at a concentration of 1 mg/mL at -80^{o}C for future use.

2.6: Dot-blots

Various amounts of peptides (as mentioned wherever applicable) were spotted on to a nitrocellulose membrane. For spotting any volume greater than 1 µL, the Bio-Dot apparatus from Bio-Rad was used. After spotting, the membrane was blocked in blocking solution (5% fat-free milk in TBS) for 1 hour. For blots involving identification of the presence of phosphorylation, phosphatase inhibitors (50 mM NaF, 20 mM Na pyrophosphate) were added to the blocking buffer. Blocking was followed by incubation with primary antibody in blocking solution for 2-4 hours, followed by three washes with TBS and incubation with secondary antibody in 5% fat-free milk in TBST for 1 hour. The

membrane was then washed 3 times in TBST. The protein present was detected using reagents for enhanced chemiluminescence (Perkin Elmer Western Lightning Plus ECL).

2.7: Cloning

2.7.1: Gateway cloning.

For cloning a gene of interest using the Gateway cloning (ThermoFisher Scientific) technology, first an attB site containing PCR product was created. The primers used for this reaction are listed in Table 2.3. A BP reaction was performed to facilitate recombination between this PCR product and a donor vector (pDNOR 221, Thermo Fisher Scientific) with an attP substrate to create an attL containing entry clone. A subsequent LR reaction was then performed to create an attB site containing expression clone. For bacterial expression, genes of interest were cloned into pDEST42 vector (Thermo Fisher Scientific) which contains two C terminal tags His6 and V5. Positive clones were selected by using appropriate antibiotic resistance and were further analyzed by DNA sequencing (Eurofins Genomics). V249 pCEP 4HA B56 delta (Addgene plasmid #14536) and V245 pCEP 4HA B56 alpha (Addgene plasmid #14532) were gifts from Dr. David Vishrup[161].

2.7.2: Classical cloning using restriction enzymes.

Using a classical cloning approach, B56 delta^{FL} and a truncated mutant B56 delta$^{\Delta 520\text{-}602}$ were cloned into pMal-C2X vector for bacterial expression. Primers and restriction sites used for this purpose are listed in Table 2.4. Both of these constructs were also cloned into pEGFP-C1 for expression in mammalian cells using restriction sites as described in Table 2.3. For expression in bacterial system, B56 alpha was subcloned in

Table 2.3: Primers used for Gateway cloning

Using the primers listed below and an PCR amplification reaction, an attB containing PCR product was generated.

Gene name	Protein name	Source vector	Target vector	Primers used (3'-5')	
				Forward	Reverse
PPP2R5D	B56 delta	pCEP-4HA	pDNOR221	GGGGACAAGTTTGTACAAAAAAGCAGGCTTCGAAGGAGATAGAACCATGCCCTATA	GGGGACCACTTTGTACAAGAAAGCTGGGTCGAGAGCCTCCTGGCTGGCAGT
PPP2R5A	B56 alpha	pCEP-4HA	pDNOR221	GGGGACAAGTTTGTACAAAAAAGCAGGCTTCGAAGGAGATAGAACCATGTCGTCGTCGTC	GGGGACCACTTTGTACAAGAAAGCTGGGTCTTCGGCACTTGTATTGCTGAGAAT

Table 2.4: Primers and restriction enzymes used for classical cloning

Using the primers and restriction enzymes listed in this table, various genes were subcloned into different vectors of choice.

Gene	Protein	Source vector	Target vector	Modifications	Primers used (5'-3')		Restriction enzymes used
					Forward	Reverse	
PPP2R5D	B56 delta	pCEP-4HA	pMAL-C2X	None	AAAAAGAATTCCCCTATAAACTGAAAAAGGAG	AAAGTCGACTCAGAGAGCCTCCTGGCTGG	EcoRI, SalI
PPP2R5D	B56 delta	pCEP-4HA	pEGFP-C1	None	AAAAAGAATTCACCCTATAAACTGAAAAAGGAG	AAAGTCGACTCAGAGAGCCTCCTGGCTGG	EcoRI, SalI
PPP2R5D	B56 delta	pCEP-4HA	pMAL-C2X	Deletion residues 520-602	AAAAAGAATTCCCCTATAAACTGAAAAAGGAG	AAAGTCGACTCAGGGATACTGGGGATTAAG	EcoRI, SalI
PPP2R5D	B56 delta	pCEP-4HA	pEGFP-C1	Deletion residues 520-602	AAAAAGAATTCACCCTATAAACTGAAAAAGGAG	AAAGTCGACTCAGGGATACTGGGGATTAAG	EcoRI, SalI
PPP2R5A	B56 alpha	pCEP-4HA	pet-MBP	None	ATACCATGGCAATGTCGTCGTCGTCGCCGCC	ATAGTCGACTTATTCGGCACTTGTATTGC	NcoI, SalI
PPP2R5A	B56 alpha	pCEP-4HA	pEGFP-C1	None	AAAACTCGAGCAATGTCGTCGTCGTCGCCGCC	ATAGTCGACTTATTCGGCACTTGTATTGC	XhoI, SalI
CEP120	Cep120	pEGFP-N2	pMAL-C2X	None	AAAAAGAATTCATGGTCTCCAAATCCGACCA	AAAGTCGACTTAATTACTGGCATTGCTTT	EcoRI, SalI

pET-MBP vector. Cep120 was subcloned in pMal-C2X using specific primers and restriction enzymes (Table 2.4) from hCEP120-EGFP (Addgene plasmid #50382) was a gift from Dr. Tang Tang[162].

2.8: Recombinant protein expression and purification

2.8.1: B56 alpha.

Arctic Express DE3 *E. coli* cells were used to express B56 alpha from pDEST42. One litre of LB was inoculated with 10 mL of an overnight saturated culture and grown at 37^{o}C for 12 hours. The cells were then pelleted and resuspended in 2 litres of LB and grown at 8^{o}C for 1 hour and then induced with 0.1 mM IPTG. After 20 hours, the cells were harvested and resuspended in ice-cold lysis buffer 1 (20 mM Tris (pH 8), 150 mM NaCl, 10 mM imidazole, 5% glycerol, 0.5% Tween-20, 1 mM PMSF, 1 mM benzamidine) and lysed under a pressure of 11000 psi using a French press. The cells were passed through the French press three times to ensure lysis. The cell debris was removed by centrifugation at 14000 rpm at 4^{o}C. The supernatant was cleared by passing through three layers of Mira-Cloth (Millipore) and then incubated end over end with 1 mL of pre-equilibrated Ni-NTA beads (GE Healthcare) at 4^{o}C for 45 minutes, following which it was poured into a pre-chilled gravity flow chromatography column and the flow-through was collected. The matrix was washed with 25 column volume (CV) of ice-cold wash buffer A1 (20 mM Tris (pH 8), 150 mM NaCl, 20 mM imidazole, 1% Tween-20, 5% glycerol) and 25 CV of ice-cold wash buffer B1 (20 mM Tris (pH 8), 300 mM NaCl, 40 mM imidazole, 5% glycerol). The bound protein was eluted using elution buffer (20 mM Tris (pH 8), 500 mM imidazole, 5% glycerol) and immediately dialyzed into Mono

Q buffer 1 (20 mM Tris (pH 8), 5% glycerol). The dialyzed protein was incubated with 1 mL Q Sepharose matrix (GE Healthcare) for 15 minutes and then poured into a gravity flow column and the flow through was collected and concentrated.

BL21 DE3 *E. coli* was used to express B56 alpha from pET-MBP. One litre of LB was inoculated with 10 mL of saturated overnight culture, grown to an OD_{600} of 0.4 at 37^{o}C and induced with 0.1 mM IPTG. Induced cells were grown at 16^{o}C for 20 hours after which cells were harvested, lysed, and B56 alpha was purified using Ni-NTA affinity chromatography as described above.

2.8.2: B56 gamma1.

BL21 DE3 *E. coli* was used to express His6-tagged B56 gamma1$^{30\text{-}380}$ from the vector pNIC28-Bsa4 (a gift from Nicola Burgess-Brown, Addgene plasmid #42369). One litre of LB was inoculated with 10 mL of saturated overnight culture, grown to OD_{600} of 0.4 at 37^{o}C and then induced with 0.1 mM IPTG. Induced cells were grown at 16^{o}C for 20 hours after which cells were harvested, lysed and purified through affinity chromatography followed by Q Sepharose anion exchange chromatography as described in section 2.8.1.

2.8.3: B56 delta.

Arctic Express DE3 *E. coli* cells were used to express B56 delta^{FL} from pDEST42. Cells were grown, induced and affinity purified using Ni-NTA affinity chromatography as described in section 2.7.1. Following affinity purification, to further purify the protein, size exclusion chromatography was used. Proteins were dialyzed into buffer1 (20 mM Tris (pH 7.5), 150 mM NaCl, 5% glycerol). The pre-packed gel

filtration column (16/60 Superdex R- 200, column volume 120 mL) (GE Healthcare) was equilibrated 2 CV of gel filtration buffer1. 0.5 mL of protein at a concentration of 1 mg/mL was passed through a 0.2 µm syringe filter and loaded onto the column and eluted with 1 CV of gel filtration buffer 1. During elution, 1 mL fractions were collected. Samples were resolved on SDS PAGE and analyzed by Coomassie staining as described in section 2.3 to check for purity of the fractions. Fractions containing the full length B56 delta were pulled together and concentrated.

Arctic Express DE3 *E. coli* cells were used to express B56 delta^{FL} and B56 delta$^{\Delta 520\text{-}602}$ from pMAL-C2X. One litre of LB was inoculated with 10 mL of an overnight saturated culture and grown at 37^{o}C till it reached an O.D$_{600}$ of 0.4. Cells were then induced with 0.5 mM IPTG and allowed to grow for 20 hours at 8^{o}C. Following this, cells were centrifuged and the cell pellet was resuspended in ice-cold lysis buffer (20 mM Tris (pH 7.5), 150 mM NaCl, 1% Tween-20, 5% glycerol, 1 mM PMSF, 1 mM benzamidine, 1 mM EDTA) and lysed and clarified as described in section 2.8.1. The supernatant was then incubated with pre-equilibrated amylose matrix (1 mL volume) for 1 hour at 4^{o}C, following which it was loaded onto a pre-chilled gravity flow chromatographic column and washed with 25 CV of wash buffer A2 (20 mM Tris (pH 7.5), 150 mM NaCl, 5% glycerol, 1 mM EDTA) and 25 CV of wash buffer B2 (20 mM Tris (pH 7.5), 500 mM NaCl, 5% glycerol, 1 mM EDTA). Bound proteins were eluted with 10 CV of elution buffer (50 mM maltose in wash buffer A2). Proteins were dialyzed in Mono S buffer 1 (25 mM MES (pH 6), 5% glycerol) and further purified by cation exchange chromatography through a Mono S 5/50 prepacked column (GE Healthcare).

Five mg of protein was filtered through a 0.2 µm filter and loaded onto a pre-equilibrated column. Bound proteins were eluted with a linear gradient of 0-1 M NaCl in MonoS buffer 1 over 36 fractions.

2.9: Preparation of cell extracts from mammalian cell lines

Unless mentioned otherwise 70-80% confluent mammalian cells were used to make cell extracts. Growth media was aspirated off and cells were washed gently with pre-warmed PBS. Cells were scraped into PBS and centrifuged at 1000 rpm for 10 minutes. To harvest cells synchronized in mitosis, the mitotic shake off method was used. To shake off mitotic cells, the plates were shaken or tapped gently against a hard surface until the adherent rounded mitotic cells were found to be detached. Cells were then resuspended in ice-cold lysis buffer (50 mM Tris-Cl (pH 7.5), 1 mM EDTA, 1 mM EGTA, 150 mM KCl, 1% Triton-X100) in presence of protein phosphatase inhibitors (50 mM NaF, 20 mM Na pyrophosphate, 0.5 µM MCLR (Cayman Chemicals), 5 mM Na orthovanadate) wherever mentioned and protease inhibitors (1 mM PMSF, 2 µg/mL leupeptin, 1 µg/mL pepstatin, 1 mM benzamidine). For immunoprecipitation experiments, cell extracts were made in RIPA buffer (50 mM Tris, 150 mM NaCl, 1% Nonidet P-40, 0.5% deoxycholate) in presence of phosphatase and protease inhibitors as previously described[154]. The resuspended cells were then sonicated for 3X10 seconds with 10 seconds pause in between each sonication using an ultrasonic cell disruptor (miroson^{TM}). Extracts were then centrifuged at 14,000 rpm for 10 minutes at 4^{o}C. The supernatant is the soluble cell extract which was either used immediately or stored at 80^{o}C for future use.

2.10: Cell cycle synchronization

For cell cycle synchronization experiments, asynchronously growing HeLa cells at 30% confluency were treated with 2 mM thymidine (Sigma-Aldrich) for 24 hours. This treatment results in blocking cells in G1/S phase of cell cycle[163]. Cells were then released into S phase by gently washing the adherent cell layer times with pre-warmed PBS and adding fresh pre-warmed growth media. Cells were grown for 3 hours and then treated with 100 ng/mL nocodazole (Sigma-Millipore) for 16 hours. Nocodazole treatment blocks cells in pro-metaphase like state by preventing microtubule assembly[163]. Adherent cell layer was washed gently with pre-warmed PBS and fresh pre-warmed growth media was added. Cells were collected as described in section 2.9 at the indicated time points over a 22-hour period. For collecting mitotic time-points, mitotic shake off method was used as described in section 2.9. Experiment was performed in triplicate.

2.11: Transfection and generation of stable cell lines

Low passage, actively dividing cells were used for all transfection experiments. Prior to transfection, cells were tested for viability using trypan blue staining to ensure that at least 90% cells are viable. The day before transfections, cells were trypsinized, counted and seeded on a 60 X 15 mm plate (21 cm^2 growth surface area) (Grenier Bio-One) such that they reached 50% confluence on the day of transfection. After the cells were attached to the surface, the cells were washed with pre-warmed PBS and allowed to grow in serum-free media, Opti-MEM (Thermo-Fisher). For each plate, 5 µg of plasmid DNA was diluted in 500 µL of Opti-MEM (mixture A) and 20 µL of Lipofectamine 2000 (Thermo-Fisher) was diluted separately in 500 µL of Opti-MEM (mixture B). Both

mixture A and B were incubated at room temperature for 10 minutes following which mixture B was added to A and mixed well. This solution was added to each plate. HeLa cells were transfected using lipofectamine 2000. HEK293T cells were transfected using polyethylene amine (PEI). PEI (molecular weight 25K) was dissolved in water and neutralized with HCl to a final pH of 7.5 and concentration of 1 mg/mL. The solution was filter sterilized and stored at -80^{o}C for long-term use. For transfecting a 15 X 60 mm plate, 5 µg of plasmid DNA and 4 µL of PEI was diluted in 500 µL of Opti-MEM and vortexed vigorously. The mixture was then incubated at room temperature for 10 minutes and then added to the cells. Twenty-four hours after transfection (either lipofectamine or PEI), serum-free media was removed, cells were washed and transferred to regular growth media (DMEM supplemented with 10% FBS, 2 mM L-glutamine, 100 IU/mL penicillin and 100 µg/mL streptomycin). Cells were assayed for transgene expression 36-48 hours post transfection. If stable cell lines were to be created, then at this stage the cells were incubated in presence of regular growth media plus the desired selection antibiotic (400 µg/mL Hygromycin for HA-tagged B56 proteins or 400 µg/mL G418 for EGFP-tagged proteins). The concentration of selection antibiotic required to create the desired selection pressure was chosen based on pre-established literature values and a kill curve experiment. Media was replaced every 48 hours until most cells died. In about 3 weeks, surviving cells started forming visible colonies. The position of the colonies was marked under a microscope. Sterile glass cylinders (Corning) were dipped in sterile grease and placed over each colony. Colonies were then separately trypsinized and passaged as described in section 2.1. Each colony was transferred to a 60 X 15 mm plate

and grown till confluent and then further passaged and frozen as described in section 2.1.

2.12: Mitotic Protein Kinase inhibition assays

HeLa cells grown to 50% confluency were synchronized in prometaphase by growing in presence of 100 ng/mL of nocodazole for 16 hours. At 15.5 hour, the kinase inhibitors were added at specific concentrations (Aurora A inhibitor I (Selleckchem, 100 nM), Hesperadin (Selleckchem, 100 nM), BI2536 (Selleckchem, 100 nM) and Roscovitine (Millipore, 50 μM), Flavopiridol (Selleckchem 2 μM), ZM447439 (Selleckchem, 5 μM) as previously described in literature[129]. At 16 hours, the cells were washed and released from the nocodazole arrest into fresh media containing only the respective kinase inhibitors. After incubation for another 30 minutes, cells were collected by mitotic shake off and cell extracts were made as described in section 2.9. All experiments were performed in triplicate.

2.13: Microscopy

Cells were grown on poly-L-lysine coated glass coverslips (VWR 12 mm no.2). To coat coverslips, they were cleaned and incubated in 50 mM HCl at room temperature for 5 minutes. They were then rinsed several times with water and then incubated with 50 μg/mL of poly-L-lysine for 30 minutes at room temperature, following which the coverslips were rinsed with autoclaved double-distilled water and then spread out on a blotting paper to dry. After drying, they were sterilized by autoclaving. Cells were seeded on coverslips. On reaching 50% confluence, cells were fixed using 2% paraformaldehyde (PFA) solution at 37ºC for 1 hour. For immunostaining, the fixed cells on coverslips were transferred to a humidified chamber. The cells were washed three times with PBS, and

blocked in blocking solution (5% (v/v) FBS, 1% (v/v) BSA in PBS) for 15 minutes, permeabilized in 0.5% (v/v)Triton-X100 in PBS and then incubated with the respective primary antibodies in blocking buffer for 1 hour. Anti Cep120 pT368 and Anti Repoman pS578 were used at a concentration of 1 ng/µL. Anti APC1 pS555 was used at a concentration of 3 ng/µL. Commercial antibodies were used at concentrations suggested by vendor datasheets. Cells were washed in washing buffer (0.05% Trition-X100 in PBS) and incubated with secondary antibodies in blocking buffer for 1 hour. Cells were washed, and the cell nuclei were counterstained by incubating with DAPI (4',6-diamino-2-phenylindole) (0.1 µg/mL) for 15 minutes. Cells were then washed in PBS three times and mounted on 1 mm glass slides (VWR) using SlowFade Diamond (ThermoFisher Scientific) mounting media. Images were acquired using a Zeiss AxioImager Z2 microscope equipped with a 100X, NA= 1.25 oil immersion objective using DAPI, GFP and dsRED filters. For each field of view, 10-14 Z stacks were taken. Z stacks were deconvoluted and combined using the Zeiss Zen Pro software. Contrast and brightness were adjusted in Adobe Photoshop using the levels function.

2.14: Peptide pull down assay

Peptide pull down assays were carried out as described in Figure 2.1. Asynchronous or mitotic HeLa cell lysate was prepared as described in 2.9. Peptide-coupled CNBr Sepharose was prepared as described in section 2.3.2. and was equilibrated in lysis buffer (composition described in section 2.9) and incubated with HeLa cell lysate for 2 hours at 4^{o}C. Non-specifically bound proteins were removed by washing the matrix three times with buffer A (25 mM Tris (pH 8), 5% glycerol, 150 mM NaCl, 75 mM LiCl,

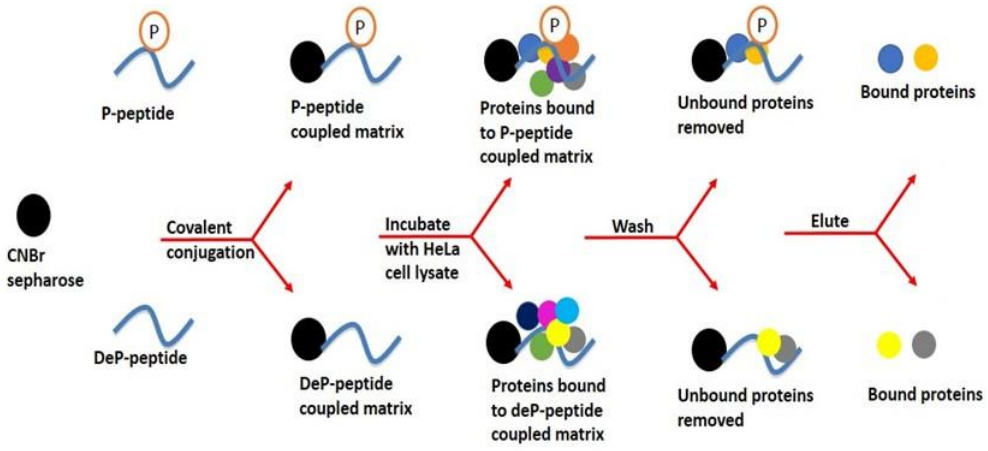

Figure 2.1: Experimental design of *in vitro* peptide binding assay. Synthetic peptides spanning the LS/TPI/V motif of the target proteins (phosphorylated and dephosphorylated variants) were covalently conjugated to a solid matrix such as CNBr Sepharose via terminal amine group mediated coupling. The peptide coupled matrix was incubated end over end with HeLa cell lysate (asynchronous or mitotic) and then washed to remove unbound or loosely associated proteins. Bound proteins were eluted by boiling with SDS sample buffer. The eluate was run on SDS PAGE to separate proteins and immunoblotted with B56 isoform specific antibodies.

0.1% NP40, 50 mM NaF, 20 mM Na pyrophosphate) followed by buffer B (25 mM Tris, 5% glycerol, 25 mM NaF and 20 mM Na pyrophosphate). Bound proteins were eluted by boiling in 1% SDS for 10 minutes at 95^{o}C. LS/TPI/V motif containing peptide used for the study and their sequences are listed in Table 2.1. As a negative control, modified peptide (RARA motif) derived from YLPM1 was used (Table 2.1). Additionally, just CNBr matrix without any coupled peptide was also used as a negative control. All experiments were performed in triplicate.

2.15: Immunoprecipitation (IP)

Mitotic and asynchronous cells were collected as described in section 2.9. Cytoplasmic, nuclear, and chromatin associated fractions were prepared as previously described[164] and were pooled together. Harvested cells were resuspended in buffer 1 (50 mM Tris pH 7.5, 0.5% Triton-X100) in presence of phosphatase inhibitors (50 mM NaF, 20 mM Na pyrophosphate, 0.5 µM MCLR) and protease inhibitors (EDTA free protease inhibitor cocktail, Sigma). Cells were then centrifuged at 1.8 X 1000g. The supernatant S1 representing the cytoplasmic fraction was collected and stored on ice. The pellet was resuspended in buffer 2 (50 mM Tris (pH 7.5), 1.5 mM $CaCl_2$) in presence of phosphatase and protease inhibitors as described above. This was then treated with 0.2 U/µL micrococcal nuclease (NEB) for 30 minutes at 37^{o}C. The cells were then centrifuged at 664g for 10 minutes. The supernatant S2 was collected and stored on ice. The pellet was resuspended in buffer 1 and sonicated briefly for 10s.The cells were then centrifuged at 14000 rpm for 10 minutes. The supernatant S3 was collected. Fractions S1, S2 and S3 were combined (S) and the concentration of protein present was measured by

Bradford assay as described in section 2.3. Two mg of combined lysate S was incubated with 2 µg of antibody against the target protein and allowed to go end over end for 1 hour at 4ºC. Next, this was incubated end over end with protein A Sepharose (GE Healthcare) for an additional 30 minutes at 4ºC, after which extracts were removed and the beads were washed three times in ice-cold PBS and bound protein eluted by boiling the beads in 1% SDS for 5 minutes. For all IP experiments, affinity purified IgG from the same species was used as control.

2.16: LC MS-MS analysis

LC MS-MS experiments were performed by SAMS center at the University of Calgary. Beads were washed 5 times with 50 mM ammonium bicarbonate and resuspended in 25 µl of 50 mM ammonium bicarbonate. Proteins bound to the beads were reduced with 10 mM dithiothreitol for 30 min at 56ºC and alkylated with 25 mM iodoacetamide for 30 min in the dark at room temperature. Proteins were then digested with 1 µg of MS grade trypsin (Pierce) for 4 hours at 37ºC following which another 1 µg of trypsin was added, and the digestion was performed overnight at 37ºC. Tryptic peptides were retrieved after centrifugation of the beads at 10000g for 1 min. Extraction solution (20 µl; 25% v/v acetonitrile (EMD), 0.1% formic acid (ThermoFisher) in water (EMD)) was added and the beads were gently vortexed for 5 min. Peptides were retrieved after centrifugation as described above and the extraction was performed twice. Samples were then lyophilized and resuspended in 30 µl of 1% formic acid in water. Tryptic peptides were analyzed on an Orbitrap Fusion Lumos Tribrid mass spectrometer (Thermo Scientific) operated with Xcalibur (version 4.0.21.10) and coupled to a Thermo Scientific

Easy-nLC (nanoflow Liquid Chromatography) 1200 system. Tryptic peptides (2 µg) were loaded onto a C18 trap (75 µm x 2 cm; Acclaim PepMap 100, P/N 164946; ThermoScientific) at a flow rate of 2 µl/min of solvent A (0.1% formic acid and 3% acetonitrile in LC-MS grade water). Peptides were eluted using a 45 min gradient from 5 to 40% of solvent B (0.1% formic acid in 80% LC-MS grade acetonitrile) at a flow rate of 0.3 µL/min and separated on a C18 analytical column (75 µm x 50 cm; PepMap RSLC C18; P/N ES803; ThermoScientific). Peptides were then electrosprayed using 2.3 kV voltage into the ion transfer tube (300°C) of the Orbitrap Lumos operating in positive mode. The Orbitrap first performed a full MS scan at a resolution of 120000 FWHM to detect the precursor ion having a *m*/*z* between 375 and 1575 and a +2 to +7 charge. The Orbitrap AGC (Auto Gain Control) and the maximum injection time were set at 4e5 and 50 ms, respectively. The Orbitrap was operated using the top speed mode with a 3 sec cycle time for precursor selection. The most intense precursor ions presenting a peptidic isotopic profile and having an intensity threshold of at least 5000 were isolated using the quadrupole and fragmented with HCD (30% collision energy) in the ion routing multipole. The fragment ions (MS^2) were analyzed in the ion trap at a rapid scan rate. The AGC and the maximum injection time were set at 1e4 and 35 ms, respectively, for the ion trap. Dynamic exclusion was enabled for 30 sec to avoid of the acquisition of same precursor ion having a similar m/z (plus or minus 10 ppm). The Lumos raw data files (*.raw) were converted into Mascot Generic Format (MGF) using RawConverter (v1.1.0.18; The Scripps Research Institute) operating in a data dependent mode. Monoisotopic precursors having a charge state of +2 to +7 were selected for conversion.

This mgf file was used to search a database specified by the customer using Mascot algorithm (Matrix Sciences; version 2.4). Search parameters for MS data included trypsin as enzyme, a maximum number of missed cleavage of 1, a peptide charge equal to 2 or higher, cysteine carbamidomethylation as fixed modification, methionine oxidation as variable modification and a mass error tolerance of 10 ppm. A mass error tolerance of 0.6 Da was selected for the fragment ions. Only peptides identified with a score having a confidence higher than 95% were kept for further analysis. The Mascot dat files were imported into Scaffold (v4.3.4, Proteome Software Inc) for comparison of different samples based on their mass spectral counting.

2.17*: In silico* analysis

2.17.1: Use of SlimSearch 4 server.

To search proteins containing LS/TPI/V motif, SlimSearch (version 4), a web based protein motif discovery tool was used[165]. SlimSearch can scan the proteome of 70 model organisms of experimental and therapeutic importance including humans. The sequence L[ST]P[IV] was used as a search query. Flank length was set at 14 to retrieve 14 amino acid residues flanking the motif in each hit instance. The motif was searched in the human proteome as well as in the proteome of *Drosophila melanogaster, Caenorhabditis elegans, Xenopus laevis, Arabidopsis thaliana, Saccharomyces cerevisiae, Escherichia coli, Bacillus subtilis* and in viruses. Wherever mentioned, disorder cut-off and accessibility cut-off scores were used to increase the stringency of the search and eliminate non-functional consensus matches. The results generated by the server in a tabular format were downloaded as a tdt file and converted to an excel

spreadsheet for analysis. Each hit instance of the motif was checked for evolutionary conservation across different species. The presence and conservation of the motif was represented by C, absence of conservation was represented by N. The absence of available information was represented by X. In addition to an overall assessment of the conservation of the motif, each amino acid residue in the motif and flanking region was also aligned. This alignment can be retrieved by clicking on the link to "view alignment" on the excel spreadsheet.

2.17.2: Multiple sequence alignment.

To align multiple sequences together, such as sequences flanking the LS/TPI/V motif in all hit instances, MultAlin server was used[54]. Output was saved as a mul file. The mul file generated from the MultAlin server was used as a search query for creating a weblogo using the Web Logo 3 server. Composition adjustment was disabled, and output was retrieved in units of probability.

2.17.3: Analysis of functional enrichment and complex signaling networks.

To analyze functional enrichment and signaling pathways, ClueGo and Cluepedia app in Cytoscape was used. Cytoscape is an open source platform for visualizing complex signaling pathways[166]. The functionalities of the core software are extensible through use of plugin and apps. ClueGo and Cluepedia are plugins that were used in this study[167]. A list of protein Uniprot identifiers were uploaded by directly pasting in the text field. Cluepedia has in-built functions to retrieve linear and non-linear dependencies between the uploaded identifiers from existing interaction databases. Functional enrichment of GO biological processes or KEGG pathways associated with the protein

identifiers were performed to generate nested networks. Proteins already known to be associated with a pathway were automatically included in the network. A minimum of 3 and a maximum of 8 GO tree intervals were selected. In the generated network, related nodes were connected by edges. Node size correlated with the number of mapped genes. Node color corresponds to the significance. Nodes were clustered together based on previous reports of their interaction.

Chapter 3: Results

3.1: LS/TPI/V motif is widespread in the human proteome

PP2A-B56 is one of the most abundant protein phosphatases and regulates numerous cellular processes and signaling pathways[40]. I speculated that the B56 binding motif, LS/TPI/V must be widespread in the human proteome. For the clarity of all discussions, the amino acid residue positions in LS/TPI/V are labelled as described in Figure 3.1A. L is in position 1 (P1) and I/V is in P4 (Figure 3.1A). SLiMSearch server was used (as described in section 2.17) to find all human proteins containing this motif[165,168]. The results and key features of this search are tabulated in Table 3.1. To help the reader better navigate Table 3.1, its key features are highlighted in Figure 3.1B. The initial computational search retrieved a total of 904 hit instances in 851 proteins, out of which 541 hits from 515 proteins have S in P2. Classical biochemistry concepts suggest that a structure-function relationship is important for protein-protein interactions. However, in the past 10 years there has been a gradual paradigm shift from this line of thought[169]. Studies have increasingly shown that regions of protein that are involved in protein-protein interactions are disordered or unstructured under native conditions, lack the ability to fold into globular domains and become structured (disorder-to-order transition) upon binding to an interacting partner[169]. This particularly holds true for SLiMs as suggested by several experimental and theoretical studies[170]. Even though there are multiple instances where globular structural domains are important for facilitating protein-protein interactions in the human proteome, these instances are outnumbered by interactions mediated through SLiMs and intrinsically disordered regions. To filter out probable non-functional consensus matches of the SLiM, LS/TPI/V, IUPRED disorder

A

B

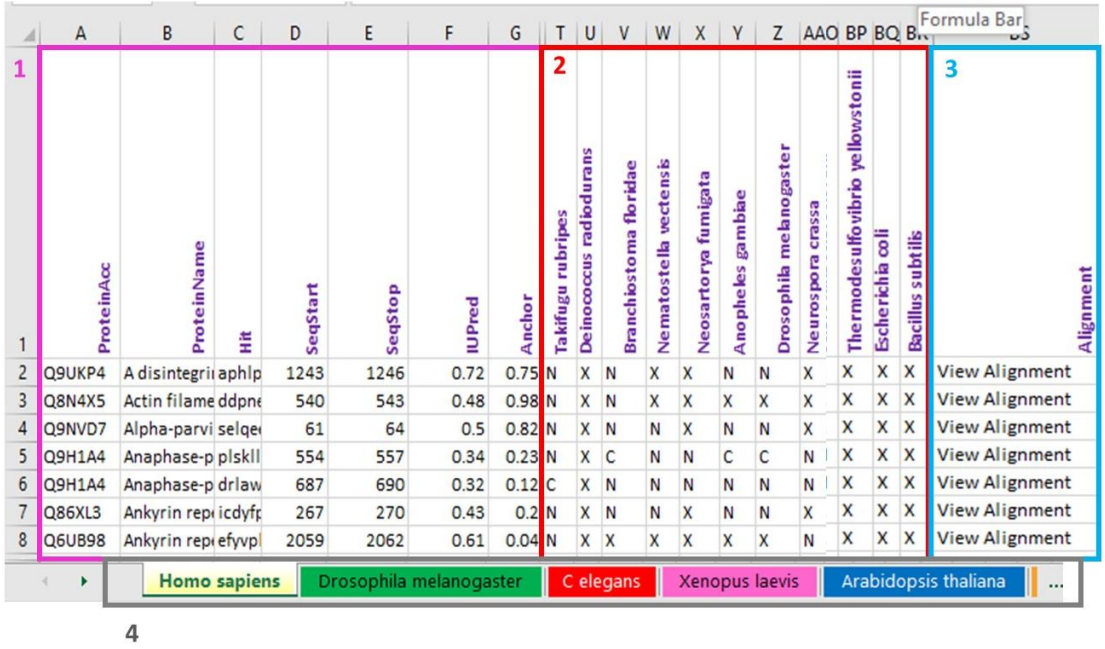

Figure 3.1: Overview of the *in silico* analysis. (A) Amino acid positions in the LS/TPI/V motif. The position of the amino acids in the LS/TPI/V motif are labelled for the clarity of all discussion. (B) Summary of the key features presented in Table 3.1. Box 1 in pink shows the hit instances and peptide annotations. Box 2 in red shows the specific columns for viewing taxonomic range and evolutionary analysis of the motif. The rows on the top represent the organisms in which the presence of the hit instance was tested. In a particular organism, C represents that the motif is conserved, N represents absence of conservation and X represent lack of available information. Box 3 in cyan blue shows the link to view alignment of each hit instance. To access alignment of the motif and the flanking sequences in each hit instance, the link "view alignment" in the corresponding row must be clicked. Box 4 in grey highlights the different tabs in this table. The results of the motif search from each model organism is summarized in each tab.

score (mean disorder score of the motif) of 0.3 was used as a disorder cut-off. The scoring system ranges from 0 to 1, 1 being a completely disordered region[171,172]. A score of 0.3 usually accounts for the majority of the structured regions and has been used in previous studies to computationally identify functional SLiMs[173]. Four hundred and twenty-eight hits in 402 human proteins passed the disorder cut-off. Mean anchor score showing the propensity of the peptide folding upon binding to a protein interactor was also calculated by the server[174]. The anchor scores are on a scale of 0 to 1, with a lower score indicating a higher propensity of folding upon binding to an interactor. Instances that have been reported to have the motif shared in more than one globular protein domain were also filtered out, resulting in 350 hits in 331 proteins (Table 3.1).

To study the diversity and the complexity of the LS/TPI/V protein signaling network, several functional enrichment analyses were performed. Data related to biological activities and functions of LS/TPI/V proteins were retrieved from two databases – Kyoto Encyclopedia of Genes and Genomes (KEGG) and Gene Ontology (GO). Functional enrichment of GO biological processes and KEGG pathways was analyzed using the ClueGO and Cluepedia application in Cytoscape as described in section 2.17. As anticipated, LS/TPI/V proteins were found to be involved in multiple signaling pathways (Figure 3.2, 3.3). GO biological processes or KEGG pathways with p value ≤ 0.05 were used to construct an interaction network. Both experimental and theoretical evidence deposited in all databases accessible by ClueGO were used for the construction of the interaction networks. Several GO biological processes related to the cell cycle, such G2/M transition, regulation of transcription involved in G1/S transition of mitotic cell

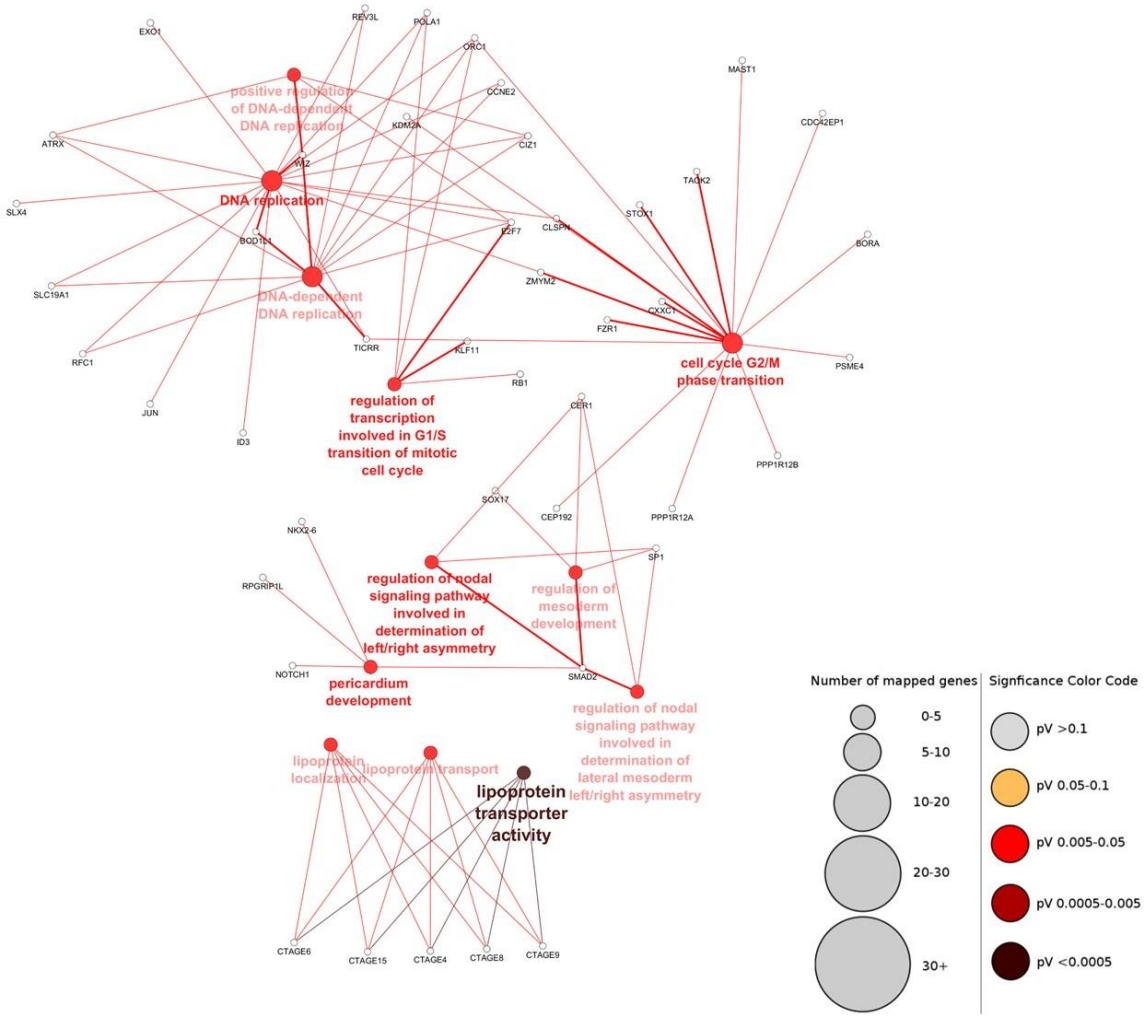

Figure 3.2: Functional enrichment analysis showing LS/TPI/V motif containing proteins in humans are involved in multiple GO biological processes. All GO biological processes (filtered using p value ≤ 0.05) associated with the selected LS/TPI/V proteins (331 proteins listed in Table 3.1) in humans were used to create this interaction map. A minimum of 3 and a maximum of 8 GO tree interval levels were selected. Analysis was performed using ClueGO and Cluepedia applications in Cytoscape. The pathways were grouped based on significance. The size and color of the legend for significance is shown on the bottom right. The node size corresponds to the number of mapped genes. The node color corresponds to the significance. Nodes are clustered together based on their Kappa score. The length and thickness of edges are not scaled.

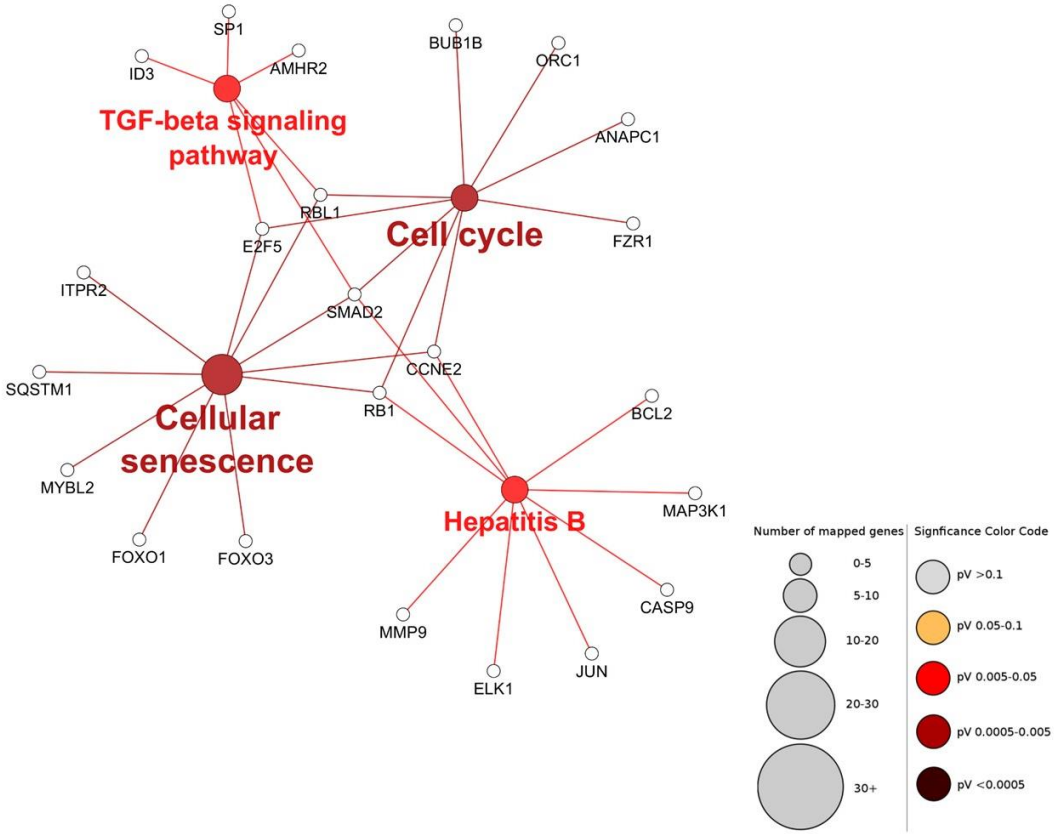

Figure 3.3: Functional enrichment analysis showing LS/TPI/V motif containing proteins in humans are involved in multiple KEGG signaling pathways in humans. All KEGG signaling pathways (filtered using p value ≤ 0.05) associated with the selected LS/TPI/V proteins (331 proteins listed in Table 3.1) in humans were used to create this interaction map. Analysis was performed using ClueGO and Cluepedia application in Cytoscape. The pathways were grouped based on significance. The size and color of the legend for significance is shown on the bottom right. The node size corresponds to the number of mapped genes. The node color corresponds to the significance. The length and thickness of edges are not scaled.

cycle, and DNA replication were found to be enriched (Figure 3.2). KEGG pathways that were enriched were related to cell cycle, cell senescence, TGFβ signaling and hepatitis virus infection (Figure 3.3).To investigate subcellular localization of LS/TPI/V proteins, the FunRich application was used[175]. Approximately 60% of the LS/TPI/V proteins were found to be localized or associated with the nucleus (Figure 3.4). LS/TPI/V proteins were also found to localize to other subcellular compartments such as the ER, lysosomes, mitochondria, centrosomes (Figure 3.4).

B56 proteins are well conserved across eukaryotes[176]. In the unicellular eukaryote *Saccharomyces cerevisiae*, there is only a single gene (RTS1) coding for the B56 protein. In humans, there are 5 genes coding for B56 proteins. In *Arabidopsis thaliana*, the B56 gene was duplicated several times resulting in 9 genes coding for B56[176]. To analyze how widespread LS/TPI/V motif proteins are across eukaryotes, proteins containing this motif were also retrieved from model organisms (using the same filters described above), in particular *Drosophila melanogaster* (416 hits in 406 proteins), *Caenorhabditis elegans* (246 hits in 242 proteins), *Xenopus laevis* (247 hits in 240 proteins), *Arabidopsis thaliana* (382 hits in 374 proteins), and *Saccharomyces cerevisiae* (63 hits in 61 proteins) (Table 3.1). Each hit instance was taxonomically aligned, and the alignment can be accessed from the corresponding "view alignment" link in Table 3.1. Using the same parameters described above diversity of the LS/TPI/V protein signaling network was studied in *Saccharomyces cerevisiae* and in *Arabidopsis thaliana*. Functional enrichment analysis was performed using the ClueGO and Cluepedia applications in Cytoscape and enriched GO biological processes and KEGG pathways were mapped. In *Saccharomyces*

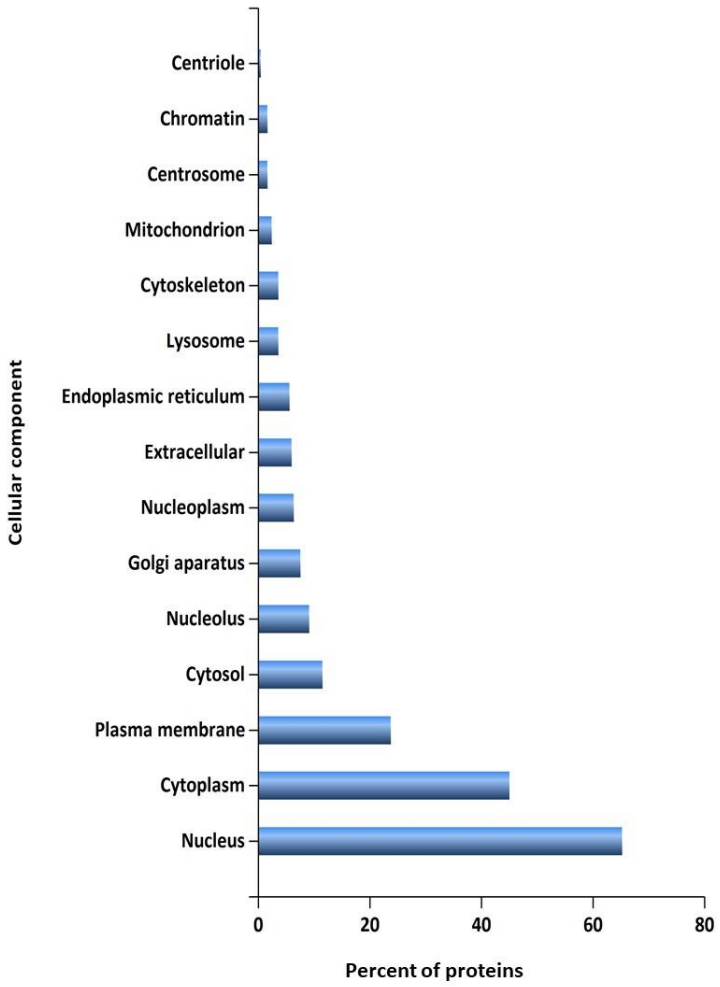

Figure 3.4: Cellular localization of LS/TPI/V proteins. The 331 human LS/TPI/V proteins were analyzed using the FunRich app (version 3.1.3) for associated of GO cellular components. The Y axis shows cellular component and X axis shows the percentage of protein present in that component.

cerevisiae, GO biological processes related to four main functions were enriched – regulation of cell cycle, protein phosphorylation, regulation of endocytosis and Rho signal transduction (Figure 3.5). The only KEGG pathway found to be enriched in *Saccharomyces cerevisiae* was cell cycle (Figure 3.6). In *Arabidopsis thaliana*, the main functional hubs found to be enriched were establishment of mitotic spindle orientation, regulation of protein kinase activity, plant organ senescence, and regulation of cellular catabolic process (Figure 3.7).

Since mitosis is tightly regulated by reversible protein phosphorylation, and several mitosis and cell cycle related pathways are enriched in the functional enrichment analysis of LS/TPI/V proteins across eukaryotes, I wanted to investigate how PP2A-B56 controlled mitosis by interacting with LS/TPI/V motif containing proteins. To study this, a selection of important mitotic regulators was chosen as representatives (Table 3.2). The LS/TPI/V motif in the chosen proteins were found to be conserved across diverse eukaryotes (Figure 3.8, 3.9). On closer examination of the motifs present in these proteins, we observed that in Repoman a LxxIxE (LPEVPE) motif is present downstream of the LSPI motif. In APC1, a LxxIxE (LGSLDE) is present upstream of the LSPV motif. The other chosen mitotic regulators have only one LS/TPI/V motif present. In addition to eukaryotes, LS/TPI/V proteins were also retrieved from organisms that do not express B56, such as *Escherichia coli* (14 hits in 14 proteins), *Bacillus subtilis* (5 hits in 5 proteins) and viruses (132 hit instances) using the same filters as described above (Table 3.1). These proteins could be non-functional consensus matches or could be proteins responsible for establishing or maintaining pathogenesis in eukaryotic hosts.

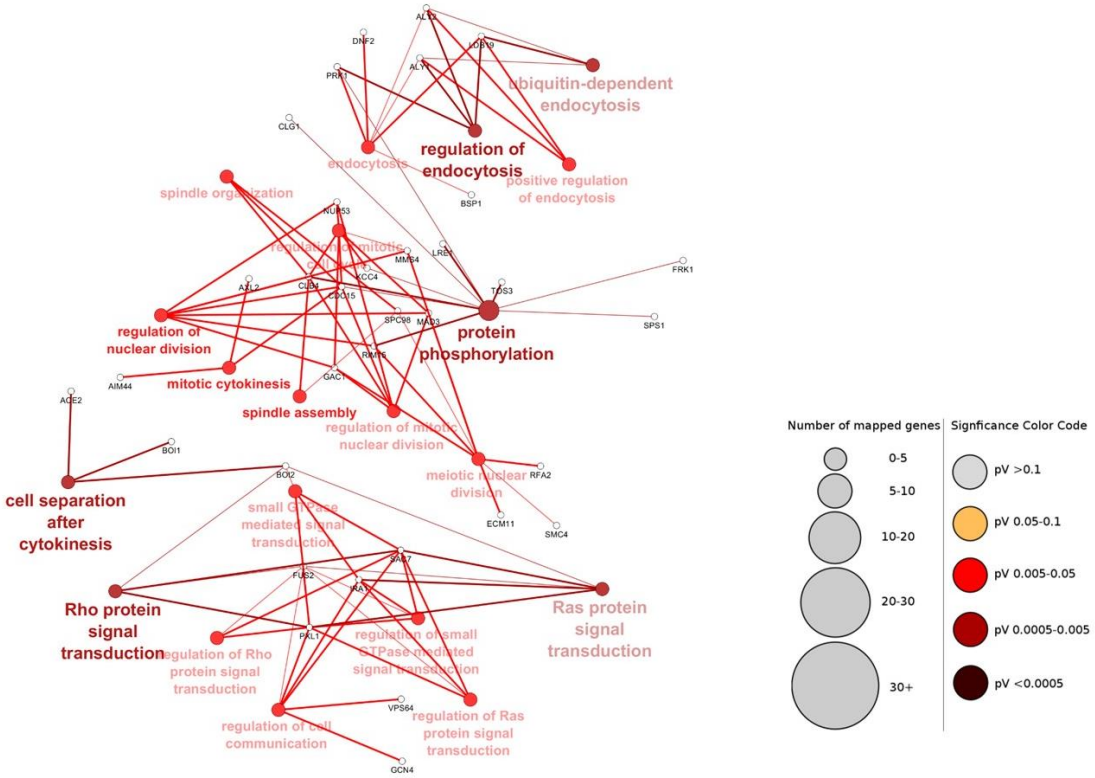

Figure 3.5: Functional enrichment analysis showing LS/TPI/V motif containing proteins in *Saccharomyces cerevisiae* are involved in multiple GO biological processes. All GO biological processes (filtered using p value ≤ 0.05) associated with the selected LS/TPI/V proteins (listed in Table 3.1) in *Saccharomyces cerevisiae* were used to create this interaction map. Analysis was performed using ClueGO application in Cytoscape. A minimum of 3 and a maximum of 8 GO Tree Interval levels were selected. The pathways were grouped based on significance. The size and color of the legend for significance is shown on the bottom right. The node size corresponds to the number of mapped genes. The node color corresponds to the significance. The length and thickness of edges are not scaled.

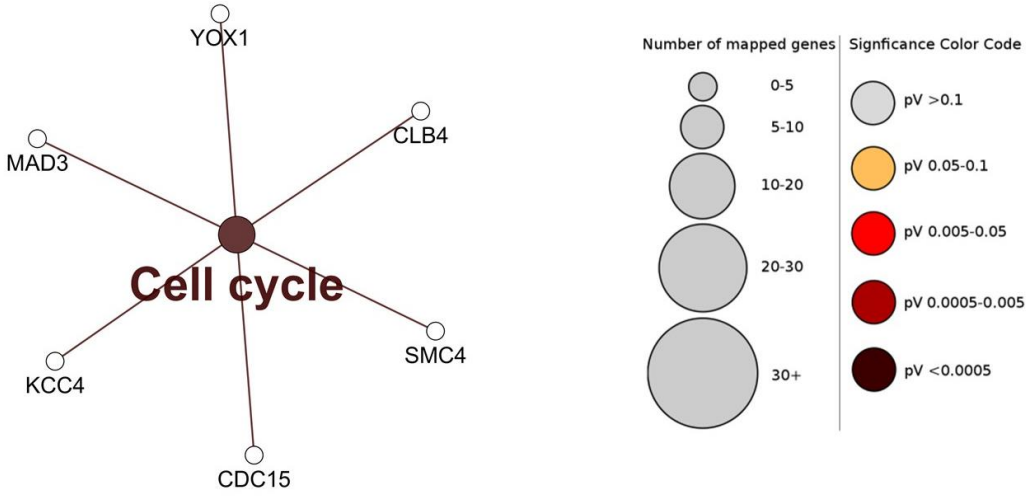

Figure 3.6: Functional enrichment analysis showing LS/TPI/V motif containing proteins in humans are involved in multiple KEGG signaling pathways in *Saccharomyces cerevisiae*. All KEGG signaling pathways (filtered using p value ≤ 0.05) associated with the selected LS/TPI/V proteins (listed in Table 3.1) in *Saccharomyces cerevisiae* were used to create this interaction map. Analysis was performed using ClueGO and Cluepedia application in Cytoscape. The pathways were grouped based on significance. The size and color of the legend for significance is shown on the bottom right. The node size corresponds to the number of mapped genes. The node color corresponds to the significance. The length and thickness of edges are not scaled.

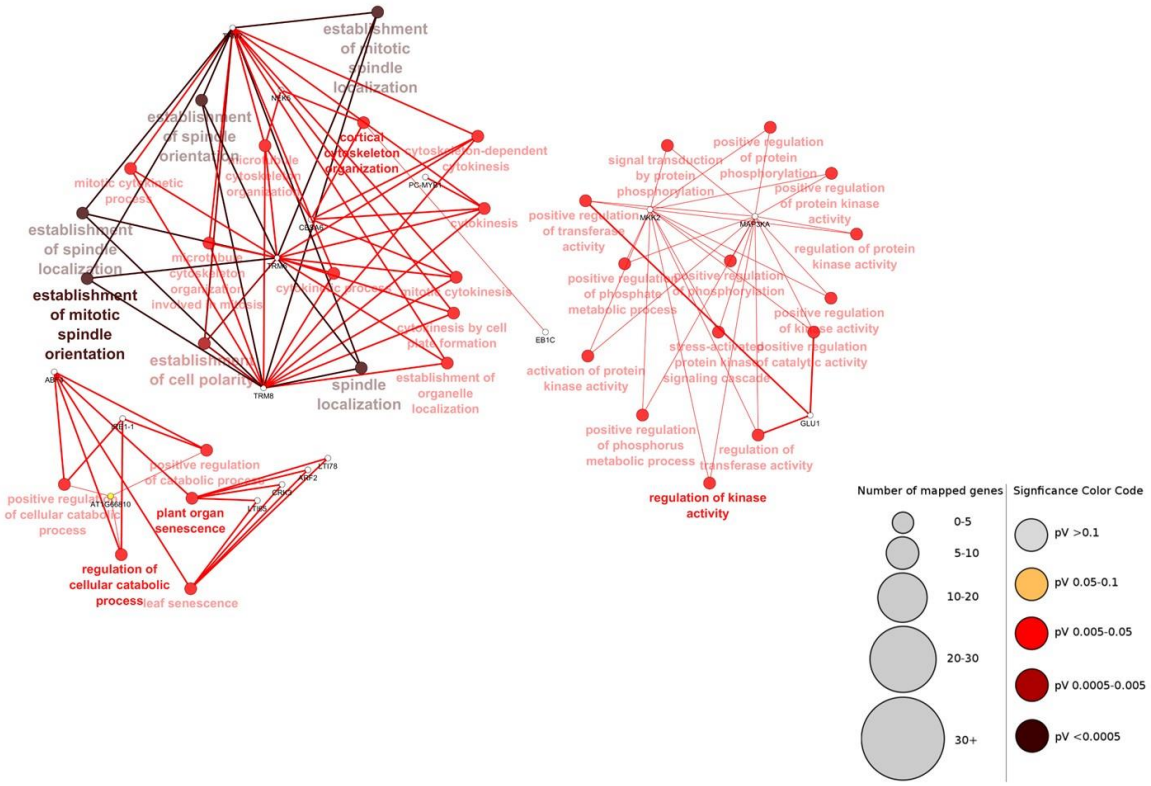

Figure 3.7: Functional enrichment analysis showing LS/TPI/V motif containing proteins in *Arabidopsis thaliana* are involved in multiple GO biological processes. All GO biological processes (filtered using p value ≤ 0.05) associated with the selected LS/TPI/V proteins (listed in Table 3.1) in *Arabidopsis thaliana* were used to create this interaction map. Analysis was performed using ClueGO and Cluepedia applications in Cytoscape. A minimum of 3 and a maximum of 8 GO Tree Interval levels were selected. The pathways were grouped based on significance. The size and color of the legend for significance is shown on the bottom right. The node size corresponds to the number of mapped genes. The node color corresponds to the significance. Nodes are clustered together based on their Kappa score. The length and thickness of edges are not scaled.

Table 3.2: LS/TPI/V containing mitotic regulator human proteins chosen for this study.

Eight mitotic regulators as tabulated below containing LS/TPI/V motif were chosen for further study.

Uniprot ID	Protein Name	Gene Name	Suggested function from literature	Motif
Q69YH5	Repoman	CDCA2	Recruits PP1 to mitotic chromatin during anaphase, regulates chromatin condensation and structure during mitosis.	ERDIASKKP LLSPIPELPE VPEMT
Q9H1A4	APC1	ANAPC1	Component of the Anaphase promoting complex/cyclosome. APC1 mainly known to act as scaffold for the other components.	LLGSLDEV VLLSPVPEL RDSSKLHD
Q8N960	Cep120	CEP120	Centrosomal protein of 120 kDa. Plays a role in centrosome cycle during cell cycle.	HEPEHSKK KVLTPIKEK TLTGPKS
Q9H410	DSN1	DSN1	Kinetochore associated protein required for chromosome alignment and segregation.	KTHDHQLE SSLSPVEVF AKTSASL
Q96GX5	GWL	MASTL	Greatwal protein kinase. Inactivates PP2A-B55 during mitosis.	GFNKKDLE LALSPIHNS SALPTTGR
Q9UM11	FZR	FZR1	Fizzy related protein homolog. Substrate of APC/C.	DDGNDVSP YSLSPVSNK SQKLLRS
P06400	RB	RB1	Retinoblastoma associated protein. Important regulator of mitosis and tumor suppressor.	QNNHTAAD MYLSPVRS PKKKGSTT
Q8WUF5	iASPP	PPP1R13L	RelA associated inhibitor. Regulates mitosis, apoptosis and takes part in Nfkappa B signaling pathway.	GPGPGGPEP ELSPITEGSE ARAGP

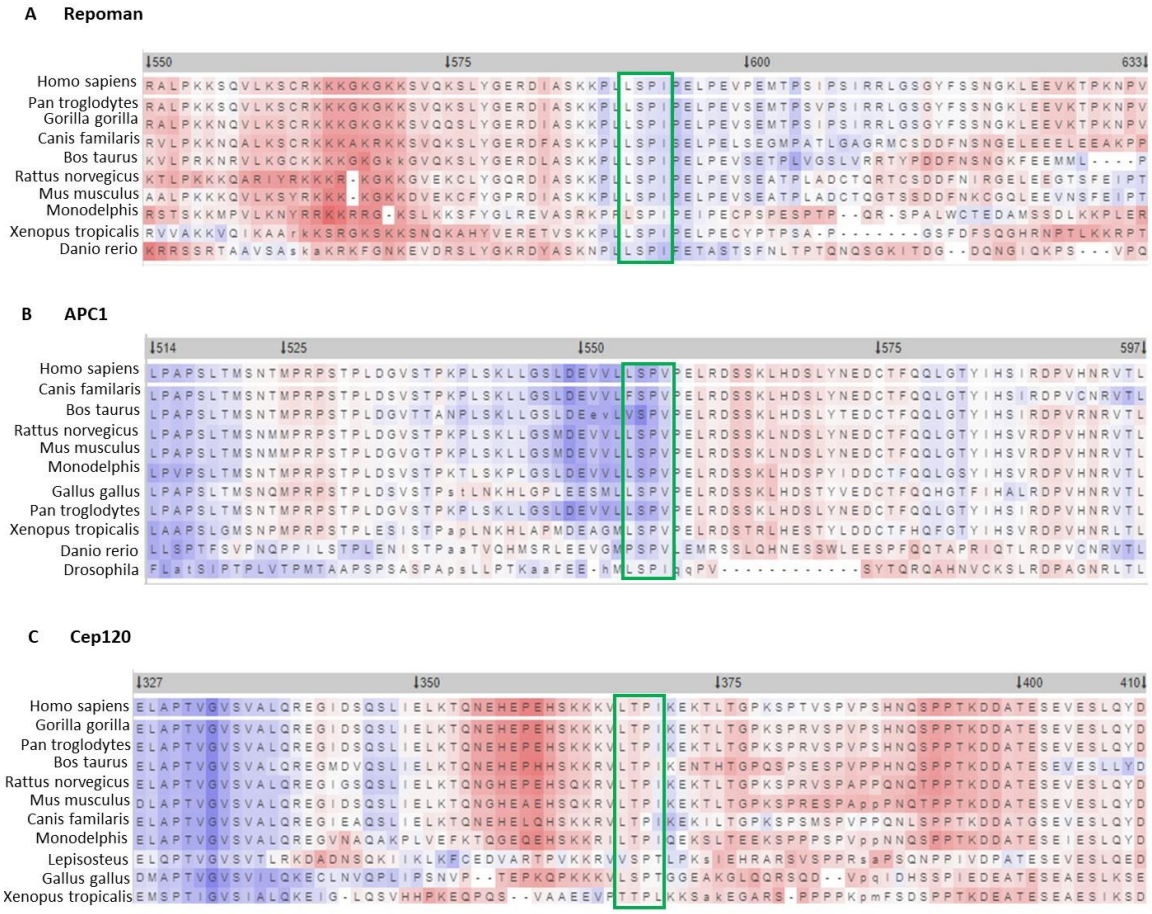

Figure 3.8: LS/TPI/V motif present in the selected proteins are conserved across eukaryotes. Amino acid sequences of the LS/TPI/V motif and its flanking region in various proteins. The amino acid sequences of the proteins and their homologues in diverse eukaryotes organisms were retrieved and aligned by SlimSearch 4 server. Panel A shows Repoman, panel B shows APC1, panel C shows Cep120. The box in green highlights the LS/TPI/V motif in each protein. The eukaryotic organism in which the protein is expressed is indicated on the left. The amino acids are colored red to blue based on the modified Kyte-Doolittle hydrophobicity scale. Red represents regions that are charged whereas blue represents hydrophobic regions.

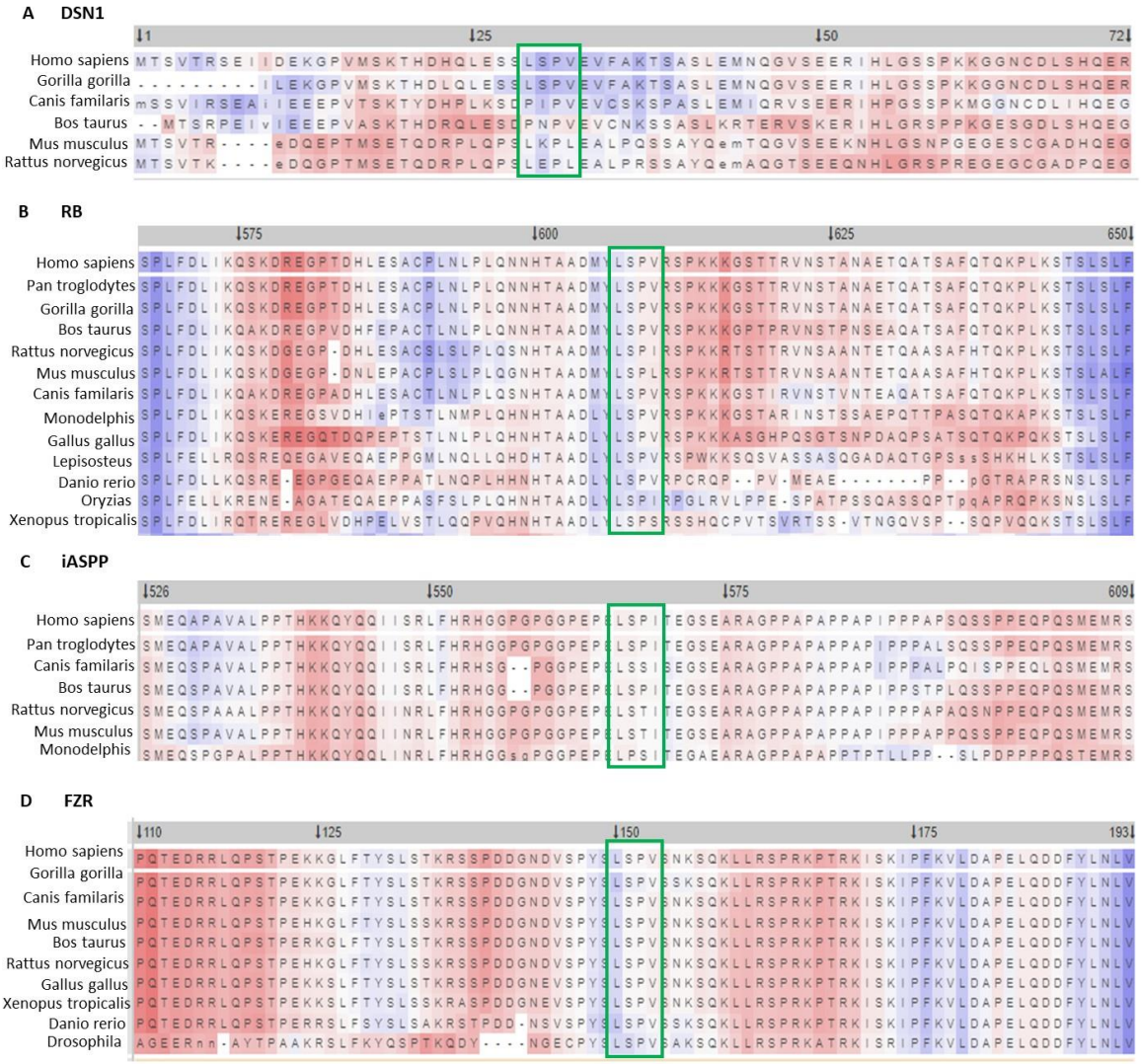

Figure 3.9: LS/TPI/V motif present in the selected proteins are conserved across eukaryotes. Amino acid sequences of the LS/TPI/V motif and its flanking region in various proteins. The amino acid sequences of the proteins and their homologues in diverse eukaryotes organisms were retrieved and aligned by SlimSearch 4 server. Panel A shows DSN1, panel B shows RB, panel C shows iASPP and panel D shows FZR. The box in green highlights the LS/TPI/V motif in each protein. The eukaryotic organism in which the protein is expressed is indicated on the left. The amino acids are colored red to blue based on the modified Kyte-Doolittle hydrophobicity scale. Red represents regions that are charged whereas blue represents hydrophobic regions.

3.2: Sequences flanking LS/TPI/V motif are enriched in specific amino acids

I wanted to investigate if there is a recurring pattern of amino acid residues in the regions flanking the LS/TPI/V motif. The 351 hit instances in human proteins were aligned according to sequence homology using the MultAlin server as described in section 2.17.2. The alignment was used to create a web logo (Web Logo 3 server) showing the probability of occurrence of different amino acid residues at each flanking position (Figure 3.10). Using the same approach, web logos were also created for LS/TPI/V proteins in other organisms including *Drosophila melanogaster* (406 proteins), *Caenorhabiditis elegans* (242 proteins), *Arabidopsis thaliana* (382 proteins), *Saccharomyces cerevisiae* (61 proteins) and *Escherichia coli* (14 proteins). In the human proteome, at position P2, S is over-represented over T (Figure 3.10). This trend also holds true for *A. thaliana*. However, in *C. elegans* and in *E. coli*, the reverse is true. At position P4, V is more prevalent over I in all eukaryotic organisms analysed in this study (Figure 3.10). At flanking positions downstream of the motif, F1 to F10, S, P and E are over-represented. T can be over-represented at positions of F1 to F4 (Figure 3.10). Upstream of the LS/TPI/V motif, at flanking positions F-1 to F-14, S and P are also over-represented. E is over-represented at positions F-3 to F-7 (Figure 3.10). This suggests that negatively charged or amino acid residues that can be phosphorylated are predominant in the flanking region of the motif. It is interesting to note that D although a negatively charged residue is not prevalent in the flanking region. The presence of S and P in the flanking regions is conserved across all the eukaryotes analyzed for this study (Figure 3.10). Interestingly, in *E. coli*, which does not express a B56 protein, a predominance of S

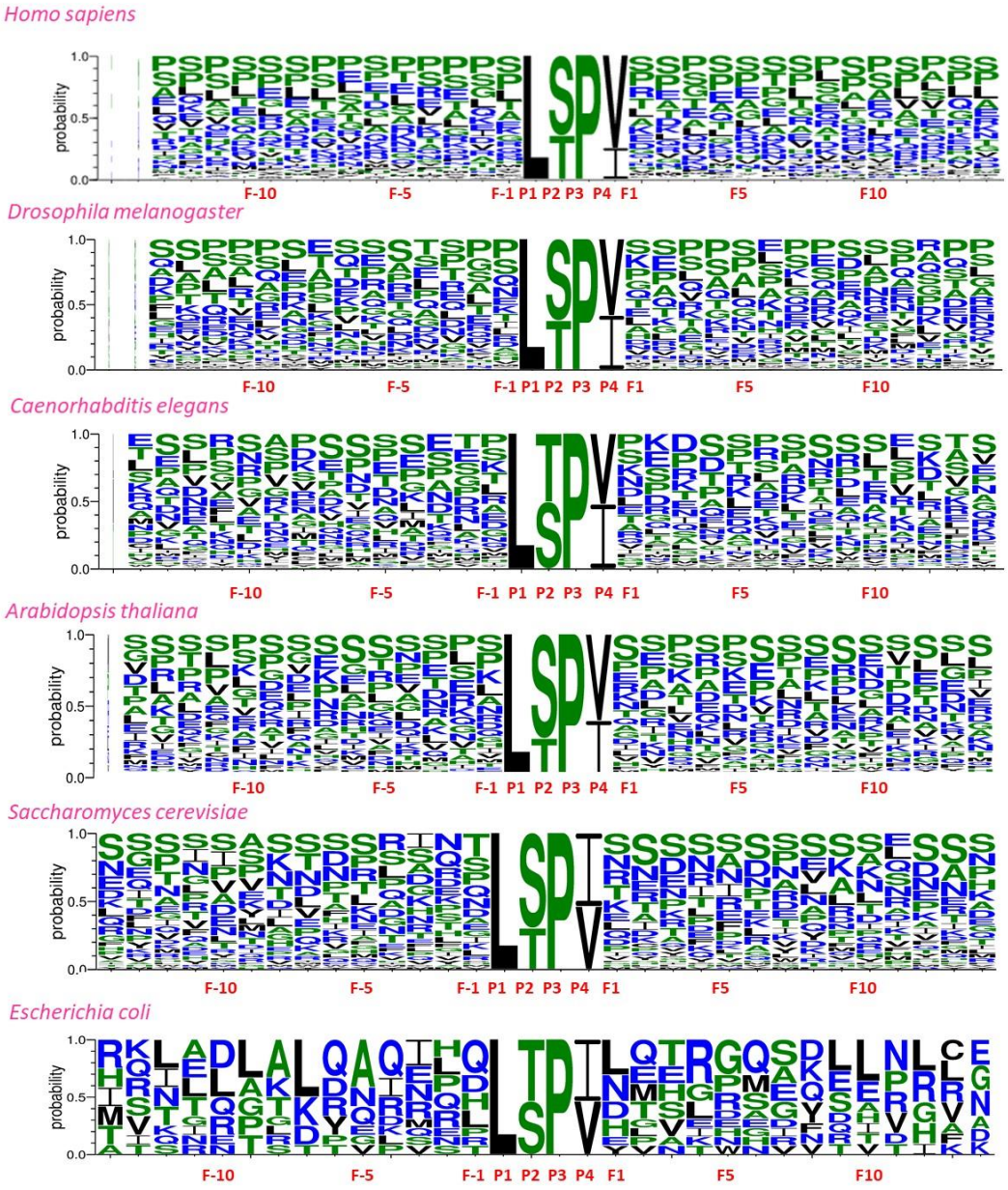

Figure 3.10: Sequence alignment of the amino acid residues flanking LS/TPI/V motif. Fourteen amino acid residues flanking either side of LS/TPI/V motif were retrieved from SLiMSearch server, aligned using MultALin, and then analyzed for the presence of recurring pattern of amino acids using Web Logo 3 server. The amino acids are colored according to the default hydrophobicity scale on the Weblogo server.

and P residues are absent in the flanking region.

3.3: *In vitro* PP2A-B56 binds LS/TPI/V motif containing peptides in a phosphorylation dependent and isoform dependent manner

Two independent studies have shown that B56 binds to LSPI motif containing peptides in a phosphorylation dependent manner and typically bind phosphorylated peptides with higher affinity[153,154]. These studies however, did not investigate if these phosphorylation dependent interactions are specific to a single isoform of B56. We wanted to examine how different B56 isoforms (α, β, γ, δ, ε) interacted with LS/TPI/V peptides and if phosphorylation status of these peptides changed the pattern of their interactions. For this purpose, we performed an *in vitro* peptide binding assay (Figure 2.1) where synthetic peptides were covalently conjugated to CNBr Sepharose matrix and incubated with asynchronous or mitotic HeLa cell lysates, washed afterwards to remove unbound proteins and peptide interacting proteins eluted and run on SDS-PAGE and immunoblotted to check for the presence B56 isoforms. The synthetic peptides were either phosphorylated (referred to as P peptides) or not phosphorylated (referred to as deP peptides) on the S/T residue of the LS/TPI/V motif. The pattern of retention of B56 proteins appear to be the same between asynchronous and mitotic extracts suggesting that any post-translational modifications on B56 during mitosis may not play a role in this association (Figure 3.11, 3.12). B56 alpha, B56 beta and B56 epsilon were not retained by the peptide coupled matrices (Figure 3.11, 3.12). B56 delta from both asynchronous and mitotic HeLa cell extracts is selectively retained by the dephosphorylated peptides, particularly by Repoman, APC1, GWL, DSN1, RB, FZR derived peptides (Figure 3.11,

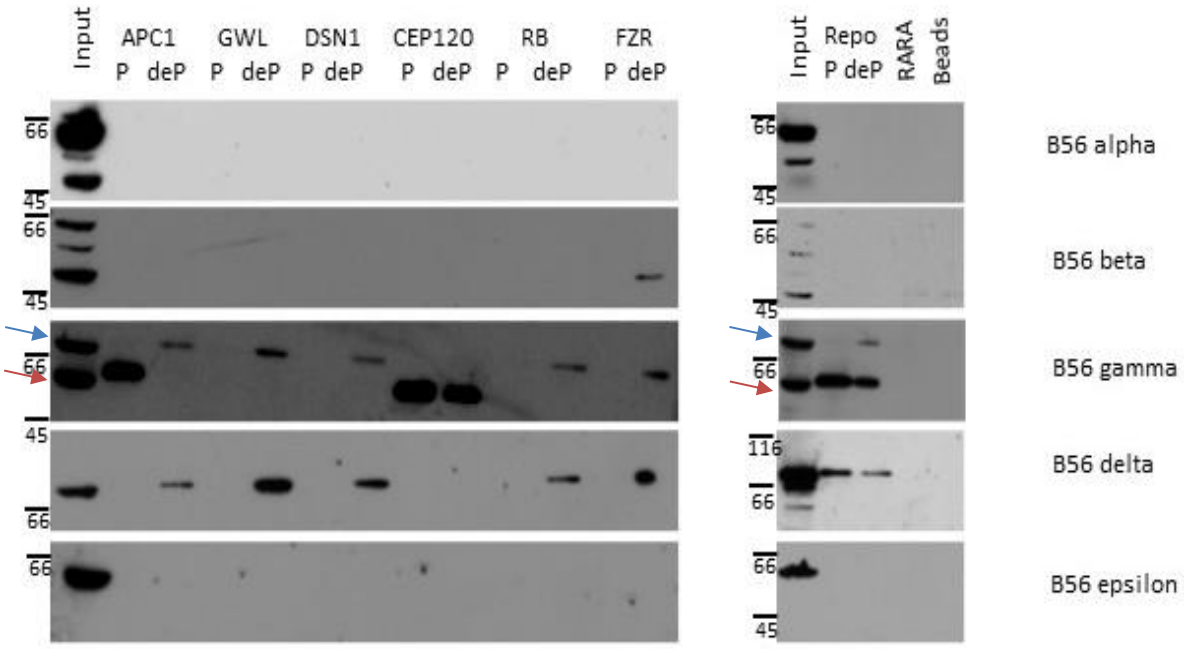

Figure 3.11: B56 proteins from asynchronous HeLa cell extract show an isoform dependent as well as phosphorylation dependent association with LS/TPI/V motif containing peptides. Pull down assays were carried out using phosphorylated (P) and not phosphorylated (deP) peptides spanning the putative LS/TPI/V motif in Repoman, APC1, GWL, DSN1, CEP120, RB, FZR. Peptides spanning the LS/TPI/V motif in Repoman were used as the positive control while RARA peptide having no LS/TPI/V sequence (GKKRARAADLE) was used as a negative control. Only beads (CNBr Sepharose matrix) was also used as a negative control. Asynchronous HeLa cell extract, made in presence of phosphatase inhibitors, was used for the pull down and was used as a positive control for the immunoblot (Input). The eluted proteins from the pull-down assay were separated by SDS PAGE. The presence of B56 isoforms in the eluate was detected by western blotting, using B56 isoform specific antibodies as indicated on the right. Molecular weight standards are shown on the left in kDa. Arrow in blue point to B56 gamma 3, arrow in red point to B56 gamma 1. All experiments were done in triplicate. Representative western blots are shown here.

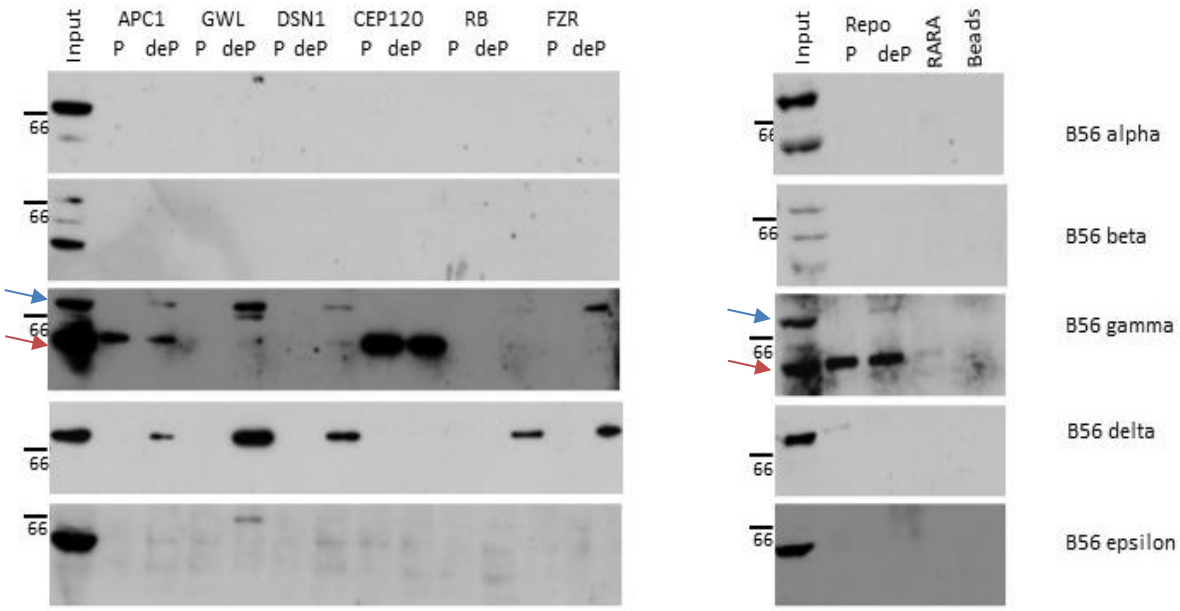

Figure 3.12: B56 proteins from mitotic HeLa cell extract show an isoform dependent as well as phosphorylation dependent association with LS/TPI/V motif containing peptides. Pull down assays were carried out using phosphorylated (P) and not phosphorylated (deP) peptides spanning the putative LS/TPI/V motif in Repoman, APC1, GWL, DSN1, CEP120, RB, FZR. Peptides spanning the LS/TPI/V motif in Repoman were used as the positive control while RARA peptide having no LS/TPI/V sequence (GKKRARAADLE) was used as a negative control. Only beads (CNBr Sepharose matrix) was also used as a negative control. HeLa cells synchronized in mitosis were collected by mitotic shake off and cell lysate made in presence of phosphatase inhibitors, was used for the pull down and was used as a positive control for the immunoblot (Input). The eluted proteins from the pull down assay were separated by SDS PAGE. The presence of B56 isoforms in the eluate was detected by western blotting, using B56 isoform specific antibodies as indicated on the right. Molecular weight standards are shown on the left in kDa. Arrow in blue point to B56 gamma 3, arrow in red point to B56 gamma 1. All experiments were done in triplicate. Representative western blots are shown here.

3.12). Since previous studies by Kruse et al. (described in section 1.6), showed interaction between Repoman and B56 gamma, I used the peptides spanning the LS/TPI/V motif of Repoman as a positive control for this peptide pull-down assay. Phosphorylated Repoman also retains B56 delta in both asynchronous and mitotic HeLa extracts (Figure 3.11, 3.12). CEP120 peptides neither in phosphorylated nor dephosphorylated form retains B56 delta (Figure 3.11, 3.12). The pattern of retention of B56 gamma3 is very similar to that of B56 delta. B56 gamma3 in both asynchronous and mitotic extracts is retained by dephosphorylated versions of Repoman, APC1, GWL, DSN1, RB and FZR (Figure 3.11, 3.12). CEP120 does not retain B56 gamma3 regardless of its phosphorylation status (Figure 3.11, 3.12). B56 gamma1 is retained by phosphorylated Repoman, phosphorylated APC1 and by CEP120 peptides irrespective of its phosphorylation status (Figure 3.11, 3.12). The only peptide showing variant behavior in terms of retaining B56 gamma3, B56 gamma1 and B56 delta is CEP120 which has a threonine instead of a serine in its LS/TPI/V motif. So next, I wanted to investigate if mutating the threonine to a serine will change the pattern of its binding to B56 isoforms (Figure 3.13). However, I found that this single amino acid change in CEP120 peptide does not alter its pattern of association with the B56 proteins. A peptide derived from the protein MPP10, which also contains a T residue was used as a negative control.

3.4: B56 proteins have a high level of sequence similarity but are unique

As suggested by our peptide pull down assay, B56 recognizes LS/TPI/V peptides in an isoform dependent and phosphorylation dependent manner (Figure 3.11, 3.12). I next wanted to investigate if there are important differences between these human B56

Peptides used	Sequence
Cep120	KKKVLTPIKEKT
Mutant Cep120	KKKVLSPIKEKT
MPP10	KESLKRVTFAL

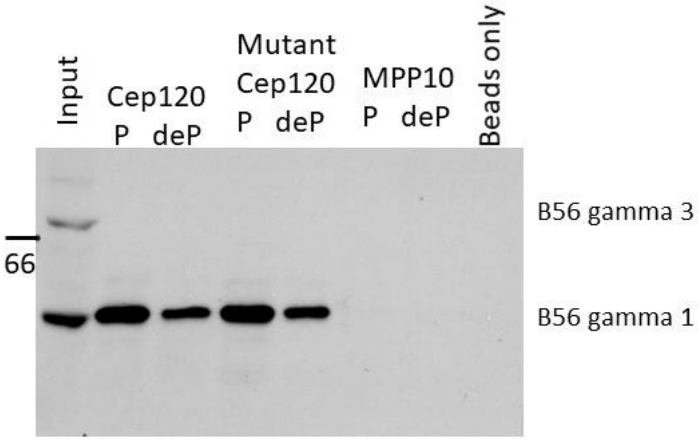

Figure 3.13: The pattern of retention of B56 gamma proteins do not change when T is changed to S in CEP120 peptides. Pull down assays were carried out with both phosphorylated (P) and not phosphorylated peptides (deP) from WT CEP120 and CEP120 (mutant) where the T is mutated to S. MPP10 peptide which has a phosphorylated T was used as a control. Only beads (CNBr Sepharose matrix) was used as a negative control. The top panel shows the peptides used for this assay. The bottom panel shows the immunoblot from the peptide pull down assay. Blot was performed with anti-B56 gamma antibody. Molecular weight standards are shown on the left in kDa. All experiments were done in triplicate. Representative western blots are shown here.

isoforms that are contributing to their binding preference. In humans, B56 proteins are, encoded by 5 genes (B56 α, β, γ, δ and ε)[176]. However, in unicellular eukaryotes such as yeast *Saccharomyces cerevisiae*, there is a single B56 gene, RTS1. Phylogenetic studies suggest that during evolution from unicellular eukaryotes to protists, fungi, plants and animals, four distinct clades (the protist clade, plant clade, fungal clade and animal clade) evolved, each of which had varying degrees of further divergence[176]. In humans, the parent B56 clade further diverged into two clusters – the B56αβε cluster and the B56γδ cluster[176]. The core domain of the human B56 isoforms, consisting of approximately 400 amino acids is highly conserved (Figure 1.4 and 3.14A). This region is also conserved across eukaryotes[152,176]. However, the amino (N) terminal region and the carboxy (C) terminal region of the proteins are quite distinct and might be responsible for isoform-specific interactions (Figure 1.4). B56 delta is the longest of all the isoforms with 602 amino acids. The 400 amino acid core region is flanked by a N-terminal region (amino acid residues 1-102) and C terminal region (amino acid residues 520-602) (Figure 3.14A). The N terminal region has a stretch of repeats of QP amino acids from residues 37 to 52 (Q-P-Q-P-Q-P-Q-P-Q-P-Q-A-Q-S-Q-P) but does not contain any other defined domains or motifs. The C terminal region on the other hand has a putative SH3 binding domain and a nuclear localization signal (Figure 3.14A). It is well-established in literature that reversible protein phosphorylation offers a dynamic way of regulating protein-protein interactions[177,178]. Phosphorylation of an amino acid residue within the binding interface can directly change the affinity of its binding as is in the case of binding of PP1 to the SLiM RVS/TF[129]. In addition, phosphorylation of amino acid residues

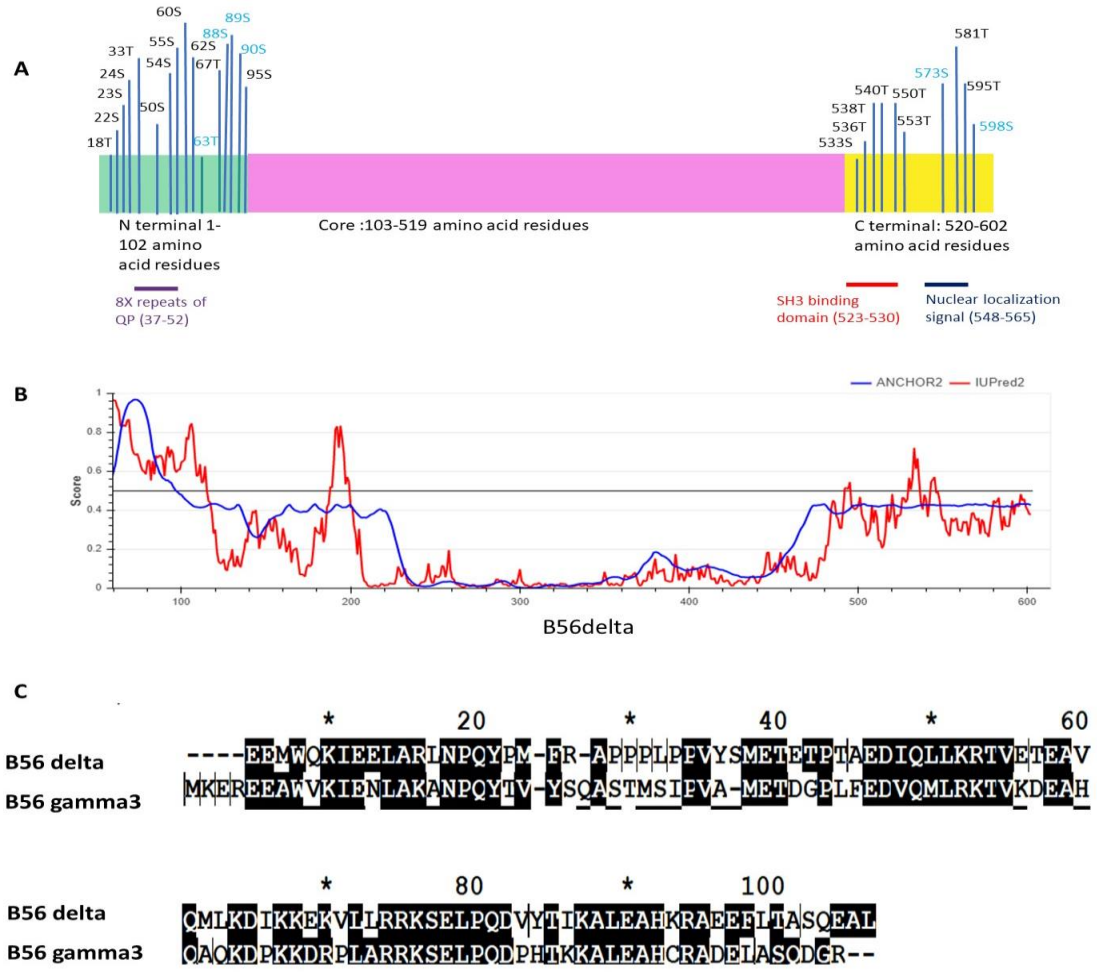

Figure 3.14: Analysis of the amino acid sequence of B56 delta. (A) In addition to the core region of approximately 400 amino acids, shown in pink, B56 delta has an N terminal region, amino acids 1-102, shown in cyan green and a C terminal region, amino acids 520-602, represented in yellow. The possible S/T phosphorylation sites on the N and C terminal are mapped. The sites labelled in blue are the ones that have been validated by individual, low throughput studies to be phosphorylated. The sites labelled in black are the predicted phosphorylation sites or sites reported to be phosphorylated by high throughput studies. All data were retrieved from Phosphosite Plus. (B) Disorder tendency of various segments of B56 delta. In red are the IUPRED2 disorder scores and in blue are the ANCHOR scores. (C) Sequence alignment of the C terminal region of human B56 delta and human B56 gamma3. Sequences were aligned using Multalin and Genedoc. Amino acid identity is marked by white on black boxes.

outside of the binding interface can cause conformational changes to the binding interface through various mechanisms. It can promote long-range conformational changes through allosteric changes, facilitate activation of the protein by releasing it from autoinhibition, or induce disorder-to-order transitions in intrinsically disordered regions[179]. I next mapped out the reported and predicted phosphorylation sites in the N terminal and the C terminal regions of B56 delta (Figure 3.14A). The data were retrieved from the Phosphosite Plus[180]. PKA has been reported to mediate the phosphorylation of 573S in B56 delta[181]. This site is also conserved in B56 gamma3. B56 delta pS573 has been reported to be overexpressed in pathological cardiac hypertrophy[181]. Another interesting phosphorylation site is 598S on B56 delta which is also conserved on B56 gamma3 (Figure 3.14A). Previous studies have reported this site to be phosphorylated in response to UV-induced DNA damage[182,183]. Interestingly, the N terminal region of B56 delta is more intrinsically disordered and has more mapped phosphorylation sites (Figure 3.14A, B). Since in the peptide pull-down assay (Figure 3.11, 3.12), B56 delta and B56 gamma3 both show a preference of binding to dephosphorylated peptides, and the C terminal region and not the N terminal region is fairly conserved between the two proteins (Figure 3.14C), I anticipated that the C terminal of these proteins might be responsible for promoting this outcome.

3.5: When C terminal region is truncated, the preference of B56 delta for dephosphorylated peptides changes

To test this hypothesis, I first proceeded to clone, express and purify recombinant full-length protein (B56 delta^{FL}) and a C terminal truncated mutant protein (B56 delta$^{\Delta 520-}$

^{602}). Initially we attempted to clone B56 delta^{FL} using the Gateway cloning system. B56 delta^{FL} was cloned upstream of two C terminal tags, His6X and V5 in pDEST42 vector as described in section 2.4. Protein expression was induced at low temperature and recombinant protein was purified using Ni-NTA affinity chromatography. Purified protein was resolved on SDS PAGE and analyzed by Coomassie blue staining. Two major bands just above the 66 kDa and 25 kDa markers, and a few minor bands were observed (Figure 3.15A). Immunoblotting with anti V5 and anti B56 delta antibodies detected two major bands, one at 72 kDa (expected molecular weight) and the other slightly lower than 45 kDa (Figure 3.15B) suggesting that along with the full-length B56 delta, a degraded or proteolytically cleaved variant of the protein was also getting purified. Since the degraded protein was also detected in the western blot using anti V5 antibody, it was speculated that the degradation is likely occurring from the N terminus of the protein. It is interesting to note that the major bands detected by Coomassie blue staining do not correspond to the bands detected by western blotting, suggesting that other proteins are being co-purified with B56 delta^{FL} during affinity chromatography. These could be bacterial proteins either rich in histidine residues or having surface exposed histidine clusters[184]. I also noticed that the whole cell lysate and the clarified supernatant do not show notable overexpression of the protein (Figure 3.15). To increase the level of recombinant protein expression, 3% ethanol and 2% glycerol were added to the growth media as suggested by a previous study[185]. However, this modification in protocol did not lead to any substantial increase in protein expression (Figure 3.16 A). One of the major challenges of expressing eukaryotic proteins in bacterial cells is the

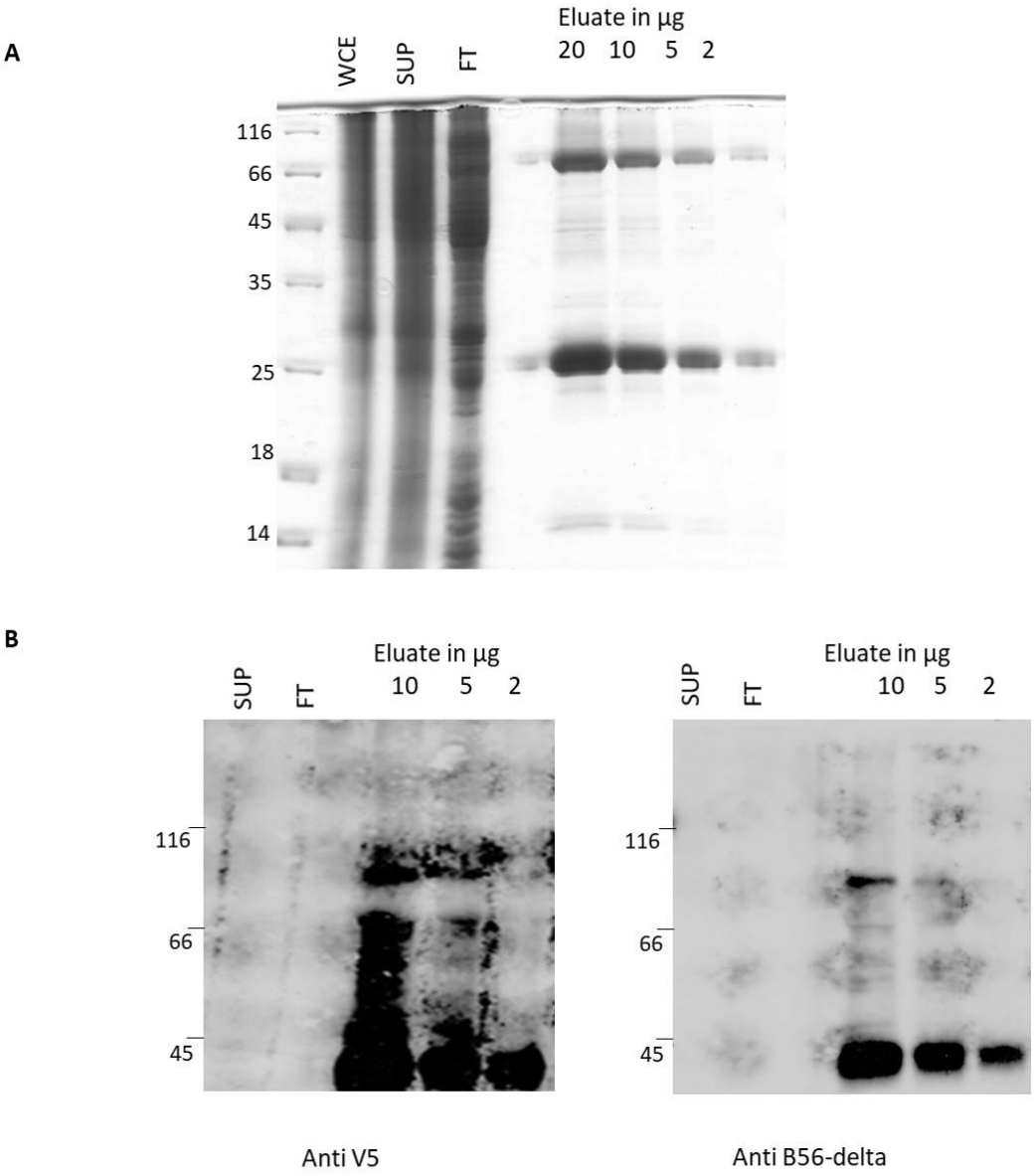

Figure 3.15: Purification of B56 delta^{FL} using Ni-NTA affinity chromatography. (A) Expression and purification of recombinant B56 delta^{FL} from Arctic Express DE3 cells. Recombinant proteins were purified using Ni-NTA affinity chromatography. Coomassie blue stained gel where WCE refers to whole cell extracts, SUP refers to supernatant after lysis and clarification, FT refers to flow-through from the Ni-NTA column. Molecular weight standards are shown on the left (B) Analysis of the samples by western blotting using anti V5 (left panel) and anti B56 delta (right panel) antibodies. Molecular weight standards are shown on the left in kDa. All experiments were done in triplicate. Representative western blots are shown here.

inability of these recombinant proteins to fold properly and exist in their native conformation. Misfolded proteins are more prone to degradation than properly folded proteins[186,187]. Improper folding of over-expressed proteins has often been attributed to limited concentration of chaperones in the cell. Studies show co-expression of recombinant proteins with chaperones, particularly heat shock chaperones, can improve protein folding. I next co-expressed B56 delta^{FL} with GroES chaperones in *E. coli* BL21 DE3 cells at low temperature and purified the recombinant B56 delta^{FL} using Ni-NTA affinity chromatography as described in section 2.4. However, I did not observe much improvement over previous purification procedures (Figure 3.16 B). Since use of these different approaches did not prevent degradation, I proceeded to further purify the full-length B56 delta from its degraded product, using size exclusion chromatography as described in section 2.4. Even though the full-length B56 delta could be successfully separated from its degraded product, the yield of the final product was very low (Figure 3.17).

Using a classical cloning approach as described in section 2.8, B56 delta^{FL} and B56 delta$^{\Delta 520-602}$ were cloned in pMAL- C2X, upstream of an MBP-tag. Protein expression was induced at low temperature and the recombinant protein was purified using amylose resin as described in section 2.4. Purified protein was resolved on SDS PAGE and analyzed by Coomassie blue staining (Figure 3.18 A, B). In addition to bands of expected molecular weight (112 kDa for B56 delta^{FL} and 102 kDa for B56 delta$^{\Delta 520-602}$), several bands of lower molecular weight were also observed, suggesting the presence of degradation products. To further purify the recombinant proteins, cation exchange

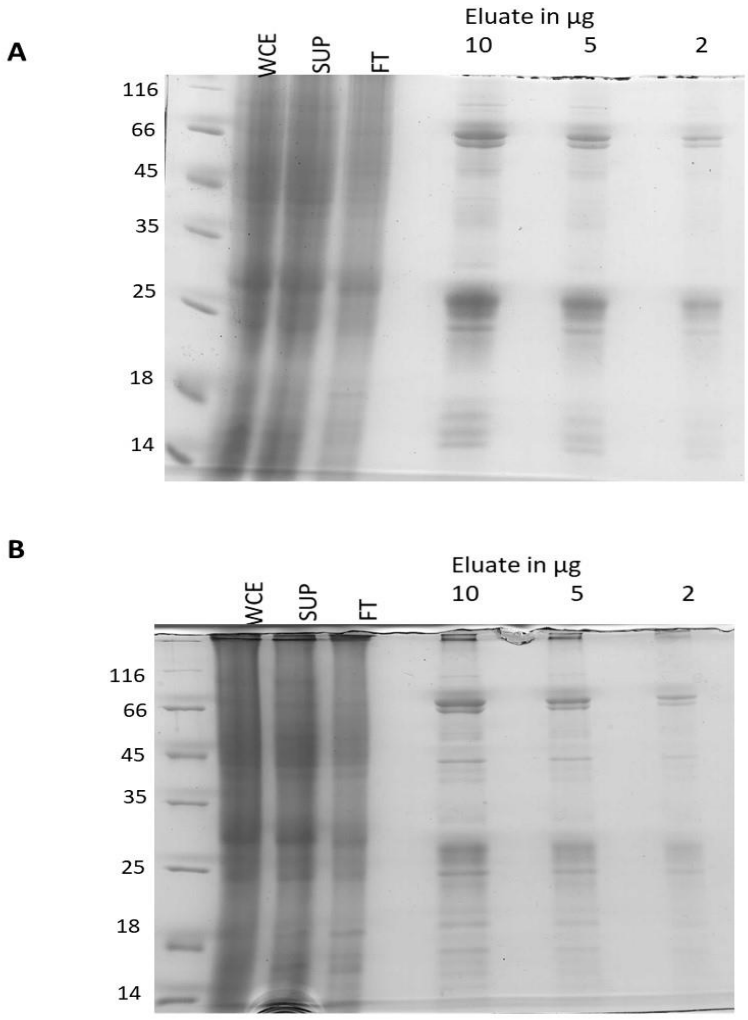

Figure 3.16: Purification of B56 delta^{FL} under different conditions using Ni-NTA affinity chromatography. (A) Expression and purification of recombinant B56 delta^{FL} from Arctic Express DE3 cells grown in presence of 3% ethanol and 2% glycerol. Recombinant proteins were purified using Ni-NTA affinity chromatography. Coomassie blue stained gel where WCE refers to whole cell extracts, SUP refers to supernatant after lysis and clarification, FT refers to flow-through from the Ni-NTA column. (B) Expression of recombinant B56 delta^{FL} in Arctic Express DE3 cells in presence of GroES chaperone. Recombinant proteins were purified using Ni-NTA affinity chromatography. Coomassie blue stained gel where WCE refers to un-lysed whole cell extracts, SUP refers to supernatant after lysis and clarification, FT refers to flow-through from the Ni-NTA column. Molecular weight standards are indicated on the left in kDa.

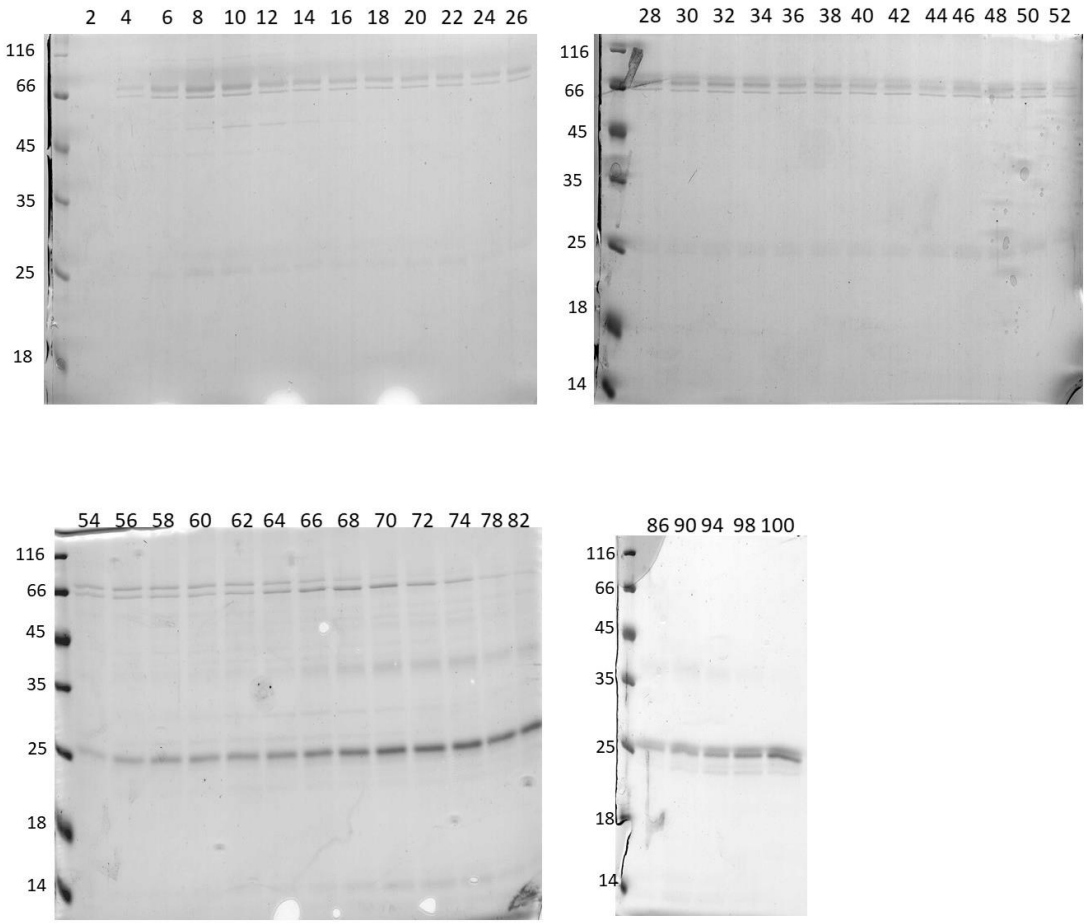

Figure 3.17: Purification of B56 delta^{FL} using size exclusion chromatography following affinity chromatography. Following purification using Ni-NTA affinity chromatography, B56 delta^{FL} was purified using size exclusion chromatography (Superdex 200 column). A total of 110 fractions, each of 1 mL volume was collected and analyzed by resolving on SDS PAGE and Coomassie blue staining. Molecular weight standards are indicated on the left in kDa. The numbers above the gel lanes indicate the number of the fraction loaded in that particular lane. Larger proteins were eluted first followed by smaller proteins, resulting in a separation between the full-length protein and its degraded product.

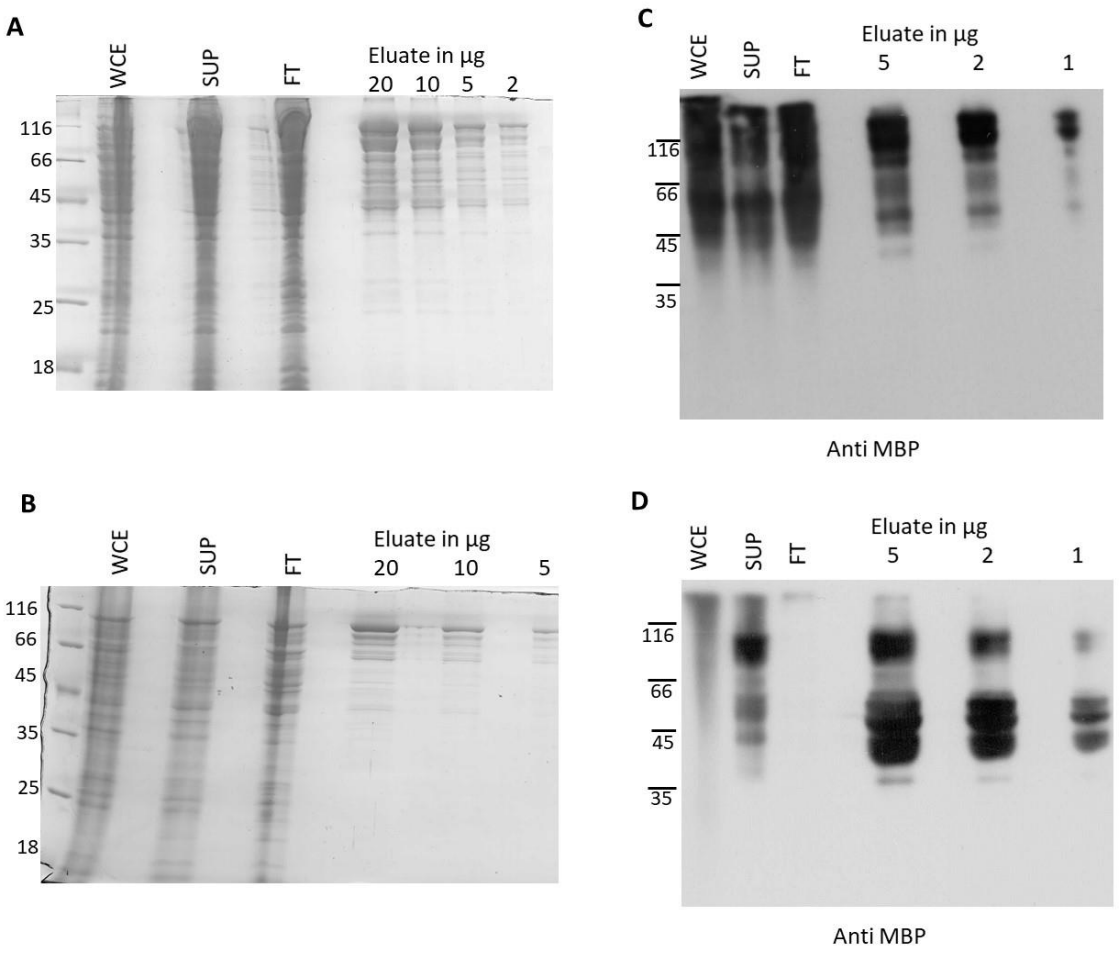

Figure 3.18: Purification of MBP-tagged B56 delta^{FL} and B56 delta$^{\Delta 520\text{-}602}$.
Expression and purification of recombinant B56 delta^{FL} (panel A) and B56 delta$^{\Delta 520\text{-}602}$(panel B). Recombinant proteins were purified using amylose resin. Samples were resolved on SDS PAGE and analyzed by Coomassie blue staining. WCE refers to un-lysed whole cell extracts, SUP refers to supernatant after lysis and clarification, FT refers to flow-through from the amylose column. (C,D) WCE, FT, SUP and eluted protein (panel C B56 delta^{FL}, panel D B56 delta$^{\Delta 520\text{-}602}$) were analyzed by western blotting with anti MBP antibody. Molecular weight standards are indicated on the left in kDa. All experiments were done in triplicate. Representative western blots are shown here.

chromatography was used as described in section 2.8. It is interesting to note that when I tried to clone, express and purify full length recombinant His tagged B56 alpha and B56 gamma1$^{30\text{-}380}$, I did not observe co-purification of any degraded protein (Figure 3.19). Since these isoforms share the core 400 amino acids (Figure 1.4), and since B56 delta^{FL} and B56 delta$^{\Delta 520\text{-}602}$ both show excessive degradation while purification, it can be speculated that the N terminal of B56 delta is contributing to this outcome.

To test if B56 delta^{FL} and B56 delta$^{\Delta 520\text{-}602}$ bound differentially to LS/TPI/V peptides, a peptide array overlay experiment was performed. Phosphorylated and non-phosphorylated LS/TPI/V peptides (listed in Table 2.1) were spotted on a nitrocellulose membrane. The membrane was blocked and then incubated with recombinant B56 delta^{FL} or B56 delta$^{\Delta 520\text{-}602}$ or the absence of any protein. The membranes were then immunoblotted with anti MBP antibody. Consistent with our previous results, B56delta^{FL} showed preference for binding to non-phosphorylated peptides (Figure 3.20). However, B56 delta$^{\Delta 520\text{-}602}$ was found to bind both phosphorylated and non-phosphorylated peptides (Figure 3.20).

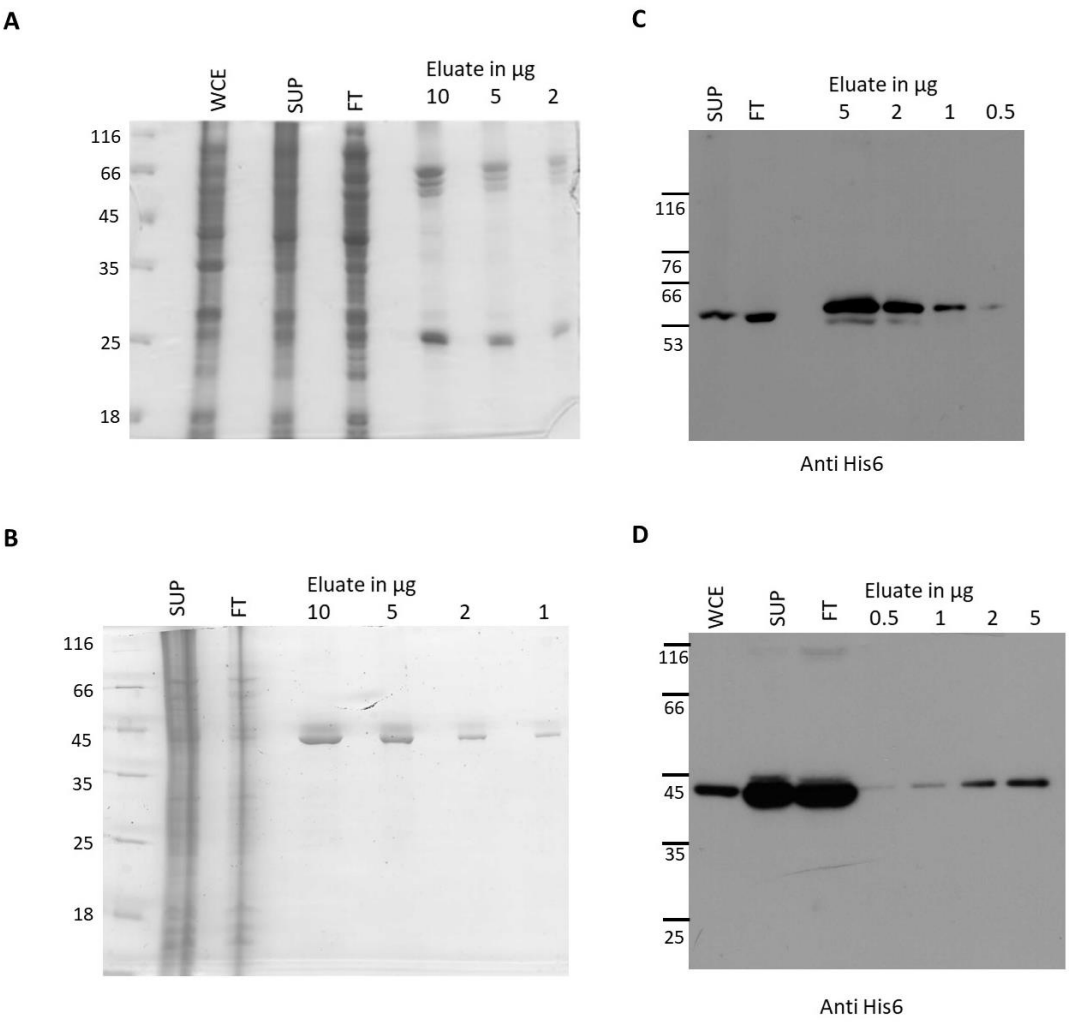

Figure 3.19: Purification of B56 alpha (panel A,C) and B56 gamma1$^{30\text{-}380}$ (panel B,D). Expression and purification of recombinant B56 alpha (panel A) and B56 gamma1$^{30\text{-}380}$ (panel B). Recombinant proteins were purified using Ni-NTA affinity chromatography. Samples were resolved on SDS PAGE and analyzed by Coomassie blue staining. WCE refers to un-lysed whole cell extracts, SUP refers to supernatant after lysis and clarification, FT refers to flow-through from the Ni-NTA column. (C,D) WCE, FT, SUP and eluted protein (panel C B56 alpha, panel D B56 gamma1$^{30\text{-}380}$) were analyzed by western blotting using anti His6 antibody. Molecular weight standards are indicated on the left in kDa.

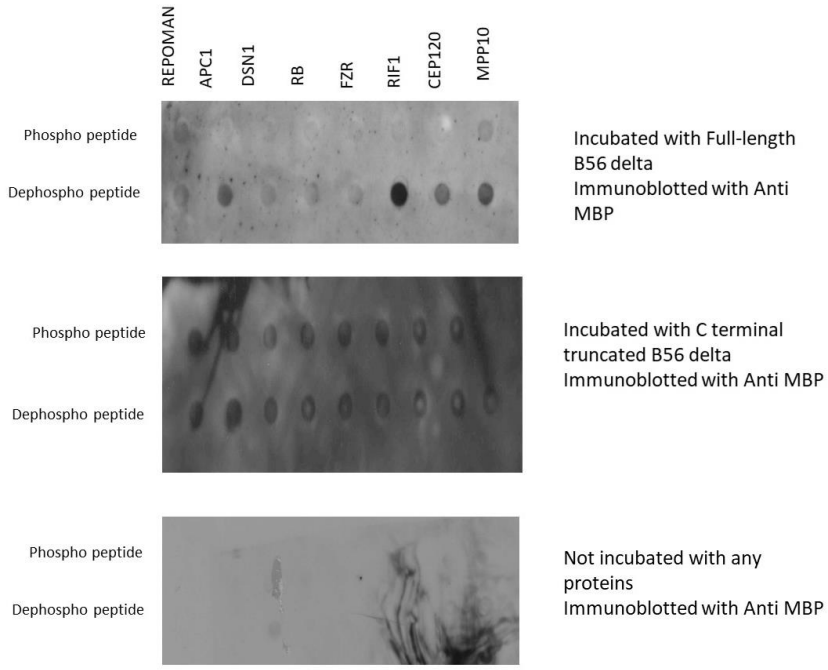

Figure 3.20: B56 delta^{FL} and B56 delta$^{\Delta 520\text{-}602}$ have different preference for binding to LS/TPI/V peptides. Phosphorylated and dephosphorylated LS/TPI/V peptides (sequences listed in Table 2.1) were spotted on a nitrocellulose membrane. Following blocking, the membranes were incubated in presence of MBP-tagged B56 delta^{FL} and B56 delta$^{\Delta 520\text{-}602}$ proteins, or in the absence of any protein (negative control) and then immunoblotted with anti MBP antibody. All experiments were performed in triplicate. Representative blots are shown here.

3.6: LS/TPI/V motifs are phosphorylated during mitosis

The findings from the peptide pull down assay (Figure 3.11, 3.12) and the peptide overlay assay (Figure 3.20) suggest that the interaction of B56 delta with the LS/TPI/V peptides is phosphorylation-dependent. The LS/TPI/V proteins chosen for this study are involved in cell cycle signaling. PP2A-B56 is an important mitotic protein phosphatase. Since mitosis and progression through cell cycle is tightly regulated by reversible protein phosphorylation, I wanted to investigate if the LS/TPI/V proteins are phosphorylated on this motif in a cell cycle-dependent manner. To study this, phospho-specific antibodies against some of the chosen LS/TPI/V protein targets such as Repoman pS597, APC1 pS555, Cep120 pT368, DSN1 pS30 and iASPP pS567 were raised in-house as described in section 2.5. The predicted molecular weights of the whole proteins are listed in Table 3.3.

Before immunization of the rabbits with phospho-peptide coupled to carrier proteins, the animals were pre-screened for the presence of endogenous antibodies. Pre-immune serum (serum prior to injection of antigens) was collected at an interval of 7 days and was used for immunoblotting asynchronous and mitotic HeLa cell lysate. No prominent bands were detected by pre-immune sera for anti Repoman pS597, anti APC1 pS555, anti Cep120 pT368 and anti DSN1 pS30 (Figure 3.21 panel A, B, D, and E). Pre-immune sera from the animal used for raising anti iASPP pS567 showed some reactivity against HeLa cell extracts (Figure 3.21, panel C). For generating an immune response, the rabbits were injected with BSA and KLH conjugated phosphorylated peptides as described in section 2.5. Briefly, the rabbit was given one primary injection followed by

Table 3.3: Predicted molecular weights of chosen LS/TPI/V proteins

The predicted molecular weights of the LS/TPI/V proteins chosen for phospho-specific antibody production are listed below.

Protein name	*Uniprot ID*	*Gene name*	*Predicted molecular weight (in kDa)*
Repoman	Q69YH5	CDCA2	112.6
APC1	Q9H1A4	ANAPC1	216.5
iASPP	Q8WUF5	PPP1R13L	89
Cep120	Q8N960	CEP120	112.6
DSN1	Q9H410	DSN1	40

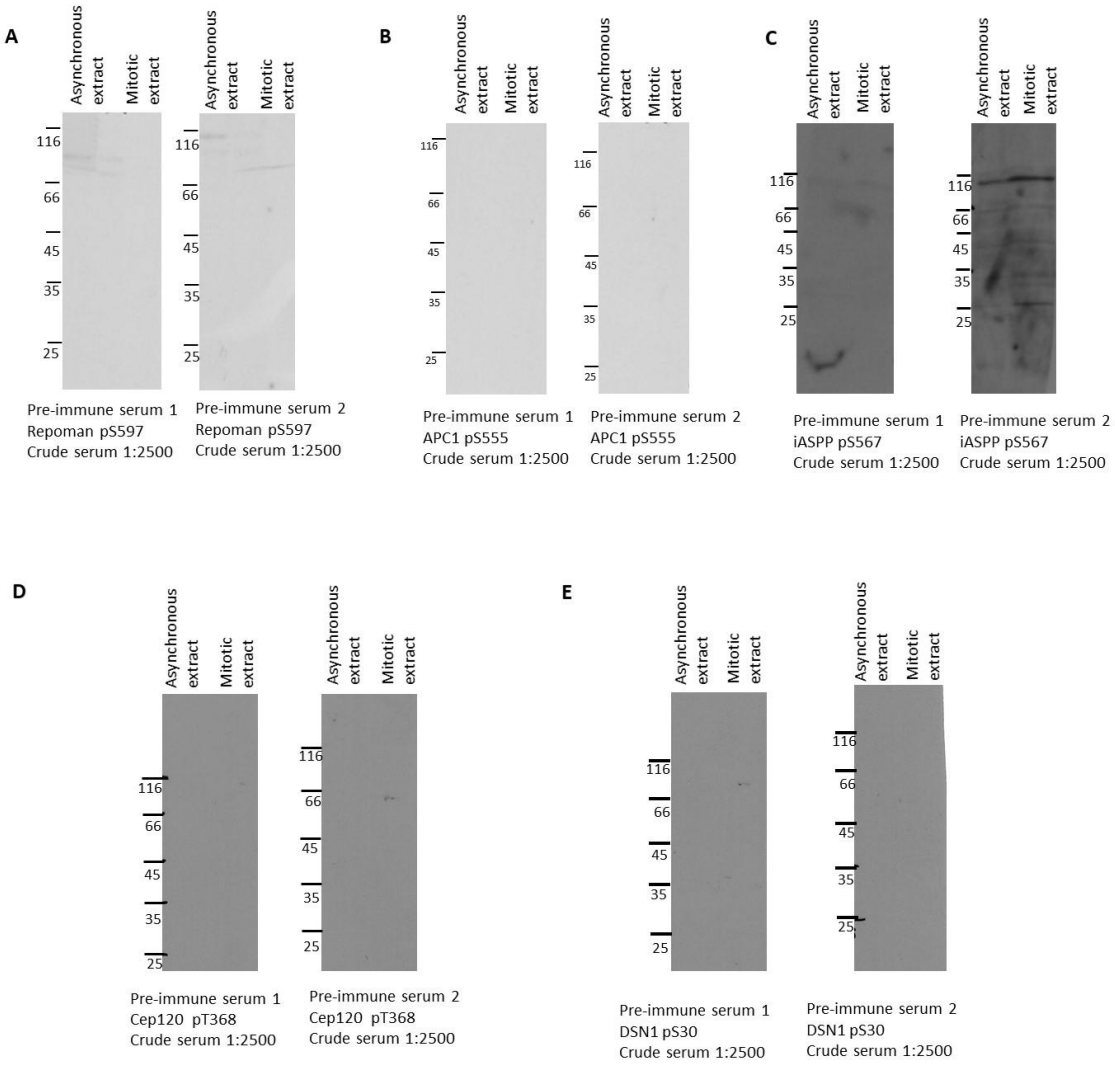

Figure 3.21: Testing of pre-immune serum from the rabbits. Rabbits were pre-screened before immunization for the presence of endogenous antibodies. 20 µg of asynchronous and mitotic HeLa cell extracts were resolved on a SDS PAGE and transferred on nitrocellulose membrane and immunoblotted with pre-immune serum from the rabbits. Pre-immune serum was collected at an interval of 7 days from each rabbit and used at a dilution of 1:2500 for immunoblotting. Molecular weight standards are shown on the left in kDa. All experiments were done in triplicate. Representative western blots are shown here.

three booster doses. Serum was collected from the rabbit after each booster injection (as described in section 2. 5) and tested for reactivity to HeLa cell extracts. The first, second and third bleeds (crude serum) showed more reactivity to HeLa cell extracts than the pre-immune serum. However, in most cases, the crude serum was unable to detect a band of the predicted size. Representative western blots are shown in Figure 3.22.

Phospho specific antibodies were purified using affinity chromatography as described in section 2.5. To validate the sensitivity and specificity of the purified antibodies, dot-blots were used as described in section 2.6. Anti Repoman pS597 and anti Cep120 pT368 used at a dilution of 1 µg/mL, could recognize as little as 1 ng of the corresponding phosphorylated peptide, but failed to recognize up to 1000 ng of the corresponding dephosphorylated peptide (Figure 3.23). Anti APC1 pS555 was less sensitive. Used at a dilution of 5 µg/mL, anti APC1 pS555 could only recognize as little as 10 ng of the corresponding phosphorylated peptide (Figure 3.23). Anti DSN1 pS30 when used at a dilution of 1 µg/mL recognized as little as 10 ng of the corresponding phosphorylated peptide (Figure 3.23). None of the antibodies showed affinity to the control peptides (phosphorylated and dephosphorylated RVSF). When the antibodies (anti Repoman pS597, anti APC1 pS555, anti Cep120 pT368 and anti DSN1 pS30) were used in presence of the corresponding phosphorylated peptides, the signal was completed abolished (Figure 3.23). Anti iASPP pS567 did not recognize any of the spotted peptides (data not shown). To further test the specificity of these antibodies, asynchronous and mitotic HeLa cell lysates were collected in presence or absence of phosphatase inhibitors as described in section 2.9. The proteins present in the cell extract were resolved on SDS

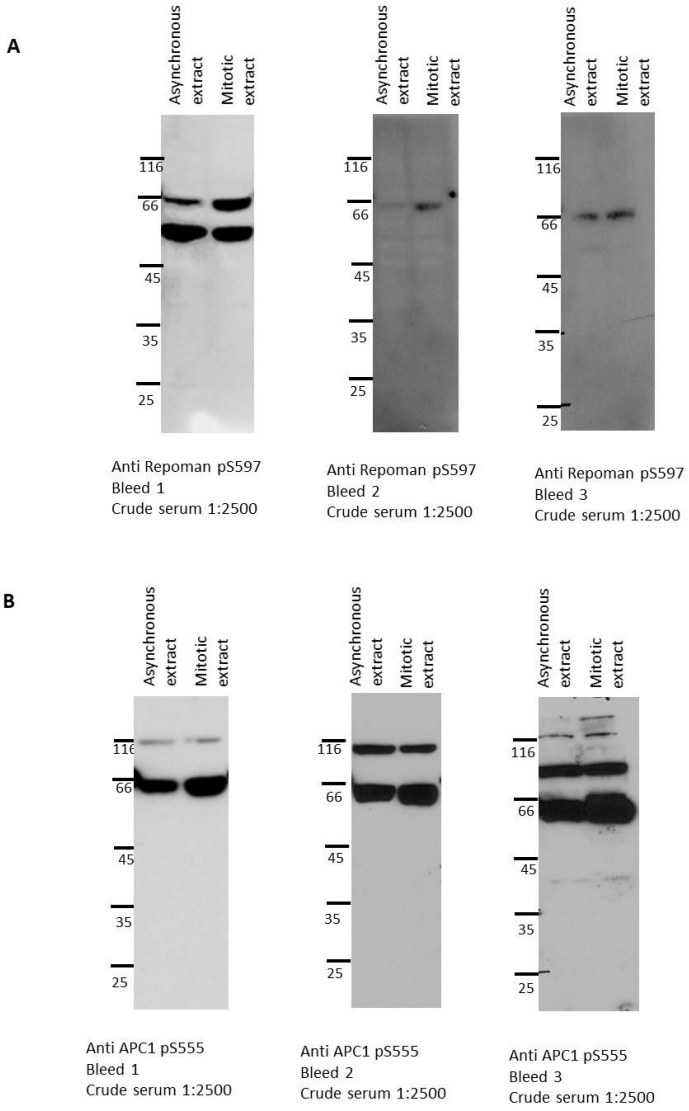

Figure 3.22: Testing the reactivity of first, second and third bleeds collected during phospho specific antibody generation. During generation of phospho specific antibodies, each booster immunization dose was followed by collection of a serum sample, 12 days post infection and has been referred to as a bleed. Asynchronous and mitotic HeLa cell lysate (20 µg) were resolved on SDS PAGE and transferred on to a nitrocellulose membrane and immunoblotted with crude serum (1:2500 dilution). Representative blots are shown. (A) Testing bleed 1, bleed 2 and bleed 3 for anti Repoman pS597. (B) Testing bleed 1, bleed 2, and bleed 3 for APC1 pS555. Molecular weight standards are shown on the left in kDa. All experiments were done in triplicate. Representative western blots are shown here.

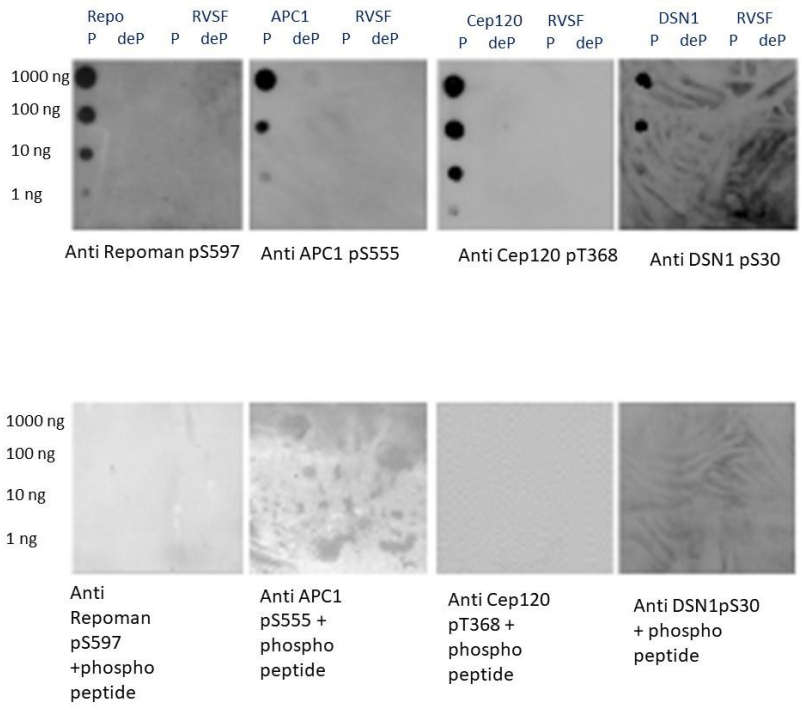

Figure 3.23: Affinity purified phospho-specific antibodies raised in house are specific to the phospho-peptide antigen used. Various amounts (1 ng to 1000 ng as indicated) of phosphorylated (P) and dephosphorylated (deP) peptides were spotted on a membrane, incubated in presence of the corresponding affinity purified antibody (top panel) or in presence of the affinity purified antibody and the corresponding phospho-peptide (bottom panel) and the dot blot assay was performed as described in section 2.6. RVSF peptides (phosphorylated and dephosphorylated) were used as negative control in all cases. Peptide sequences are listed in Table 2.1. All experiments were done in triplicate. Representative blots are shown here.

PAGE and immunoblotted. Anti Repoman pS597, anti APC1 pS555, anti Cep120 pT368 antibodies detected a band of the predicted size (Table 3.3) (Figure 3.24). Anti DSN1 pS30 detected a band much higher than predicted size (Table 3.3) (Figure 3.24). Mitotic lysates collected in presence of phosphatase inhibitors show higher levels of protein phosphorylation than those collected in absence of phosphatase inhibitors. Asynchronous cell lysates show little or no phosphorylation. The low levels of phosphorylation of APC1 pS555 observed in asynchronously growing cells is likely due to the small percentage of mitotic cells in this population. Following validation, the phospho-specific antibodies were used to monitor the phosphorylation status of the LS/TPI/V motif present in Repoman, APC1 and Cep120 during cell cycle. Anti DSN1 pS30 was not used further in this study as it is most likely detecting a non-specific protein.

HeLa cells were arrested in mitosis using a thymidine/nocodazole block and then released into fresh media and allowed to progress through the cell cycle as described in section 2.10. Cells were collected at various time points over the following 22 hours. Time point 0 represents an untreated asynchronous cell population, cells collected between 0.5 hour to 2 hour represent cells in mitosis, 3 hour to 11 hour represent cells in G1 and 12 hour to 20 hour represents S phase. The 22 hour sample represents late G2 and the onset of the next mitotic cycle. Increased phosphorylation of Repoman pS597, APC1 pS555 and Cep120 pT368 during mitosis when compared to other stages of the cell cycle (Figure 3.25). The protein levels however, remained constant throughout the cell cycle (Figure 3.25). Levels of cyclin proteins, Cyclin B and Cyclin E were found to vary dynamically and appropriately as predicted by previous studies[188]. Histone3 is

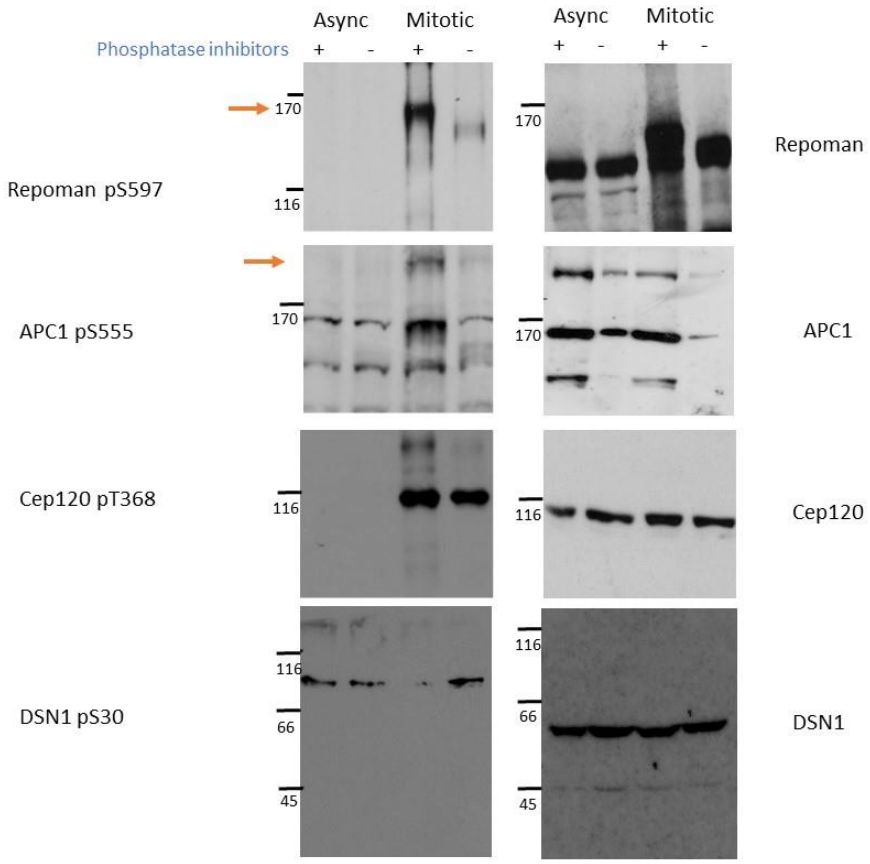

Figure 3.24: Validation of phospho-specific antibodies by western blotting of asynchronous and mitotic lysates. Asynchronous and mitotic Hela cell lysates were collected in presence and absence of phosphatase inhibitors and were resolved on SDS PAGE (20 µg of each extract) and transferred to a nitrocellulose membrane. Immunoblotting was performed with in house raised and affinity purified phospho-specific antibodies and the corresponding commercial antibodies. Arrows point to the protein of interest. Molecular weight standards are shown on the left in kDa. All experiments are done in triplicate. Representative blots are shown here.

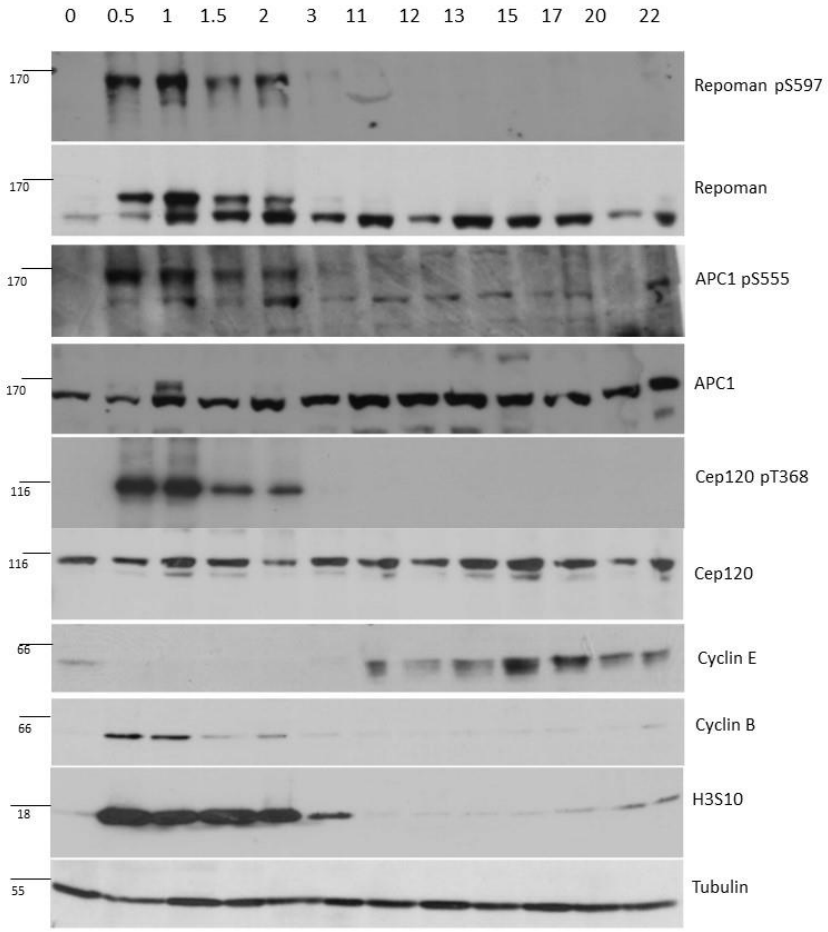

Figure 3.25: LS/TPI/V motif is phosphorylated during mitosis. HeLa cells were synchronized using thymidine/nocodazole block. Cell lysates were collected over a 22-hour period. Numbers at the top indicate time of release from nocodazole block. Asynchronous sample is represented by time point 0. Time points 0.5 hour to 2 hour represent mitosis. 3 hour to 11 hour samples represent cells in G1 phase, 12 hour to 20 hour samples represents cells in S phase. At 22 hour, cells start getting back in mitosis. The cell lysates were resolved on SDS PAGE and transferred to nitrocellulose membrane and immunoblotted with the indicated antibodies. Molecular weight standards are indicated on the left in kDa. All experiments were done in triplicate. Representative western blots are shown here.

phosphorylated on S10 residue in a cell cycle dependent manner and was used as an additional control to evaluate the efficacy of cell synchronization.

To further investigate the phosphorylation status of Repoman S597, APC1 S555, Cep120 T368, immunofluorescence assays were performed as described in section 2.13. HeLa cells were grown on coverslips and fixed in 2% paraformaldehyde and processed for microscopy as described in section 2.13. Cells stained with the phospho-specific antibody were co-stained for tubulin. Nuclei were visualized by staining with DAPI. Cells were imaged in interphase, prophase, metaphase and telophase. A minimum of five hundred cells were imaged for each phospho-specific antibody. Representative images are shown in Figure 3.26, 3.27 and 3.28. Cells in interphase showed minimal phosphorylation on Repoman S597, APC1 S555 and Cep120 T368 (Figure 3.26, 3.27 and 3.28). As cells entered prophase as evidenced by condensation of the DNA, the levels of phosphorylation were found to increase. The high level of phosphorylation was maintained throughout metaphase and anaphase. In telophase, the phosphorylation was either diminished or completely abolished (Figure 3.26, 3.27 and 3.28). No phosphorylation of APC1 pS555 and Repoman pS597 were detected in telophase. However, Repoman S597 showed some phosphorylation in the interphase (Figure 3.28). Cep120 T368 remained phosphorylated in telophase and the phosphorylation was negligible during interphase (Figure 3.27). To further investigate if the localization pattern of the whole proteins, APC1, Cep120 and Repoman were similar to that of the corresponding phosphorylated LS/TPI/V proteins, immunofluorescence assays using commercial antibodies against the whole proteins were performed. Barely any signal was

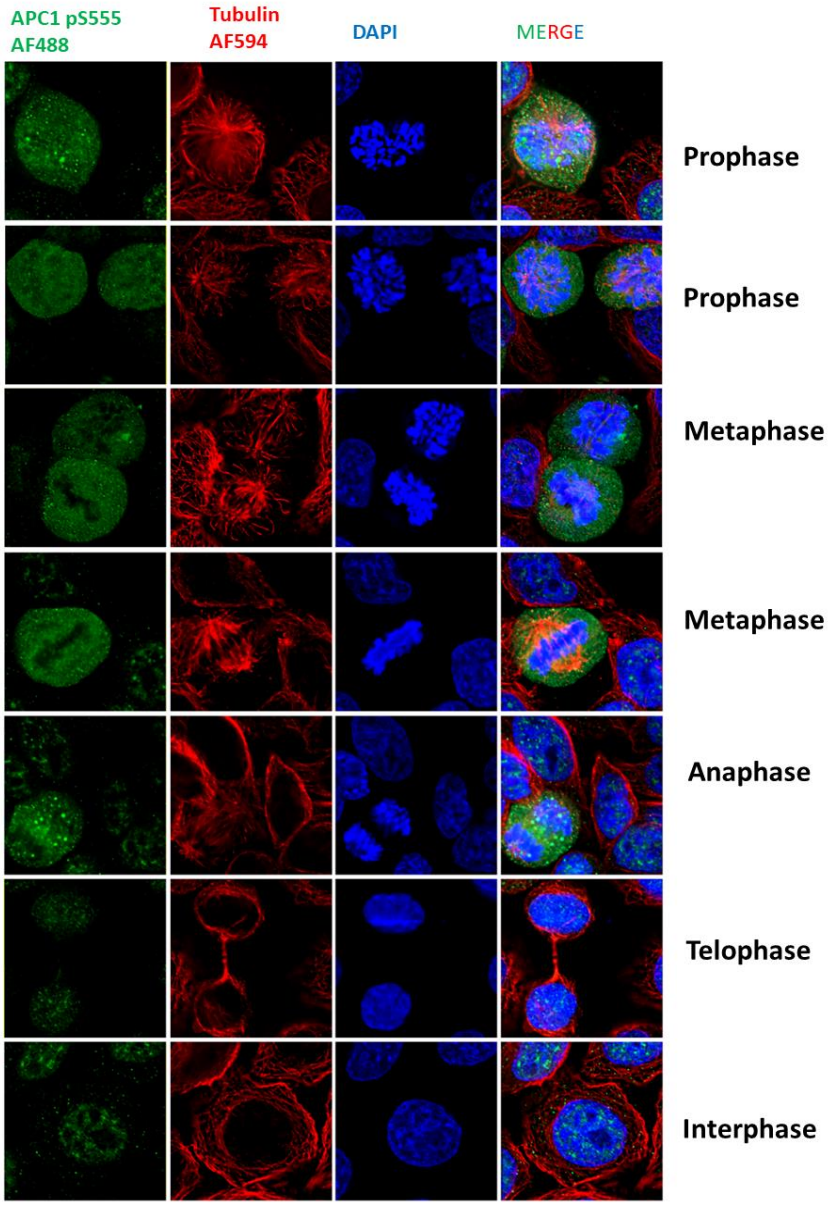

Figure 3.26: LS/TPI/V motif is phosphorylated during mitosis. Hela cells were grown on coverslips and fixed in 2% paraformaldehyde. Cells were permeabilized then stained for APC1 pS555 (AF488 or green) and tubulin (AF594 or red). Nuclei were stained with DAPI (blue). Cells were imaged using oil immersion 100X objective on a Zeiss Axio Imager Z2 microscope. 10-14 Z stacks were taken per field of view. Z stacks were reconstructed by using the extended depth of focus (wavelets) function on the Zeiss Pro Software. Reconstructed Z stack image was deconvoluted using the default parameters.

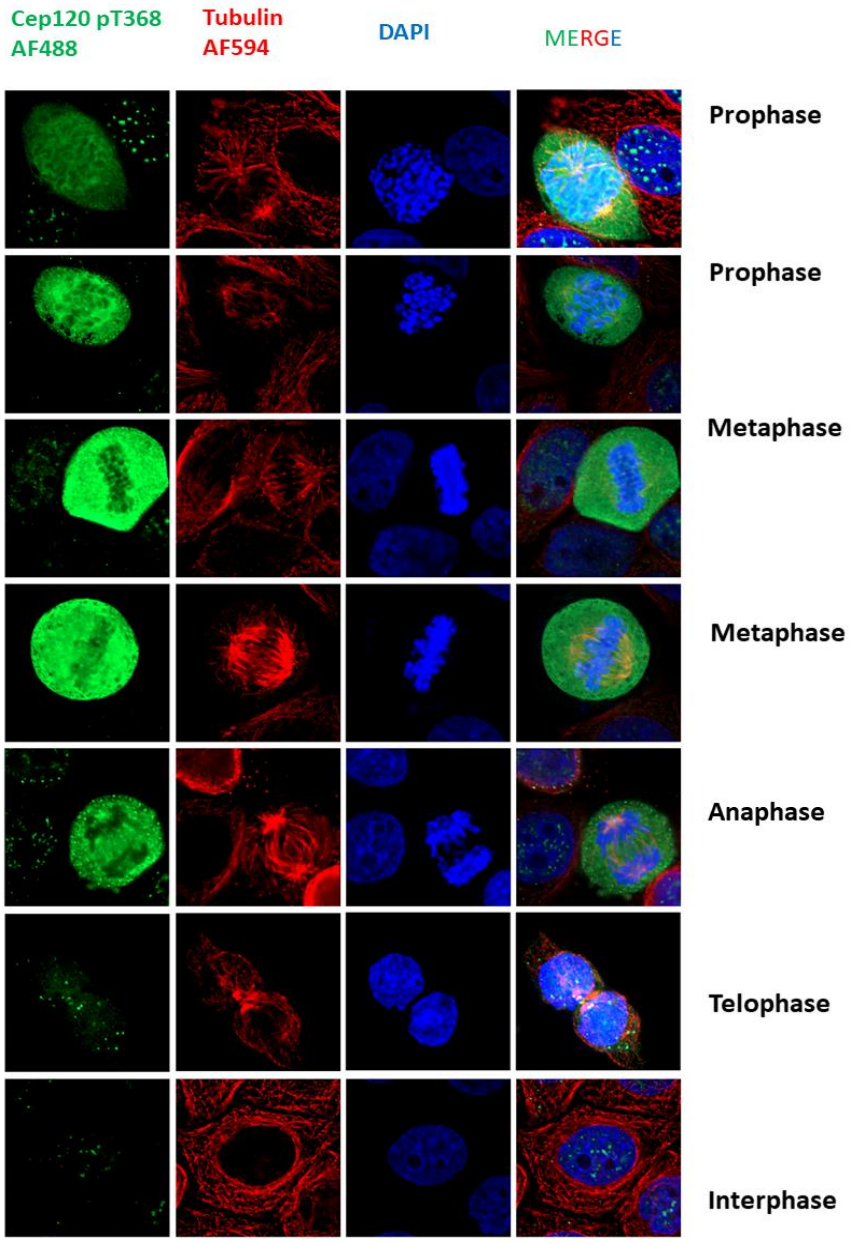

Figure 3.27: LS/TPI/V motif is phosphorylated during mitosis. Hela cells were grown on coverslips and fixed in 2% paraformaldehyde. Cells were permeabilized then stained for Cep120 pT368 (AF488 or green) and tubulin (AF594 or red). Nuclei were stained with DAPI (blue). Cells were imaged using oil immersion 100X objective on a Zeiss Axio Imager Z2 microscope. 10-14 Z stacks were taken per field of view. Z stacks were reconstructed by using the extended depth of focus (wavelets) function on the Zeiss Pro Software. Reconstructed Z stack image was deconvoluted using the default parameters.

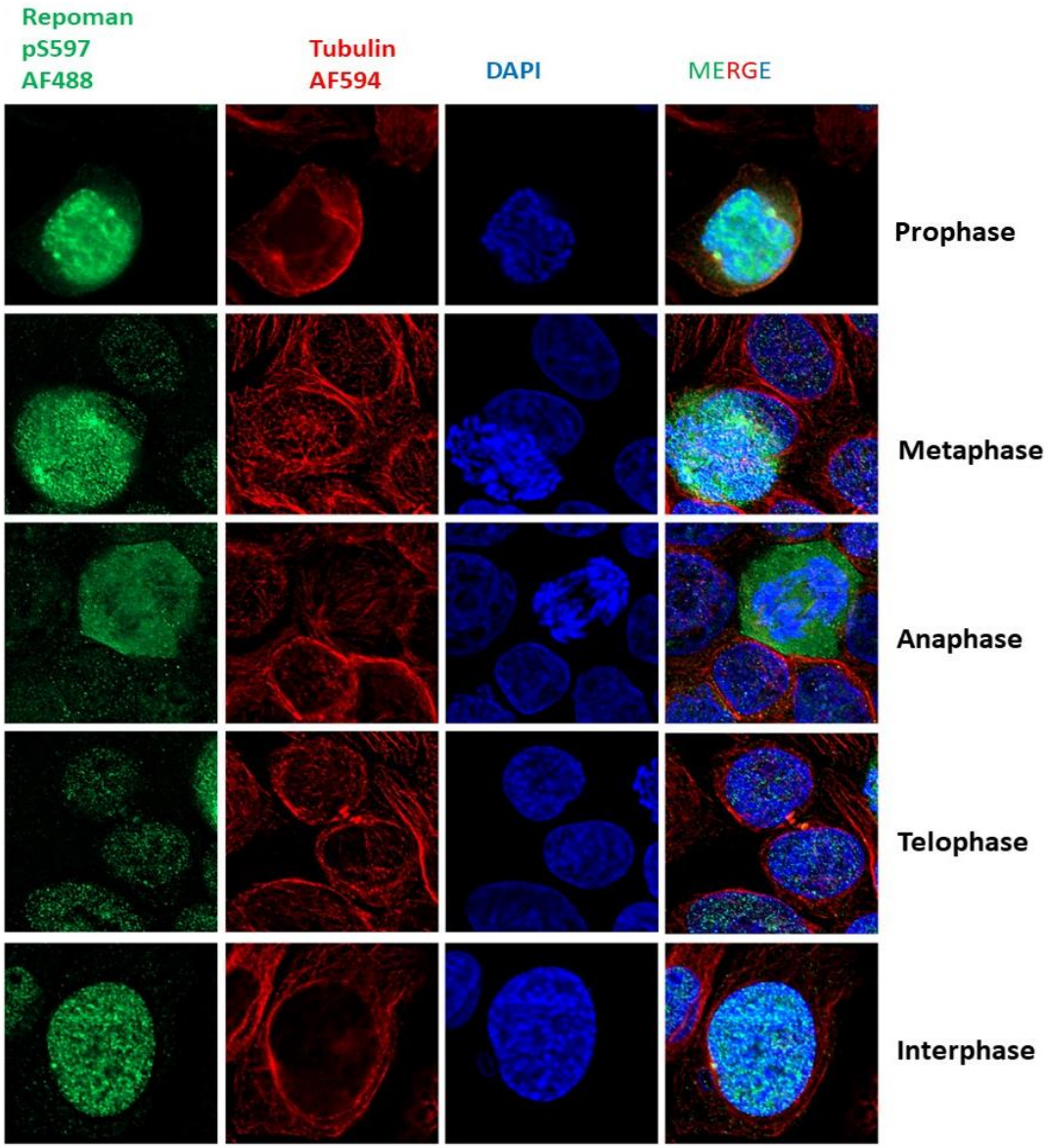

Figure 3.28: LS/TPI/V motif is phosphorylated during mitosis. Hela cells were grown on coverslips and fixed in 2% paraformaldehyde. Cells were permeabilized then stained for Repoman pS597 (AF488 or green) and tubulin (AF594 or red). Nuclei were stained with DAPI (blue). Cells were imaged using oil immersion 100X objective on a Zeiss Axio Imager Z2 microscope. 10-14 Z stacks were taken per field of view. Z stacks were reconstructed by using the extended depth of focus (wavelets) function on the Zeiss Pro Software. Reconstructed Z stack image was deconvoluted using the default parameters.

detected from anti Cep120 and anti Repoman suggesting that these antibodies are not suited for microscopy (data not shown). During interphase, APC1 is present in the cytoplasm (Figure 3.29). During prophase and metaphase, APC1 surrounds the DNA and is localized to the mitotic spindle, similar to APC1 pS555. Levels of APC1 decrease during anaphase (Figure 3.29). A probable explanation could be the global proteolysis that takes place after fulfillment of SAC to promote mitotic exit.

3.7: Aurora Kinase B controls the phosphorylation on the LS/TPI/V motifs during mitosis

Having established that the LS/TPI/V motif on Repoman, Cep120 and APC1 gets phosphorylated during mitosis (Figure 3.25, 3.26, 3.27 and 3.28), I next wanted to investigate which mitotic protein kinase is responsible for phosphorylating this motif. HeLa cells were either untreated (asynchronous) or treated with nocodazole (mitotic) as described in section 2.10 and 2.12. Wherever indicated, mitotic cells (after 15 hours of nocodazole treatment) were incubated in the presence of selective inhibitors of mitotic protein kinases –Aurora A (Aurora A Inhibitor 1, 100 nM), Aurora B (Hesperadin, 100 nM), PLK1 (BI2536, 100 nM) and CDK1 (Roscovitine, 50 μM) for 30 minutes, followed by mitotic shake off and collection of cell lysate as described in section 2.9. The cell lysates were resolved on SDS PAGE and analyzed by immunoblotting. S/TP is a well-established CDK1 recognition site[89]. However, when CDK1 was inhibited, a reduction but not abolition of phosphorylation of Repoman pS597, APC1 pS555 and Cep120 pT368 was observed (Figure 3.30). Interestingly, when Aurora B was inhibited, the phosphorylation on Repoman pS597 and APC1 pS555 were abolished and that on

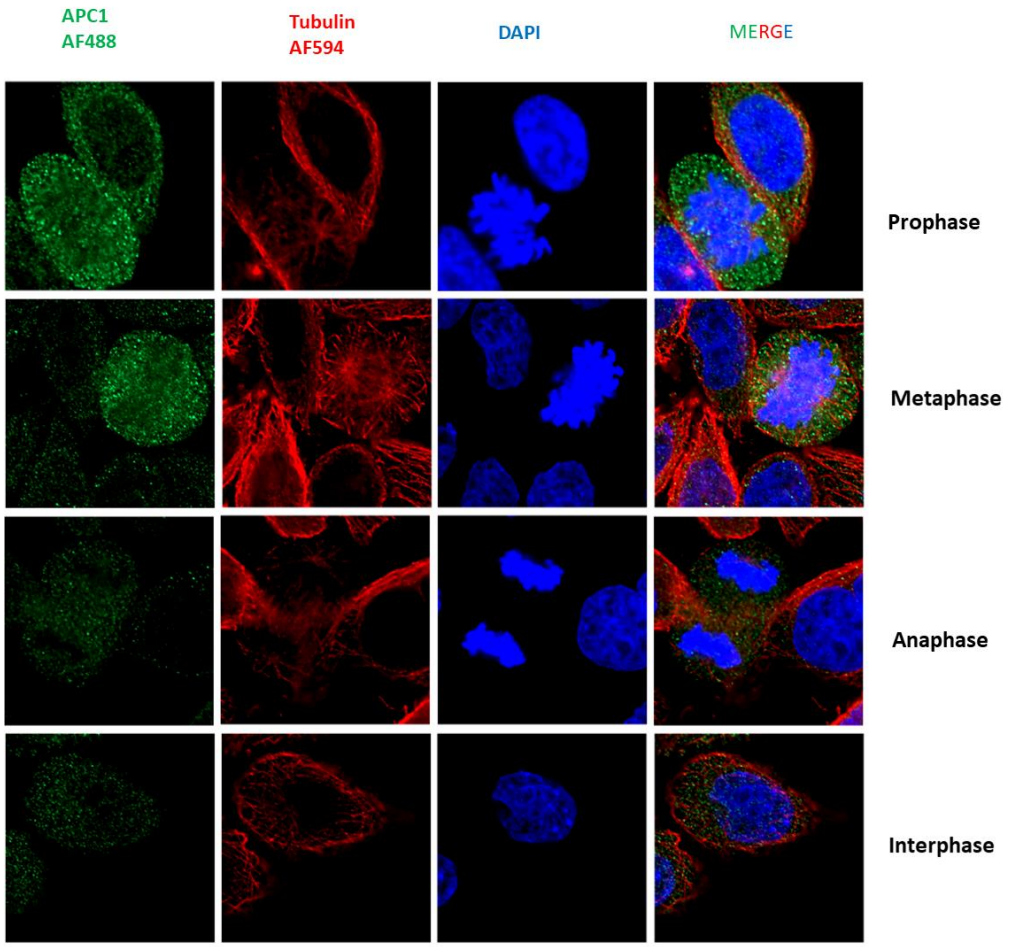

Figure 3.29: Localization of APC1 during different stages of cell cycle. Hela cells were grown on coverslips and fixed in 2% paraformaldehyde. Cells were permeabilized then stained for APC1 (AF488 or green) and tubulin (AF594 or red). Nuclei were stained with DAPI (blue). Cells were imaged using oil immersion 100X objective on a Zeiss Axio Imager Z2 microscope. 10-14 Z stacks were taken per field of view. Z stacks were reconstructed by using the extended depth of focus (wavelets) function on the Zeiss Pro Software. Reconstructed Z stack image was deconvoluted using the default parameters.

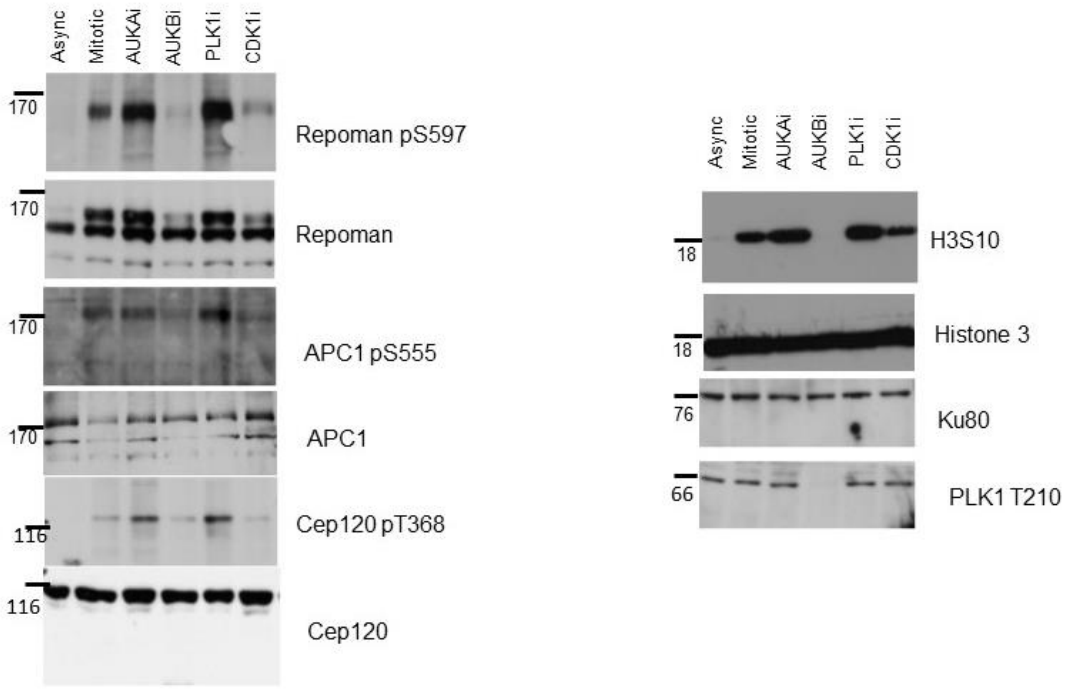

Figure 3.30: Aurora B controls the phosphorylation of LS/TPI/V motifs during mitosis. HeLa cells were synchronized in mitosis using a nocodazole block. After 15 hours of incubation, cells were treated with the indicated inhibitors. AURKAi (100 nM Aurora A Inhibitor 1), AURKBi (100 nM Hesperadin), PLKi (100 nM BI2536), CDKi (50 µM Roscovitine) were used in this assay. At 16th hour, the cells were released from nocodazole arrest into pre-warmed fresh media containing the indicated inhibitors. The cells were then collected after 30 minutes, cell lysate prepared as previously described, resolved on SDS PAGE, transferred on nitrocellulose membrane and immunoblotted using the indicated antibodies. Molecular weight markers are shown on the left in kDa. All experiments were done in triplicate. Representative western blots are shown here.

Cep120pT368 was highly reduced (Figure 3.30). Inhibition of Aurora A and PLK1 did not change the phosphorylation status of any of these sites. These results suggest that Aurora B is responsible for controlling the phosphorylation on Repoman pS597, APC1 pS555, Cep120 pT368. However, CDK1 might be also contributing to this event. To validate this further, I performed immunostaining of mitotic HeLa cells. HeLa cells, grown on coverslips were treated with nocodazole for 15 hours and then incubated in presence of kinase inhibitors (where indicated) for 30 minutes before fixing as described in section 2.12. Cells were stained for Cep120 pT368, and counterstained for tubulin. Nuclei was visualized by DAPI staining. Consistent with the immunoblotting results, immunostaining showed that mitotic cells had high levels of phosphorylation of Cep120 pT368 (Figure 3.31). Mitotic cells when treated with inhibitors of Aurora A kinase and Plk1 showed phosphorylation comparable to that of untreated cells. However, when treated with Aurora B kinase inhibitor, phosphorylation was almost abolished. When treated with CDK1 inhibitor, less cells showed formation of an intact metaphasic plate or mitotic spindle. However, in cells with intact mitotic structures, phosphorylation of Cep120 pT368 was still observed (Figure 3.31). Together these results suggest that in the signaling cascade, Aurora B might be functioning upstream of CDK1.

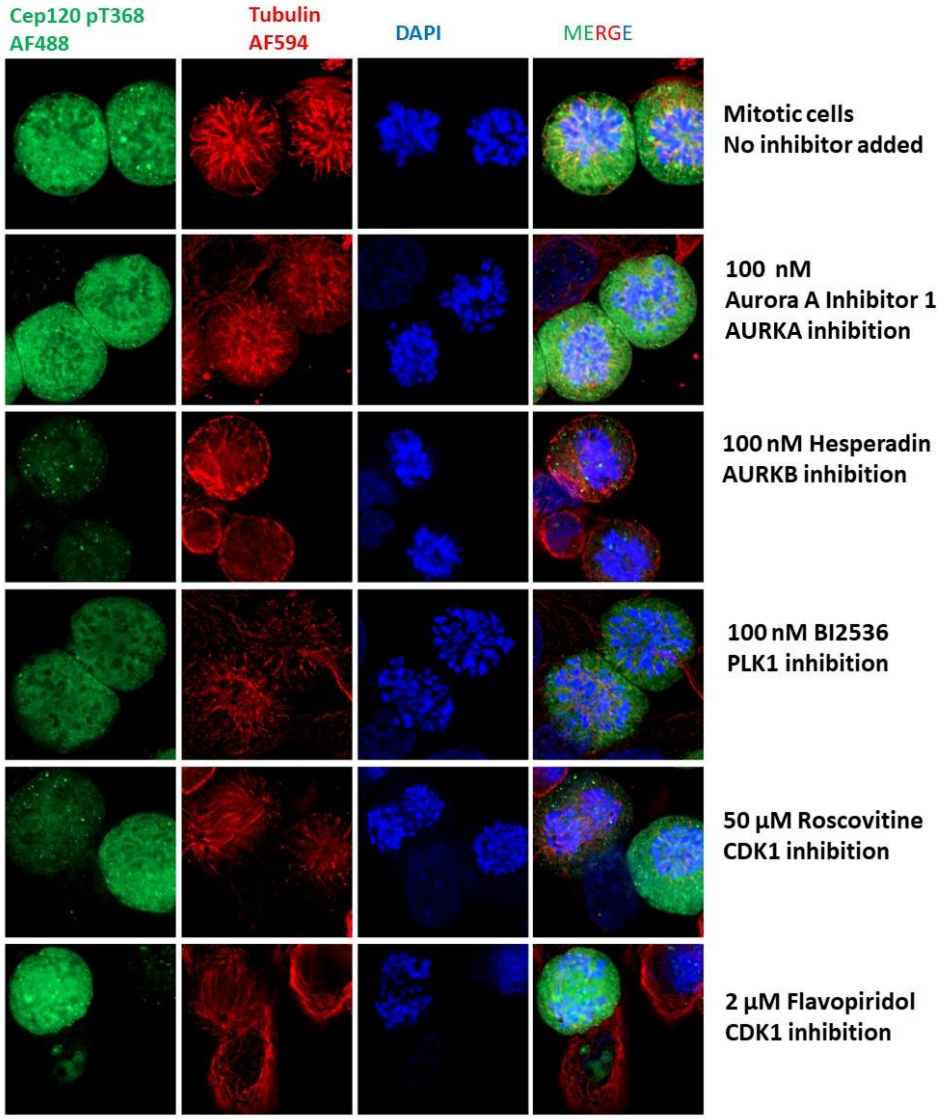

Figure 3.31: Aurora B phosphorylates Cep120 pT368. Hela cells were grown on coverslips, synchronized in mitosis by using a nocodazole block for 15 hours and then treated with the indicated inhibitors. At 16h cells were released from nocodazole into fresh media containing inhibitors. After 30 minutes of further treatment, cells were fixed in 2% paraformaldehyde. Cells were permeabilized then stained for Cep120 pT368 (AF488 or green) and tubulin (AF594 or red). Nuclei were stained with DAPI (blue). Cells were imaged using oil immersion 100X objective on a Zeiss Axio Imager Z2 microscope. 10-14 Z stacks were taken per field of view. Z stacks were reconstructed by using the extended depth of focus (wavelets) function on the Zeiss Pro Software. Reconstructed Z stack image was deconvoluted using the default parameters.

3.8. B56 delta differentially interacts with protein interactors during cell cycle

Using the peptide pull down assay (Figure 3.11, 3.12) and the peptide array overlay assay (Figure 3.20), I showed that B56 delta binds to LS/TPI/V peptides in a phosphorylation-dependent manner. I also showed that LS/TPI/V motifs are phosphorylated in a cell cycle-dependent manner (Figure 3.25, 3.26, 3.27, 3.28). Next, I wanted to investigate if in human cells, B56 delta interacted with LS/TPI/V proteins in a cell cycle-dependent manner. A stable HEK293T cell line expressing HA tagged B56 delta was created as described in section 2.11. HEK293T cells were used for their ease of transfection. The cells were arrested in mitosis by treating with 100 ng/mL of nocodazole for 16 hours and then released into fresh prewarmed media without nocodazole. Cells were collected at various time points after release and tested for the expression of HA tagged B56 delta by immunoblotting with anti HA antibody (Figure 3.32). Immunoprecipitation experiments were performed using anti HA antibody and control IgG, using asynchronous and mitotic cell lysate as described in section 2.15. Immunoblotting with specific antibodies revealed enrichment and co-purification of PP2A catalytic subunit in the IP with anti HA antibody under both asynchronous and mitotic conditions (Figure 3.33). However, LS/TPI/V motif containing proteins such as APC1, iASPP, Cep192 and Bora were not found to be retained by the immunoprecipitation (Figure 3.33). To further analyze the proteins enriched in the IP under asynchronous and mitotic conditions, mass spectrometric analysis was performed. Total spectral count, defined as the total number of spectra identified for the protein of interest, was used to semi quantitatively compare the interactors between the samples.

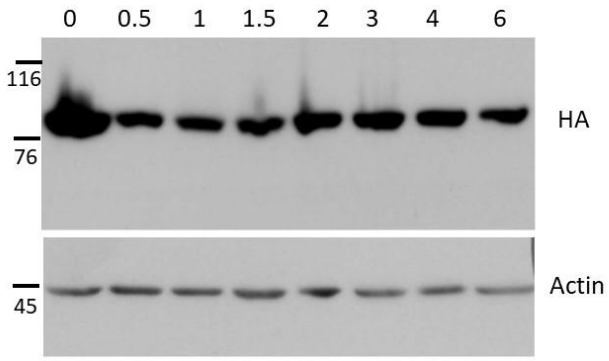

Figure 3.32: HEK293T -B56 delta cells express B56 delta through different phases in cell cycle. HEK293T cells were transfected with HA tagged B56 delta. Cells expressing HA tagged B56 delta were selected through antibiotic resistance and a stable cell line was established. The stable cell line was synchronized in mitosis using a nocodazole block. Cells were collected at various time points after release from nocodazole as indicated by the numbers above the western blot. Cell lysate was as previously described, quantified using Bradford assay and equal amounts of cell lysate were resolved on SDS PAGE and transferred to nitrocellulose membrane. Western blotting was performed with anti actin antibody to shows equal loading of samples. Western blotting with anti HA antibody shows expression of HA-tagged B56 delta. Molecular weight standards are shown on the left in kDa. All experiments were done in triplicate. Representative western blots are shown here.

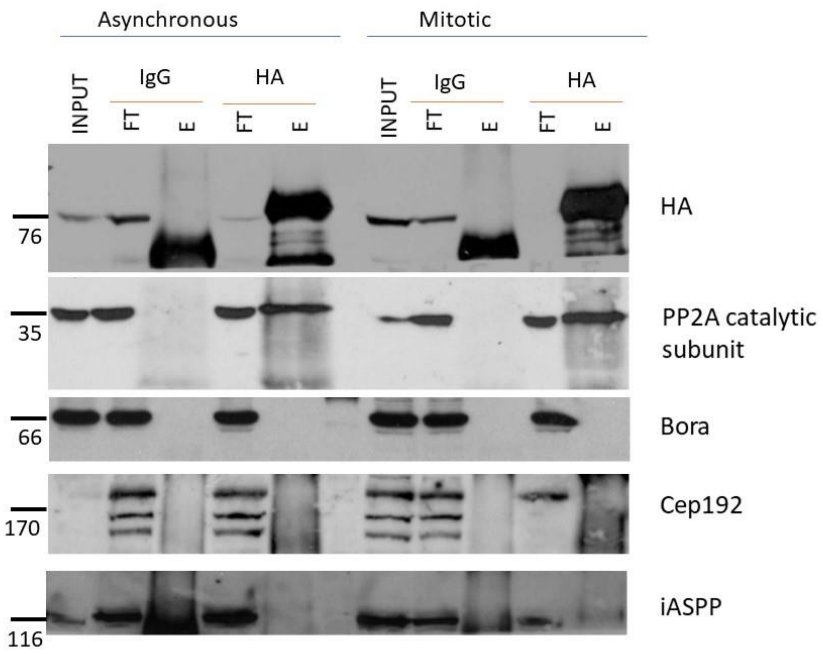

Figure 3.33: LS/TPI/V proteins were not enriched in the immunoprecipitation using anti HA antibodies with HEK293T cells expressing HA tagged B56 delta. HEK293T cells stably expressing HA tagged B56 delta were used for immunoprecipitation (IP) experiments using anti HA antibody and the corresponding species-specific IgG as a control. Asynchronous and mitotic cell extracts were used. Bound proteins were eluted from the beads by boiling with 1% SDS. Samples were resolved on SDS PAGE and transferred on to nitrocellulose membrane and western blotted with the indicated antibodies. FT refers to flow through from the column, E refers to eluate from the column. 1% of the input was loaded on the gel. Molecular weight standards are mentioned on the left in kDa. All experiments were done in triplicate. Representative western blots are shown here.

Protein threshold was set at 95% and only proteins with at least 3 identified peptides were considered in the analysis (Appendix A). To compare the two samples, at least a two-fold difference in total spectral count between the samples was considered to be a significant difference (Appendix A). B56 delta, PP2A catalytic subunit, PP2A A subunit were equally retained between asynchronous and mitotic samples (Appendix A). I speculated that since B56 delta preferentially binds LS/TPI/V proteins in their dephosphorylated form (Figure 3.11, 3.12, 3.20) and since these proteins are phosphorylated during mitosis (Figure 3.25), the IP eluate from the asynchronous cell extract will be enriched in LS/TPI/V proteins. However, LS/TPI/V proteins such as Repoman, APC1, iASPP, FZR, DSN1, RB, Cep120, Bora, Raver1 were not found to be retained under either condition. One probable explanation could be that the pattern of phosphorylation of LS/TPI/V proteins in HEK293T – B56 delta cells is different from that observed in HeLa cells. To test this, HEK293T -B56 delta cells were synchronized in mitosis using a thymidine/nocodazole block and then released from the block and allow to progress through the cell cycle. Cell lysates were collected at various points in the cell cycle, resolved on SDS PAGE and then immunoblotted using the phospho-specific antibodies. The preliminary data (Appendix B) shows that in these cells, Repoman pS597 remains phosphorylated in the asynchronous cell population and through all stages of cell cycle. Further experiments need to be done to validate the phosphor status of Cep120 pT368 and APC1 pS55 in these cells under asynchronous conditions. This could explain why none of the LS/TPI/V proteins were found to be retained in the IP (Figure 3.3).

Interestingly, some proteins containing the RVS/TF motif such as RIF1, ELYS, TACC3, SFI1, MPP10 were found to be enriched in the IP (Appendix A). RVS/TF is a PP1 binding motif. Previous studies have shown that PP1 can bind to B56 gamma in a cell cycle dependent manner[154]. However, understanding why B56 delta might be binding to PP1 regulatory proteins needs further investigation.

Chapter 4: Discussion

4.1: Summary of the key findings from this study

Eukaryotic cell cycle is one of these many processes that are tightly regulated by reversible protein phosphorylation. PP2A-B56 is an important mitotic protein phosphatase. In this study, I show that many mitotic interactors of PP2A-B56 bind to B56 through a LS/TPI/V motif. LS/TPI/V proteins are widespread in the human proteome (Table 3.1). LS/TPI/V proteins are involved in multiple signaling pathways including pathways related to the cell cycle (Figure 3.2, 3.3). In addition to humans, LS/TPI/V proteins also regulate cell cycle in *Saccharomyces cerevisiae* and in *Arabidopsis thaliana* (Figure 3.5, 3.6, 3.7). A few important mitotic regulators containing LS/TPI/V motifs were chosen for this study – Repoman, APC1, iASPP, DSN1, FZR, Cep120, GWL, RB (Table 3.2). The LS/TPI/V motif in these proteins are found to be conserved across eukaryotes (Table 3.1, Figure 3.8, 3.9). It is interesting to note that the amino acid sequences flanking the LS/TPI/V motif are enriched in specific amino acids. Using a computational approach, LS/TPI/V proteins were retrieved from different eukaryotic organisms such as *Homo sapiens, Drosophila melanogaster, Caenorhabditis elegans, Arabidopsis thaliana*, and *Saccharomyces cerevisiae* (Table 3.1). The amino acid sequences flanking the LS/TPI/V motif were aligned and a weblogo was created with the alignment (Figure 3.10). Certain amino acids such as S, P and E were found to be enriched downstream of the LS/TPI/V motif in all eukaryotic organisms. In *E. coli*, which does not contain a B56 protein, this trend was not observed (Figure 3.10).

Using an *in vitro* peptide pull-down assay, I showed that B56 proteins bind to LS/TPI/V peptides in a phosphorylation-dependent and isoform-dependent manner. B56

alpha, B56 beta, and B56 epsilon were not found to bind to peptides spanning the LS/TPI/V motif in Repoman, APC1, Cep120, DSN1, GWL, FZR, RB, and iASPP. B56 gamma3 and B56 delta were mainly found to bind to the dephosphorylated peptides (Figure 3.11, 3,12). B56 proteins are conserved across eukaryotes and share more than 80% sequence similarity (Figure 1.4). In humans, the 5 main B56 isoforms share a conserved core domain which consist of approximately 400 amino acids (Figure 1.4, 3.14). B56 delta is the longest of all the isoforms and contain an extra N terminal and C terminal region (Figure 3.14). B56 gamma3 also has a C terminal region flanking the core region. The C terminal region between these isoforms are conserved (Figure 3.14) and were speculated to be responsible for promoting the observed pattern of binding to LS/TPI/V peptides. To test this hypothesis, MBP-tagged B56 delta^{FL} (full-length protein) and B56 delta$^{\Delta 520\text{-}602}$ (a C terminal truncated protein) were cloned, expressed and purified (Figure 3.19). Using the recombinant purified proteins, a peptide overlay assay was performed. LS/TPI/V peptides (Table 2.1) were spotted on a nitrocellulose membrane and incubated in presence of the recombinant proteins. To test binding of the recombinant proteins to the peptides, the membranes were then western blotted using anti-MBP antibodies. B56 delta^{FL} was found to bind to the dephosphorylated but not the phosphorylated peptides (Figure 3.20). However, B56 delta$^{\Delta 520\text{-}602}$ was found to bind to both phosphorylated and dephosphorylated peptides (Figure 3.20).

To investigate if LS/TPI/V proteins are phosphorylated in a cell-cycle dependent manner, I designed, raised and purified polyclonal antibodies in rabbits which specifically recognize the phosphorylated LS/TPI/V motif in Repoman, APC1 and Cep120 (Figure

3.23). The antibodies were found to be highly sensitive, and specifically recognized only the phosphorylated peptides spotted on a nitrocellulose membrane (Figure 3.23). I also showed that the LS/TPI/V motif on Repoman, APC1 and Cep120 were phosphorylated during mitosis and not in other stages of the cell cycle (Figure 3.25). Using immunofluorescence assays, it was shown that the cells on entering prophase gets phosphorylated on the LS/TPI/V motif (Figure 3.26, 3.27, 3.38). This phosphorylation is maintained through metaphase and anaphase and decreases as the cells enter telophase (Figure 3.26, 3.27, 3.28). The phosphorylation on different mitotic substrates is carried out by four main mitotic kinases, AURKA, AURKB, Plk1 and CDK1-cyclinB (section 1.6). Using a kinase inhibition assay, I showed that the phosphorylation on the LS/TPI/V motif is controlled by AURKB (Figure 3.30). These findings were also validated by immunofluorescence assay (Figure 3.31).

To investigate if B56 delta interacts with LS/TPI/V proteins in a cell-cycle dependent manner, HA-tagged B56 delta was stably expressed in HEK293T cells. Immunoprecipitation (IP) experiments were performed using anti HA antibodies and the corresponding IgG was used as a control. The proteins enriched in the IP assays were analyzed by western blotting and mass spectrometry. HA tagged proteins and PP2A catalytic subunits were retained by the anti-HA antibody but not by the control IgG suggesting that the IP was successful (Figure 3.33). None of the LS/TPI/V proteins of our interest were found to be retained (Figure 3.33, Appendix A).

The key findings from this study are summarized in Figure 4.1.

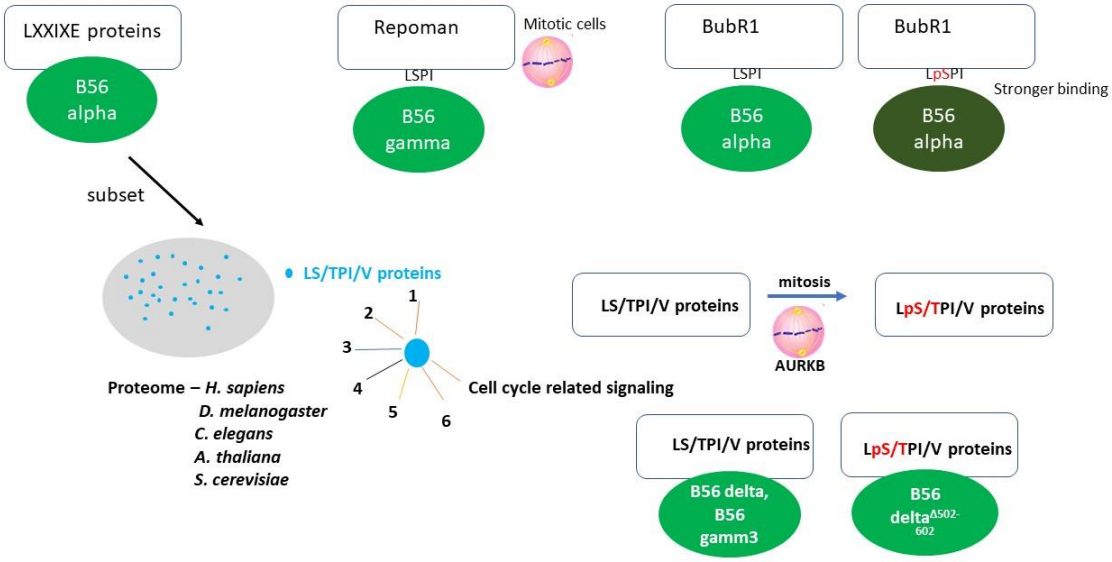

Figure 4.1: Key findings from this study. This study investigates how PP2A-B56 controls mitosis by interacting with LS/TPI/V motif containing proteins. The key findings from this study that enriched the existing literature are summarized in this figure. This study shows that LS/TPI/V proteins are widespread not only in the human proteome but also in the proteome of other eukaryotic organisms LS/TPI/V proteins are involved in multiple signaling pathways, represented as pathways 1, 2,3, 4,5, 6 and particularly in cell cycle related signaling. This functional enrichment of LS/TPI/V proteins are conserved across eukaryotes. LS/TPI/V peptides in dephosphorylated form has a preference for binding B56 delta and B56 gamma3. B56 delta$^{\Delta 520\text{-}602}$, a C terminal truncated mutant of B56 delta binds to both phosphorylated and dephosphorylated LS/TPI/V peptides. LS/TPI/V proteins are phosphorylated during mitosis and this phosphorylation is controlled by AURKB.

4.2: The LS/TPI/V motif is widespread in human proteome

In 2016, Hertz et al. showed that PP2A-B56 can bind to interactors through a six amino acid motif LxxIxE[36]. The evidence for this was primarily generated from a proteomic study in which HeLa cells stably expressing YFP tagged B56 alpha and YFP tagged B55 alpha (two separate cell lines) were used for immunoprecipitation using anti YFP. The interactors that were enriched for B56 alpha were analyzed and their consensus interaction motif was retrieved. Using biochemical assays such as ITC and peptide scanning mutagenesis overlay, the authors show that position 1 in this motif can be occupied by L, or by F and M, X in P2 and P3 could be any amino acid residue. However, if the amino acid residue in P2 is phosphorylated, the binding affinity for B56 alpha increases. P4 could be occupied by I, V, L, C, W, listed in the decreasing order of affinity for binding. According to their findings, E in P6 cannot be substituted by any other amino acid. To support this hypothesis, they have used data from ITC experiments and from an invitro peptide array overlay assay. For this purpose, peptides derived from the LSPIIE motif present in BubR1 were used. The amino acids in each position was replaced and the affinity of binding to B56 alpha was evaluated in the peptide overlay array experiment. Through this assay, they showed that E in the P6 was irreplaceable and its absence leads to the abolishment of the interaction with B56. However, in their assay, they did not evaluate the binding between B56 and the peptide when E was present at a different position, for example in P5 or P7 instead of P6. Additionally, the presence of phosphorylated S (which shows similar biochemistry to E) in P5 or P6 was not evaluated. In the ITC experiments, the E in P5 was only replaced by D or A in P5. From the findings

of the *in vitro* assays performed in my study (Figure 3.11, 3.12, 3.20) and sequence alignment of the flanking region of all the LS/TPI/V proteins across eukaryotes, it can be speculated that the presence of E in P6 of the peptide tested in their study is important but not mandatory. To further validate this, ITC and peptide array overlay experiments can be done with peptides having E in different positions and with peptides having phosphorylated S or T in P6. Using the same parameters described in section 2.17, an *in silico* search was performed to retrieve all LxxIxE proteins present in the human proteome. These proteins were then compared with the LS/TPI/V proteins. It was found that only 34 proteins belonged to both sets (Figure 4.2). Since reversible protein phosphorylation is a mechanism that tightly regulates mitosis, and since this study shows that LS/TPI/V is dynamically and reversibly phosphorylated during mitosis (Figure 3.25, 3.26, 3.27, 3.28), it can be speculated that LS/TPI/V is an important motif for cell cycle regulators that interact with B56.

4.2.1: Presence of two adjacent LS/TPI/V motifs

On closer examination of the motifs present in the proteins chosen for this study (Table 3.2), we observed that in Repoman a LxxIxE (LPEVPE) motif is present downstream of the LSPI motif. In APC1, a LxxIxE (LGSLDE) is present upstream of the LSPV motif. The other chosen mitotic regulators have only one LS/TPI/V motif present. Further studies need to be done to understand the importance of this double motif present in selected interactors.

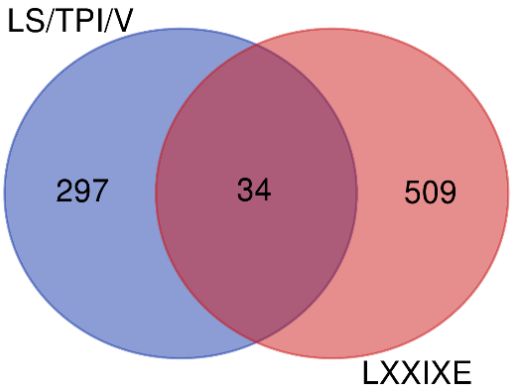

Figure 4.2: Venn diagram showing overlap between LS/TPI/V proteins retrieved in this study and LxxIxE proteins retrieved using the same parameters. LS/TPI/V and LxxIxE proteins were retrieved from the human proteome using the SlimSearch server as described in section 3.1. The proteins subsets were compared, and a Venn diagram was drawn using the Venn diagram drawing tool on Yves Van de Peer lab.

4.3: Degeneracy of B56 isoforms

Historically studies have assumed that the B56 proteins exhibit degeneracy in function. This assumption stems from the fact that B56 proteins are highly conserved (Figure 1.4). However, the high conservation is restricted to the 400 amino acids in the core region as previously described in chapter 1 and chapter 3. In this study, I show that B56 proteins bind to LS/TPI/V proteins in an isoform dependent manner and speculate that the B56 delta is a unique isoform. In 2011, using GFP tagged B56 protein constructs, Foley et al. showed that B56 proteins get recruited to the metaphasic plate and localizes to the centromere/kinetochore of unattached sister chromatids[151]. In 2013, Kruse et al. showed that BubR1, a pseudokinase recruits PP2A-B56 to the metaphasic plate during mitosis using the LSPI motif[189]. In all their experiments, they used B56 alpha and extrapolated their findings to all B56 proteins. However, a study by Bastos et al. showed that the localization of B56 proteins during mitosis is isoform dependent[190]. Additionally, they found that B56 gamma and B56 epsilon, and not the other B56 isoforms counteracted the activities of AURKB. Vallardi et al. in 2019 showed isoform specific localization of B56 proteins during mitosis[191]. B56 alpha and B56 epsilon mainly localize to the centromere during prophase and this localization is facilitated by their interaction with Sgo2. B56 delta and B56 gamma were shown to localize to the kinetochore after being recruited by BubR1 through the LSPI motif. Sgo2 and BubR1 bind distinct regions on B56.

While analyzing the localization of B56 proteins in the cell using immunofluorescence assays, I had observed some of the isoforms, particularly B56 alpha

form cytoplasmic aggregates which structurally resemble P bodies or stress granules (Appendix B). It is possible that in addition to phosphorylation, geographic location of the B56 isoforms in the cell contribute to isoform specific interactions. For example, B56 alpha interacts with LS/TPI/V proteins in the P body and are important for related stress signaling pathways. Another example is unpublished data from our lab showing that in *Arabidopsis thaliana*, B56 theta (but not the other B56 isoforms) localizes to the peroxisome. In the past, since B56 isoforms were considered to be redundant in function. the study of isoform specific functions was neglected. Many studies in the literature were done with one isoform, without any scientific rationale for the choice.

4.4: Phosphorylation of LS/TPI/V during mitosis provides an additional mechanism of regulation

This study shows that the LS/TPI/V motif is phosphorylated as the cells enter mitosis and is dephosphorylated at mitotic exit. This phosphorylation is controlled by AURKB and CDK1. S/TP is a consensus recognition site for CDK1-cyclinB. However, according to the data presented in this study AURKB controls phosphorylation of this motif. When AURKB is inhibited, phosphorylation on this motif is abolished. It is possible that AURKB is acting as a priming kinase and phosphorylating a different residue outside the LS/TPI/V motif. This phosphorylated residue is then facilitating the recruitment of CDK1-cyclin B which is in turn phosphorylating LS/TPI/V. So AURKB is acting upstream of CDK1 to control the phosphorylation of this motif. To test this, phosphomimetics of residues close to the LS/TPI/V motif could be created. Phosphorylation of the LS/TPI/V motif provides an additional level of control of binding

with specific B56 proteins. When phosphorylated B56 delta does not bind this motif as shown by this study. However, as shown by previous studies, B56 alpha has a preference for binding to phosphorylated LS/TPI/V motif. It is possible that through phosphorylation, isoform specific recruitment of PP2A-B56 is being monitored.

4.5: Novel functions of PP2A-B56 can be speculated from studying the LS/TPI/V protein signaling network

4.5.1: Participation of B56 in novel signaling pathways.

In this study, I show that LS/TPI/V motif is widespread in the human proteome (Table 3.1) and LS/TPI/V proteins participate in diverse signaling pathways (Figure 3.2, 3.3). Since LS/TPI/V is the B56 binding motif, by studying the diversity and role of the LS/TPI/V network, potential novel roles of PP2A-B56 can be unveiled. In humans, in addition to cell cycle, LS/TPI/V proteins are also involved in various other signaling pathways including positive regulation of neuronal cell death, pericardium development and lipoprotein transporter activity. FOXO3, ELK1, and JUN are three LS/TPI/V transcription factors involved in positive regulation of neuronal cell death and are also implicated in various other disease conditions (Figure 4.3A). Transcriptional factor FOXO3 has been shown to interact directly with B56 alpha *in vitro*[36]. Studies have shown that FOXO3 is responsible for inhibiting age-dependent degeneration of neurons[192]. The mechanism though not completely worked out is speculated to be both overlapping and distinct from the regulation of cell death by the mTOR pathway[192]. PP2A is a key signaling molecule in the mTOR pathway but its role in regulating FOXO3 in this context has not been studied and could offer valuable insights. ELK1 and JUN are

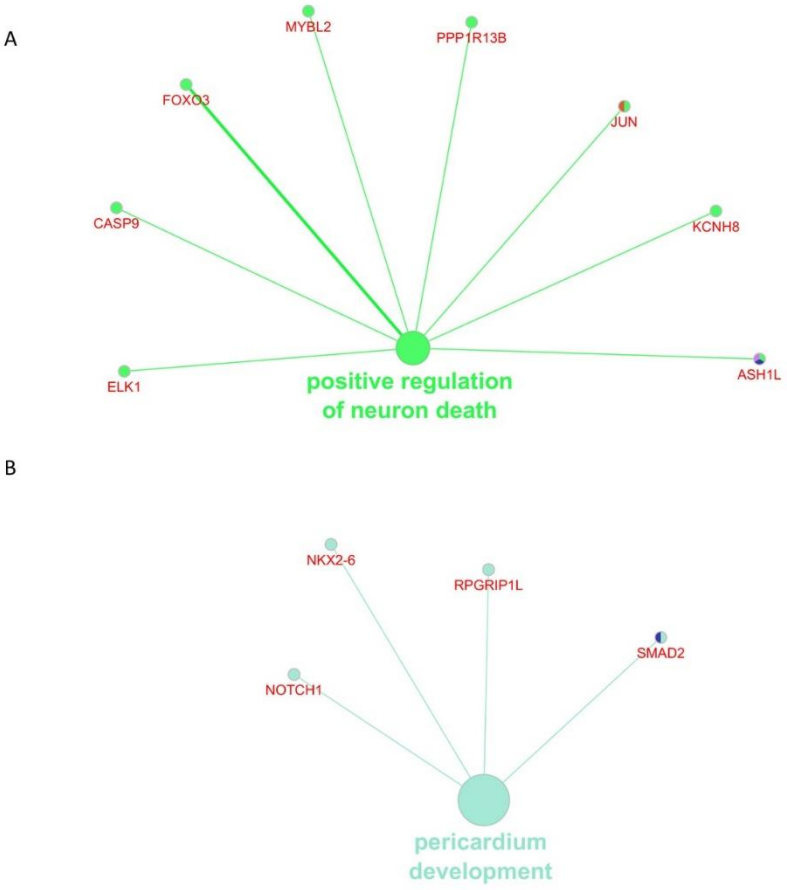

Figure 4.3: Functional enrichment analysis showing LS/TPI/V motif containing proteins in humans are involved in (A) positive regulation of neuronal death and (B) pericardium development. All GO biological processes (filtered using p value ≤ 0.1) associated with the pre-filtered and selected LS/TPI/V proteins (331 proteins listed in Table 3.1) in humans were used to create an interaction map. Specific functions on the interaction were zoomed on to find the LS/TPI/V proteins involved and are presented here. Analysis was performed using Clue-GO plug-in in Cytoscape. GO Tree Interval levels were selected at a minimum of 3 and maximum of 15. The pathways were grouped based on significance. The size and color of the legend for significance is shown on the bottom right. The node size corresponds to the number of mapped genes. The node color corresponds to the significance. Nodes are clustered together based on their Kappa score. The length and thickness of edges are not scaled.

transcription factors that are implicated in various diseases including age dependent neuropathology and cancer (Figure 4.3A). They regulate multiple signaling pathways that are also regulated by PP2A. However, how a direct interaction between PP2A-B56 and these transcription factors impact the neuronal death signaling pathway has not been studied and can provide further insight into the signaling network. Another example is that of pericardium development. Previous studies have shown that PP2A catalytic subunit is highly expressed in embryonic heart tissue compared to an adult heart tissue[193]. Dephosphorylation of targets by PP2A has been speculated to be important for heart development[193]. The functional enrichment analysis presented in this thesis shows that Notch1, Nkx2-6, Smad2 and Rpgrip1l are LS/TPI/V proteins involved in pericardium development (Figure 4.3B) and are potential interactors of B56 (Figure 4.3B). These LS/TPI/V proteins might be responsible for recruiting PP2A to the heart tissue. Studying how PP2A-B56 influences pericardium development might fill in gaps in our knowledge about the process.

4.5.2: Localization of B56 to novel cellular organelles.

LS/TPI/V proteins are localized to various components of the cell (Figure 3.4). It can be speculated that LS/TPI/V proteins recruit PP2A-B56 to these different cellular components. Whether B56 proteins get recruited by LS/TPI/V proteins in an isoform dependent manner remains to be validated.

Among other organelles, LS/TPI/V proteins localize to the centrosome (Figure 3.4). Some of the obvious centrosome localized LS/TPI/V proteins are Cep44, Cep120, Cep164 and Cep192 (Table 3.1). Centrosomes are microtubules organizing centers of

mammalian cells and are crucial for mitotic spindle formation[194]. Centrosomes consist of a pair of centrioles surrounded by peri centriolar matrix (PCM)[194]. The PCM is rich in proteins which can be classified into four main groups based on their function – proteins responsible for maintaining structure and acting as scaffold to recruit other proteins, proteins involved in microtubule nucleation, various regulatory proteins, and signaling molecules including protein kinases and protein phosphatases. Proteomic studies have identified many of these centrosomal proteins. However, the biological functions of many of these proteins are yet to be explored by individual functional studies. Thirty-two centrosomal protein family (CEP) of proteins have been identified so far. CEP family of proteins are important for controlling cell cycle progression and control various aspects of cell cycle signaling. The centrosome cycle occurs in sync with the cell cycle and involves duplication of the centrosomes as well as centrosome maturation. During G1 phase, the centrioles separate from each other and duplicate in a semiconservative manner which is completed by the end of S phase[194]. During mitosis, each daughter cell receives a pair of centrioles and a cloud of PCM. Centrosomal duplication and maturation has been reported to be regulated by mitotic kinases such as AURKA, Plk1, Nek2A[195]. Various centrosomal proteins have been reported to be heavily phosphorylated by mitotic kinases during a cell's entry into mitosis. Given the reversible and dynamic nature of protein phosphorylation, it can be anticipated that these proteins must dephosphorylated at mitotic exit for proper functioning of the cell cycle and centrosomal cycle. In this study I show how phosphorylation of LTPI motif of Cep120 changes during cell cycle. The motif is phosphorylated in mitosis and dephosphorylated as cells exit mitosis (Figure

3.25). A previous study from our research group shows how phosphorylation on RVSF motif on Cep192 is regulated in the same fashion. Till date only a few studies have investigated the protein phosphatases regulating dephosphorylation of centrosomal proteins. We have previously shown that PP1 is recruited by Cep192 to the centrosome[196]. Since several of the CEP proteins have the LS/TPI/V motif and since Cep120 interacts with B56 (Figure 3.9, 3.10), I speculate that PP2A-B56 has an important role to play in cell cycle dependent centrosomal dephosphorylation.

Chapter 5: Future Directions

5.1: Crystallization of B56 delta

To further understand why B56 delta prefers binding to dephosphorylated peptides, and the contribution of its C terminal region in this interaction, the elucidation of the crystal structure of B56 delta is very important. For protein crystallization, it is important to have highly pure, homogeneous protein sample in large quantities. The first choice for recombinant protein expression and purification is often the bacterial system as it is easy to handle, inexpensive and well characterized. However, in some cases (as is the case of B56 delta) producing a highly pure human protein in bacteria in high quantities could be challenging. A future aim of this study is to clone, express and purify B56 delta in human cells (HEK293F cells) using the system developed by Schellenberg et al[183]. In this system a YFP tagged recombinant protein is expressed from a Gateway expression vector in suspension HEK293K cells and purified using the anti YFP nanobody support. Since the recombinant human proteins are being expressed in native conditions, in human cells, misfolding is limited and folding is facilitated by native chaperones. The recombinant protein also gain the correct post-translational modifications which in turn aid its folding and stability[183]. Another common approach used for purifying unstable proteins for crystallization studies is to co-express them with an interactor. B56 delta could be co-expressed with the other subunits of PP2A for crystallization.

X-ray crystallography has been the primary method of choice for structural biology studies over the years. However, recent times has seen the rise of the use of cryo-EM in structural biology studies. Combined with powerful computational tools for single-particle analysis, cryo-EM has been used to determine the structures of complex

macromolecules at near- atomic resolution. For determination of B56 delta structure, the use of cryo-EM could be considered.

5.2: Studying cell-cycle dependent isoform-specific interactome of B56

Previous proteomic studies have characterized the interactome of B56 alpha in asynchronous cells. In this study, I show that the interactome of B56 delta changes between asynchronous and mitotic conditions. To further understand the regulation of mitosis by PP2A-B56, it is important to study the isoform-dependent interactome of B56 under asynchronous and mitotic conditions. In this study, I have created stable HEK293T cell lines expressing HA-tagged B56 isoforms. Using anti HA antibody, immunoprecipitation experiments can be performed under asynchronous and mitotic conditions and the enriched interactors can be analyzed by mass spectrometry.

5.3: Dephosphorylation of the LS/TPI/V motif at mitotic exit

In this study, I show that LS/TPI/V proteins get dephosphorylated at mitotic exit (Figure 3.25, 3.26, 3.27, 3.28). To further understand, the significance of this dephosphorylation, it is important to determine the mitotic phosphatase responsible for this reaction. To study that, HeLa cells can be synchronized in mitosis using a thymidine/nocodazole block and then treated with phosphatase inhibitors on being released from the block. Cells can be collected at various time points; cell lysates can be prepared and can be analyzed by western blotting. The western blotting studies can be validated further by microscopy. The two important mitotic phosphatases that dephosphorylate most proteins at mitotic exit are PP1 and PP2A.

5.4 Therapeutic potential of PP2A-B56

As discussed in Chapter 1, protein phosphatases have not been sufficiently explored by the pharmaceutical industry as drug targets even though their counterparts, protein kinases are the second largest group of drug targets. The loss of cell cycle regulation is one of the hallmarks of cancer. Many cancer drugs have targeted inhibition of mitotic kinases such as AURKA, AURKB, Plk1 and CDK1. In recent years, some inhibitors of mitotic phosphatases, particularly that of PP1 have been developed. Recent drug development studies show that the use of a drug combination therapy targeting two different aspects of cancer is more effective than a single drug in chemotherapy. An example is the development of histone deacetylase inhibitors in conjugation with immune check point inhibitors. PP2A has been reported by many studies as a tumor suppressor. A novel approach to drug development would include designing and testing PP2A activators and using them in combination therapy for cancer.

APPENDIX A: **MASS SPECTROMETRIC ANALYSIS:**

Table showing proteins enriched in the mass spectrometry analysis. Immunoprecipitation experiments were performed using HEK293T cells expressing HA tagged B56 delta. Anti- HA antibodies Asynchronous and mitotic cell lysates were used. Table showing total spectral counts of proteins detected in the asynchronous vs mitotic extracts. To limit false positives, peptide threshold was set to 95% and minimum spectral count to 3.

Identified Proteins	**Accession Number**	**Asynchronous - total spectral count**	**Mitotic - total spectral count**	**Ratio of total spectral count**
desmoplakin isoform I	gi|58530840	0	4	0
angiomotin isoform 1	gi|166064029 (+3)	0	8	0
filamin-B isoform 2	gi|105990514 (+5)	0	7	0
PREDICTED: catenin beta-1 isoform X2	gi|578805674 (+1)	0	3	0
tropomyosin alpha-3 chain isoform Tpm3.1cy	gi|24119203	0	5	0
elongation factor Tu, mitochondrial precursor	gi|34147630	0	4	0
protein-L-isoaspartate(D-aspartate) O-methyltransferase isoform 1	gi|226530908 (+4)	0	5	0
exportin-1	gi|4507943 (+4)	0	4	0
dolichyl-diphosphooligosaccharide--protein glycosyltransferase subunit 1 precursor	gi|4506675	0	4	0
ankycorbin isoform a	gi|224809468 (+16)	0	6	0
sphingomyelin phosphodiesterase 4 isoform 2	gi|102467481 (+3)	0	4	0
60S ribosomal protein L32	gi|4506635 (+2)	0	4	0
gelsolin isoform b	gi|189083772 (+26)	0	5	0
PREDICTED: splicing factor U2AF 65 kDa subunit isoform X2	gi|578833896 (+3)	0	4	0
PREDICTED: gamma-adducin isoform X1	gi|530393070 (+10)	0	6	0
cytoskeleton-associated protein 4	gi|19920317	0	4	0
trifunctional enzyme subunit beta, mitochondrial isoform 1 precursor	gi|4504327 (+1)	0	3	0
leucine--tRNA ligase, cytoplasmic	gi|108773810 (+3)	0	3	0
replication factor C subunit 3 isoform 2	gi|108773789 (+6)	0	4	0
calnexin precursor	gi|10716563 (+3)	0	4	0
sperm-specific antigen 2 isoform 1	gi|194363771 (+6)	0	4	0
basigin isoform 3	gi|38372921	0	4	0
heat shock protein HSP 90-alpha isoform 1	gi|153792590 (+2)	0	3	0
D-3-phosphoglycerate dehydrogenase	gi|23308577 (+2)	0	5	0
phosphate carrier protein, mitochondrial isoform b precursor	gi|4505775 (+2)	0	3	0
60S ribosomal protein L8	gi|15431306 (+2)	0	4	0

filamin-A isoform 1	gi|116063573 (+6)	0	3	0
prohibitin-2 isoform 1	gi|221307584	0	4	0
protein phosphatase 1 regulatory subunit 12A isoform a	gi|219842212 (+8)	0	4	0
THO complex subunit 4	gi|238776833	0	3	0
tropomodulin-1	gi|260763922 (+1)	0	3	0
cytochrome c oxidase subunit II (mitochondrion)	gi|251831110	0	3	0
prohibitin isoform 1	gi|4505773 (+2)	0	4	0
40S ribosomal protein S5	gi|13904870	0	4	0
supervillin isoform 1	gi|150417971 (+13)	0	4	0
epiplakin	gi|525507390 (+1)	0	4	0
PREDICTED: kinesin-like protein KIF14 isoform X3	gi|767911132 (+1)	0	3	0
inositol 1,4,5-trisphosphate receptor type 2	gi|95147335	0	5	0
myosin light polypeptide 6 isoform 1	gi|17986258 (+1)	0	4	0
mitochondrial import inner membrane translocase subunit TIM50	gi|48526509 (+1)	0	3	0
PREDICTED: unconventional myosin-VI isoform X1	gi|530383142 (+5)	0	3	0
cytochrome b-c1 complex subunit 2, mitochondrial precursor	gi|50592988	0	3	0
calcium/calmodulin-dependent protein kinase type II subunit gamma isoform 4	gi|26667191 (+21)	0	3	0
SWI/SNF-related matrix-associated actin-dependent regulator of chromatin subfamily E member 1	gi|21264355	0	3	0
C-Myc-binding protein	gi|57242777	0	3	0
cytochrome b-c1 complex subunit 1, mitochondrial precursor	gi|46593007	0	3	0
unconventional myosin-XVIIIa isoform a	gi|28416946 (+1)	0	3	0
sodium/potassium-transporting ATPase subunit alpha-1 isoform a	gi|21361181 (+3)	0	3	0
succinate dehydrogenase [ubiquinone] flavoprotein subunit, mitochondrial isoform 1	gi|156416003 (+2)	0	3	0
exportin-2 isoform 1	gi|29029559 (+1)	3	10	0.3
ATP synthase subunit beta, mitochondrial precursor	gi|32189394	3	9	0.3333
inositol 1,4,5-trisphosphate receptor type 3	gi|153945846 (+2)	4	11	0.3636
myosin-9	gi|12667788 (+1)	16	41	0.3902
lupus La protein	gi|10835067 (+1)	3	7	0.4286
40S ribosomal protein S3a isoform 1	gi|4506723	5	10	0.5
alpha-enolase isoform 1	gi|4503571	3	6	0.5
tropomodulin-3	gi|7657649	3	6	0.5
catenin alpha-1 isoform 1	gi|55770844 (+3)	3	6	0.5
spectrin beta chain, non-erythrocytic 1 isoform 1	gi|112382250 (+3)	32	60	0.5333
myosin-10 isoform 2	gi|367460087 (+2)	37	68	0.5441
PREDICTED: myosin phosphatase Rho-interacting protein isoform X1	gi|767991900 (+1)	5	9	0.5556
PREDICTED: tight junction protein ZO-1 isoform	gi|530406350 (+3)	5	9	0.5556

X4				
78 kDa glucose-regulated protein precursor	gi|16507237	7	12	0.5833
cytoskeleton-associated protein 2 isoform 2	gi|148664201 (+3)	6	10	0.6
voltage-dependent anion-selective channel protein 3 isoform 2	gi|208879465 (+1)	3	5	0.6
protein LYRIC	gi|223555917	3	5	0.6
polyadenylate-binding protein 1	gi|46367787 (+1)	3	5	0.6
plectin isoform 1c	gi|47607492 (+1)	28	43	0.6512
translational activator GCN1	gi|54607053	12	18	0.6667
poly(rC)-binding protein 2 isoform a	gi|14141168 (+2)	4	6	0.6667
14-3-3 protein zeta/delta	gi|208973238 (+9)	4	6	0.6667
elongation factor 1-gamma	gi|4503481	4	6	0.6667
serine/threonine-protein phosphatase 2A catalytic subunit alpha isoform	gi|4506017	10	14	0.7143
bifunctional glutamate/proline--tRNA ligase	gi|62241042	5	7	0.7143
myosin regulatory light chain 12B	gi|15809016 (+7)	5	7	0.7143
PREDICTED: spectrin beta chain, non-erythrocytic 2 isoform X1	gi|530397182 (+4)	6	8	0.75
isoleucine--tRNA ligase, cytoplasmic	gi|94721239 (+1)	6	8	0.75
40S ribosomal protein S6	gi|17158044	3	4	0.75
complement component 1 Q subcomponent-binding protein, mitochondrial precursor	gi|4502491	3	4	0.75
spectrin alpha chain, non-erythrocytic 1 isoform 2	gi|154759259 (+2)	61	81	0.7531
heterogeneous nuclear ribonucleoprotein A/B isoform a	gi|55956919 (+1)	7	9	0.7778
liprin-alpha-1 isoform a	gi|29171753 (+15)	20	25	0.8
ATP synthase subunit alpha, mitochondrial isoform b precursor	gi|382546007 (+2)	4	5	0.8
60S ribosomal protein L10a	gi|15431288	4	5	0.8
60S ribosomal protein L4	gi|16579885	4	5	0.8
calcium/calmodulin-dependent protein kinase type II subunit delta isoform 5	gi|212549753 (+18)	4	5	0.8
voltage-dependent anion-selective channel protein 2 isoform 1	gi|296317337 (+4)	4	5	0.8
40S ribosomal protein S7	gi|4506741	5	6	0.8333
40S ribosomal protein S2	gi|15055539	5	6	0.8333
60S ribosomal protein L12	gi|4506597	5	6	0.8333
60S ribosomal protein L23a	gi|17105394	5	6	0.8333
F-actin-capping protein subunit alpha-1	gi|5453597	5	6	0.8333
heat shock protein beta-1	gi|4504517	6	7	0.8571
tubulin beta chain isoform b	gi|29788785	13	15	0.8667
PREDICTED: RNA-binding protein Raly isoform X1	gi|530417947 (+3)	7	8	0.875

serine/threonine-protein phosphatase PP1-alpha catalytic subunit isoform 1	gi|4506003	7	8	0.875
heat shock protein HSP 90-beta isoform a	gi|20149594 (+3)	9	10	0.9
elongation factor 1-alpha 1	gi|4503471 (+1)	9	10	0.9
keratin, type II cytoskeletal 8 isoform 1	gi|372466572 (+2)	13	14	0.9286
actin, cytoplasmic 2	gi|316659409 (+2)	29	31	0.9355
serine/threonine-protein phosphatase 2A 56 kDa regulatory subunit delta isoform isoform 1	gi|5453954	22	23	0.9565
serine/threonine-protein phosphatase 2A 65 kDa regulatory subunit A alpha isoform	gi|21361399	25	25	1
60S ribosomal protein L6	gi|16753227 (+6)	11	11	1
LIM domain and actin-binding protein 1 isoform 1	gi|165905589 (+1)	7	7	1
60 kDa heat shock protein, mitochondrial	gi|31542947 (+2)	10	10	1
neurofilament light polypeptide	gi|105990539	9	9	1
unconventional myosin-Id isoform 1	gi|51100974 (+1)	8	8	1
insulin-like growth factor 2 mRNA-binding protein 1 isoform 1	gi|56237027 (+1)	8	8	1
40S ribosomal protein S18	gi|11968182	7	7	1
ADP/ATP translocase 2	gi|156071459	6	6	1
keratin, type I cytoskeletal 18	gi|40354195 (+1)	6	6	1
60S ribosomal protein L7a	gi|4506661	6	6	1
lamin-B receptor	gi|37595750 (+4)	6	6	1
reticulocalbin-2 isoform b precursor	gi|426214088 (+1)	7	7	1
60S ribosomal protein L9	gi|15431303 (+2)	6	6	1
60S ribosomal protein L3 isoform a	gi|4506649 (+1)	4	4	1
histone H1.0	gi|4885371	5	5	1
neurabin-2	gi|140972063 (+1)	4	4	1
ribosome biogenesis regulatory protein homolog	gi|14719402	5	5	1
TAR DNA-binding protein 43	gi|6678271	5	5	1
KRR1 small subunit processome component homolog	gi|117676403	5	5	1
heterogeneous nuclear ribonucleoprotein D0 isoform c	gi|14110414 (+1)	3	3	1
40S ribosomal protein S16	gi|4506691	4	4	1
serine/threonine-protein phosphatase 2A 65 kDa regulatory subunit A beta isoform isoform a	gi|32455246	3	3	1
40S ribosomal protein S27	gi|4506711	5	5	1
aspartate--tRNA ligase, cytoplasmic isoform 1	gi|45439306	3	3	1
PREDICTED: erlin-2 isoform X1	gi|530387549 (+1)	3	3	1
serine/arginine-rich splicing factor 7 isoform 2	gi|306482694 (+3)	4	4	1
RNA-binding protein 39 isoform c	gi|336176064 (+8)	3	3	1
DBIRD complex subunit ZNF326 isoform 1	gi|33946297	4	4	1

small nuclear ribonucleoprotein Sm D1 isoform 1	gi|5902102	4	4	1
U3 small nucleolar ribonucleoprotein protein IMP3	gi|8922794	4	4	1
ATP-dependent RNA helicase DDX51	gi|154759257 (+1)	3	3	1
DAZ-associated protein 1 isoform b	gi|25470886 (+2)	3	3	1
charged multivesicular body protein 4b	gi|28827795	3	3	1
alpha-adducin isoform a	gi|29826319 (+9)	3	3	1
replication factor C subunit 1 isoform 1	gi|32528306 (+1)	3	3	1
40S ribosomal protein S15a	gi|14165469 (+1)	3	3	1
10 kDa heat shock protein, mitochondrial	gi|4504523	3	3	1
40S ribosomal protein S25	gi|4506707	3	3	1
40S ribosomal protein S19	gi|4506695	3	3	1
DNA-dependent protein kinase catalytic subunit isoform 2	gi|126032350 (+3)	26	25	1.04
X-ray repair cross-complementing protein 6 isoform 1	gi|4503841 (+1)	14	13	1.0769
heat shock cognate 71 kDa protein isoform 1	gi|5729877 (+1)	13	12	1.0833
40S ribosomal protein S3 isoform 1	gi|15718687 (+1)	11	10	1.1
ribosomal L1 domain-containing protein 1	gi|118498359	11	10	1.1
tubulin alpha-1B chain	gi|57013276	17	15	1.1333
60S ribosomal protein L7	gi|15431301	8	7	1.1429
voltage-dependent anion-selective channel protein 1	gi|4507879 (+1)	8	7	1.1429
nucleolin	gi|55956788	15	13	1.1538
116 kDa U5 small nuclear ribonucleoprotein component isoform a	gi|217272892 (+2)	15	13	1.1538
splicing factor, proline- and glutamine-rich	gi|4826998 (+2)	7	6	1.1667
ATPase family AAA domain-containing protein 3A isoform 1	gi|283436220 (+1)	7	6	1.1667
protein DEK isoform 1	gi|4503249	7	6	1.1667
60S acidic ribosomal protein P2	gi|4506671	7	6	1.1667
non-POU domain-containing octamer-binding protein isoform 1	gi|224028244 (+2)	13	11	1.1818
importin subunit beta-1 isoform 1	gi|19923142	13	11	1.1818
40S ribosomal protein S8	gi|4506743	6	5	1.2
pinin	gi|33356174	6	5	1.2
cellular tumor antigen p53 isoform a	gi|120407068 (+4)	6	5	1.2
stress-70 protein, mitochondrial precursor	gi|24234688	6	5	1.2
PREDICTED: alpha-actinin-4 isoform X2	gi|530417302 (+1)	10	8	1.25
40S ribosomal protein S9	gi|14141193 (+19)	5	4	1.25
PREDICTED: transmembrane protein 43 isoform X1	gi|767924288	10	8	1.25

insulin receptor substrate 4	gi|4504733 (+3)	5	4	1.25
60S ribosomal protein L23	gi|4506605	5	4	1.25
interleukin enhancer-binding factor 2 isoform 1	gi|24234747 (+1)	18	14	1.2857
clathrin heavy chain 1 isoform 1	gi|4758012 (+5)	9	7	1.2857
40S ribosomal protein S4, X isoform X isoform	gi|4506725	9	7	1.2857
60S acidic ribosomal protein P0	gi|16933546 (+1)	9	7	1.2857
ELAV-like protein 1	gi|38201714 (+1)	8	6	1.3333
heterogeneous nuclear ribonucleoprotein H	gi|381342476 (+12)	8	6	1.3333
40S ribosomal protein S11	gi|4506681	8	6	1.3333
nucleolar pre-ribosomal-associated protein 1	gi|194394141	4	3	1.3333
liprin-alpha-3	gi|32189362 (+1)	4	3	1.3333
small nuclear ribonucleoprotein Sm D3	gi|4759160 (+1)	4	3	1.3333
40S ribosomal protein S14	gi|5032051 (+2)	4	3	1.3333
60S ribosomal protein L27a	gi|4506625	4	3	1.3333
neurofilament medium polypeptide isoform 1	gi|157738649	39	29	1.3448
poly [ADP-ribose] polymerase 1	gi|156523968	22	16	1.375
thymopoietin isoform alpha	gi|4507555	11	8	1.375
nucleolar RNA helicase 2 isoform 1	gi|50659095	21	15	1.4
unconventional myosin-Ib isoform 1	gi|194328685 (+7)	14	10	1.4
WD repeat-containing protein 3	gi|5803221	14	10	1.4
nuclease-sensitive element-binding protein 1	gi|34098946	7	5	1.4
keratin, type II cytoskeletal 1	gi|119395750	38	27	1.4074
PREDICTED: vimentin isoform X1	gi|578818565 (+2)	102	72	1.4167
N-acetyltransferase 10 isoform b	gi|221316741	17	12	1.4167
probable ATP-dependent RNA helicase DDX5	gi|4758138 (+3)	10	7	1.4286
nucleophosmin isoform 1	gi|10835063	23	16	1.4375
PREDICTED: double-stranded RNA-specific adenosine deaminase isoform X4	gi|578800406 (+3)	13	9	1.4444
drebrin isoform a	gi|18426915	13	9	1.4444
X-ray repair cross-complementing protein 5	gi|10863945	19	13	1.4615
heterogeneous nuclear ribonucleoprotein R isoform 2	gi|5031755 (+1)	24	16	1.5
heterogeneous nuclear ribonucleoprotein K isoform b	gi|14165435 (+1)	24	16	1.5
heat shock 70 kDa protein 1A/1B	gi|167466173 (+1)	21	14	1.5
unconventional myosin-Ic isoform a	gi|124494238 (+2)	15	10	1.5
heterogeneous nuclear ribonucleoprotein H3 isoform a	gi|14141157 (+5)	6	4	1.5
nucleolar complex protein 2 homolog	gi|157694511	9	6	1.5

ruvB-like 2	gi|5730023	9	6	1.5
GTP-binding nuclear protein Ran isoform 1	gi|5453555	6	4	1.5
FACT complex subunit SPT16	gi|6005757 (+1)	6	4	1.5
RNA 3'-terminal phosphate cyclase-like protein isoform a	gi|157426877	6	4	1.5
emerin	gi|4557553	6	4	1.5
probable 28S rRNA (cytosine(4447)-C(5))-methyltransferase isoform 2	gi|385198059 (+2)	17	11	1.5455
polypyrimidine tract-binding protein 1 isoform b	gi|14165464 (+4)	17	11	1.5455
heterogeneous nuclear ribonucleoproteins C1/C2 isoform b	gi|117190174 (+3)	25	16	1.5625
lamin-B2	gi|388240801	22	14	1.5714
nucleolar protein 58	gi|7706254	24	15	1.6
guanine nucleotide-binding protein-like 3 isoform 1	gi|45593130 (+2)	8	5	1.6
ATP-dependent RNA helicase DDX3X isoform 2	gi|301171467 (+2)	8	5	1.6
chromobox protein homolog 3	gi|15082258 (+2)	8	5	1.6
ribosome biogenesis protein WDR12	gi|217330644	8	5	1.6
PREDICTED: splicing factor 3B subunit 2 isoform X1	gi|530396224 (+2)	8	5	1.6
heterogeneous nuclear ribonucleoprotein L isoform a	gi|52632383	21	13	1.6154
rRNA 2'-O-methyltransferase fibrillarin	gi|12056465 (+4)	15	9	1.6667
DNA damage-binding protein 1	gi|148529014	10	6	1.6667
nucleolar and coiled-body phosphoprotein 1 isoform 2	gi|148596949 (+3)	10	6	1.6667
alpha-internexin	gi|14249342	10	6	1.6667
MICOS complex subunit MIC60 isoform 2	gi|154354962 (+5)	5	3	1.6667
60S ribosomal protein L13 isoform 1	gi|15431295 (+1)	5	3	1.6667
pogo transposable element with ZNF domain isoform 3	gi|302699211 (+11)	5	3	1.6667
U2 small nuclear ribonucleoprotein A'	gi|50593002	5	3	1.6667
60S ribosomal protein L18 isoform 1	gi|4506607	5	3	1.6667
ribosome production factor 2 homolog isoform 1	gi|39930469 (+1)	5	3	1.6667
H/ACA ribonucleoprotein complex subunit 2 isoform a	gi|8923444	5	3	1.6667
40S ribosomal protein S23	gi|4506701	5	3	1.6667
PREDICTED: heterogeneous nuclear ribonucleoprotein M isoform X1	gi|530427501 (+1)	22	13	1.6923
RNA-binding protein 14 isoform 1	gi|5454064	17	10	1.7
PREDICTED: nuclear pore complex protein Nup107 isoform X1	gi|530400597 (+1)	12	7	1.7143

heterogeneous nuclear ribonucleoprotein U isoform b	gi|14141161	26	15	1.7333
lamin-B1 isoform 1	gi|5031877	33	19	1.7368
ATP-dependent RNA helicase A	gi|100913206	35	20	1.75
ribosome biogenesis protein BRX1 homolog	gi|55770900	7	4	1.75
targeting protein for Xklp2	gi|20127519 (+4)	7	4	1.75
lamin isoform A	gi|27436946	37	21	1.7619
probable ATP-dependent RNA helicase DDX17 isoform 1	gi|38201710	16	9	1.7778
PREDICTED: treacle protein isoform X1	gi|530380665 (+2)	18	10	1.8
probable ATP-dependent RNA helicase DDX27	gi|224593278 (+1)	9	5	1.8
far upstream element-binding protein 2	gi|154355000 (+2)	9	5	1.8
heterogeneous nuclear ribonucleoprotein U-like protein 1 isoform d	gi|21536320 (+12)	9	5	1.8
KH domain-containing, RNA-binding, signal transduction-associated protein 1 isoform 1	gi|5730027	9	5	1.8
serine/arginine-rich splicing factor 1 isoform 1	gi|5902076	9	5	1.8
heterogeneous nuclear ribonucleoproteins A2/B1 isoform B1	gi|14043072 (+1)	56	31	1.8065
matrin-3 isoform a	gi|21626466 (+3)	29	16	1.8125
DNA topoisomerase 2-alpha	gi|19913406 (+1)	20	11	1.8182
nucleoprotein TPR	gi|114155142	31	17	1.8235
keratin, type I cytoskeletal 10	gi|195972866 (+1)	33	18	1.8333
interleukin enhancer-binding factor 3 isoform d	gi|212549553 (+1)	33	18	1.8333
RNA-binding motif protein, X chromosome isoform 1	gi|56699409	11	6	1.8333
pre-rRNA processing protein FTSJ3	gi|194097365	11	6	1.8333
ruvB-like 1	gi|4506753	11	6	1.8333
nucleolar GTP-binding protein 1	gi|55953087	13	7	1.8571
heterogeneous nuclear ribonucleoprotein Q isoform 1	gi|228008291 (+1)	15	8	1.875
H/ACA ribonucleoprotein complex subunit 4 isoform 1	gi|4503337	17	9	1.8889
mediator of DNA damage checkpoint protein 1	gi|132626688 (+47)	36	19	1.8947
keratin, type II cytoskeletal 2 epidermal	gi|47132620	19	10	1.9

nuclear pore membrane glycoprotein 210 precursor	gi|27477134	14	7	2
SWI/SNF-related matrix-associated actin-dependent regulator of chromatin subfamily A member 5	gi|325651836	8	4	2
WD repeat-containing protein 36	gi|21281677	14	7	2
core histone macro-H2A.2	gi|8923920	12	6	2
putative pre-mRNA-splicing factor ATP-dependent RNA helicase DHX15	gi|68509926	8	4	2
U3 small nucleolar RNA-interacting protein 2	gi|4759276	8	4	2
U3 small nucleolar ribonucleoprotein protein MPP10	gi|31317305	8	4	2
nuclear pore glycoprotein p62	gi|24497603 (+4)	8	4	2
DNA replication licensing factor MCM7 isoform 1	gi|33469968	8	4	2
reticulocalbin-1 precursor	gi|4506455	6	3	2
proline-, glutamic acid- and leucine-rich protein 1 isoform 1	gi|503774453	8	4	2
nucleolar transcription factor 1 isoform b	gi|115529449 (+5)	6	3	2
polymerase delta-interacting protein 3 isoform 1	gi|29837655 (+2)	6	3	2
actin-like protein 6A isoform 1	gi|4757718	6	3	2
nucleolar protein 56	gi|32483374	21	10	2.1
heterogeneous nuclear ribonucleoprotein A3	gi|34740329 (+2)	19	9	2.1111
nuclear pore complex protein Nup155 isoform 1	gi|24430149 (+1)	13	6	2.1667
thyroid hormone receptor-associated protein 3	gi|167234419	13	6	2.1667
structural maintenance of chromosomes protein 3	gi|4885399	13	6	2.1667
HEAT repeat-containing protein 1	gi|73695475 (+1)	24	11	2.1818
core histone macro-H2A.1 isoform 2	gi|4758496 (+5)	33	15	2.2
PREDICTED: pescadillo homolog isoform X1	gi|578837026 (+1)	11	5	2.2
nucleolar complex protein 4 homolog	gi|13129068	11	5	2.2
scaffold attachment factor B1 isoform 3	gi|21264343 (+1)	20	9	2.2222
heterogeneous nuclear ribonucleoprotein A1 isoform a	gi|4504445	36	16	2.25
heterogeneous nuclear ribonucleoprotein U-like protein 2	gi|118601081	9	4	2.25
PC4 and SFRS1-interacting protein isoform 2	gi|190014588 (+1)	9	4	2.25
probable rRNA-processing protein EBP2 isoform 2	gi|237649015	9	4	2.25
spliceosome RNA helicase DDX39B	gi|18375623 (+1)	9	4	2.25
PREDICTED: RNA-binding protein 28 isoform X1	gi|767948194	9	4	2.25
nuclear pore complex protein Nup205	gi|57634534	25	11	2.2727
myb-binding protein 1A isoform 2	gi|157694492 (+1)	23	10	2.3
keratin, type I cytoskeletal 9	gi|55956899	30	13	2.3077
ATP-dependent RNA helicase DDX18	gi|38327634	14	6	2.3333

probable ATP-dependent RNA helicase DDX56 isoform 2	gi|380692328 (+1)	7	3	2.3333
importin subunit alpha-1	gi|4504897 (+1)	7	3	2.3333
DNA replication licensing factor MCM3 isoform 1	gi|394582093	7	3	2.3333
PREDICTED: sister chromatid cohesion protein PDS5 homolog B isoform X3	gi|530402180 (+4)	7	3	2.3333
E3 SUMO-protein ligase RanBP2	gi|150418007 (+5)	33	14	2.3571
transducin beta-like protein 3	gi|19913369	12	5	2.4
splicing factor 3B subunit 3	gi|54112121	12	5	2.4
periodic tryptophan protein 2 homolog	gi|48762926 (+2)	12	5	2.4
deoxynucleotidyltransferase terminal-interacting protein 2	gi|54633315	12	5	2.4
heterogeneous nuclear ribonucleoprotein D-like isoform a	gi|14110407 (+1)	12	5	2.4
U5 small nuclear ribonucleoprotein 200 kDa helicase	gi|40217847	29	12	2.4167
histone H1.2	gi|4885375	27	11	2.4545
regulator of chromosome condensation isoform c	gi|114796642 (+3)	20	8	2.5
pumilio domain-containing protein KIAA0020	gi|109948283	10	4	2.5
bcl-2-associated transcription factor 1 isoform 4	gi|666335584 (+1)	8	3	2.6667
histone-binding protein RBBP4 isoform a	gi|5032027	8	3	2.6667
RNA-binding protein FUS isoform 3	gi|283135173 (+5)	8	3	2.6667
splicing factor 3B subunit 1 isoform 1	gi|54112117	14	5	2.8
ran GTPase-activating protein 1	gi|4506411 (+7)	14	5	2.8
nuclear pore complex protein Nup93 isoform 1	gi|208609990 (+1)	17	6	2.8333
tyrosine-protein kinase BAZ1B	gi|14670392	15	5	3
probable ATP-dependent RNA helicase DDX52 isoform 1	gi|612407837 (+2)	12	4	3
nucleoporin p54 isoform 1	gi|26051237	9	3	3
60S ribosomal protein L7-like 1	gi|50053872 (+1)	9	3	3
zinc finger RNA-binding protein	gi|34101286	16	5	3.2
RRP12-like protein isoform 1	gi|223278379	23	7	3.2857
histone H4	gi|11415030 (+13)	106	32	3.3125
histone H2B type 1-J	gi|20336754 (+1)	53	16	3.3125
DNA topoisomerase 1	gi|11225260 (+1)	10	3	3.3333
ribosome biogenesis protein BOP1	gi|21327667	14	4	3.5
PREDICTED: heterochromatin protein 1-binding protein 3 isoform X1	gi|530361109 (+4)	14	4	3.5

PREDICTED: nuclear mitotic apparatus protein 1 isoform X1	gi|578821444 (+12)	54	15	3.6
PREDICTED: protein RRP5 homolog isoform X2	gi|530393314 (+3)	33	9	3.6667
PREDICTED: apoptotic chromatin condensation inducer in the nucleus isoform X4	gi|767980045	15	4	3.75
pre-mRNA-processing-splicing factor 8	gi|91208426	20	5	4
telomere-associated protein RIF1 isoform 2	gi|295054210 (+6)	12	3	4
nuclear pore complex protein Nup98-Nup96 isoform 1	gi|21264365 (+7)	18	4	4.5
polyubiquitin-B precursor	gi|11024714 (+6)	14	3	4.6667
antigen KI-67 isoform 1	gi|103472005	37	7	5.2857
nuclear pore complex protein Nup153 isoform 2	gi|24430146 (+1)	17	3	5.6667
structural maintenance of chromosomes protein 1A isoform 1	gi|30581135	17	3	5.6667
nuclear pore complex protein Nup133	gi|26051235	19	0	INF
protein ELYS	gi|262359929 (+2)	18	0	INF
CCAAT/enhancer-binding protein zeta	gi|42542392	14	0	INF
splicing factor 3A subunit 1	gi|5032087	11	0	INF
small subunit processome component 20 homolog	gi|120587023	9	0	INF
SUN domain-containing protein 1 isoform a	gi|195972890	13	0	INF
RNA-binding protein 34 isoform 1	gi|238859597	14	0	INF
probable ATP-dependent RNA helicase DDX10	gi|13514831	11	0	INF
nucleolar protein 14 isoform 1	gi|55769587 (+2)	10	0	INF
ribosomal RNA processing protein 1 homolog B	gi|57863269	11	0	INF
nucleolar protein 8 isoform a	gi|46048234 (+4)	3	0	INF
PREDICTED: nuclear pore complex protein Nup214 isoform X3	gi|578817905	14	0	INF
U3 small nucleolar RNA-associated protein 14 homolog A isoform 1	gi|21361348	15	0	INF
ribosome biogenesis protein BMS1 homolog	gi|224589071 (+2)	14	0	INF
bystin	gi|51173724	7	0	INF
protein SON isoform F	gi|520261969	8	0	INF
60S ribosomal protein L13a isoform 1	gi|6912634	4	0	INF
cirhin	gi|186928847	10	0	INF
keratin, type I cytoskeletal 14	gi|15431310	10	0	INF
transcription elongation factor SPT6	gi|27597090 (+1)	11	0	INF
WD repeat-containing protein 75 isoform 1	gi|29789283	8	0	INF
serine/arginine-rich splicing factor 9	gi|4506903	9	0	INF
nucleolar protein 11 isoform 1	gi|21361468	8	0	INF
nuclear pore complex protein Nup160	gi|54859722	11	0	INF

eukaryotic initiation factor 4A-III	gi|7661920	9	0	INF
keratin, type II cytoskeletal 6A	gi|5031839	8	0	INF
MKI67 FHA domain-interacting nucleolar phosphoprotein	gi|222352111	7	0	INF
WD repeat-containing protein 46 isoform 1	gi|256773176	8	0	INF
zinc finger protein 638 isoform 1	gi|21626468 (+6)	6	0	INF
U3 small nucleolar RNA-associated protein 15 homolog isoform 1	gi|50980309 (+1)	8	0	INF
nucleolar protein 6 alpha isoform	gi|18644728	6	0	INF
aladin isoform 1	gi|12962937 (+1)	6	0	INF
DNA-directed RNA polymerase II subunit RPB1	gi|4505939	5	0	INF
remodeling and spacing factor 1	gi|38788333 (+1)	7	0	INF
PPAN-P2RY11 protein isoform 2	gi|310923196 (+2)	4	0	INF
guanine nucleotide-binding protein subunit beta-2-like 1	gi|5174447	3	0	INF
transcription factor A, mitochondrial isoform 1 precursor	gi|4507401	4	0	INF
heterogeneous nuclear ribonucleoprotein A0	gi|5803036	6	0	INF
transcription intermediary factor 1-beta	gi|5032179	5	0	INF
splicing factor 3A subunit 3	gi|5803167	5	0	INF
DDB1- and CUL4-associated factor 13	gi|229892270	7	0	INF
nuclear RNA export factor 1 isoform 1	gi|15487670	5	0	INF
probable U3 small nucleolar RNA-associated protein 11	gi|156415994	6	0	INF
cleavage and polyadenylation specificity factor subunit 1	gi|56676371 (+5)	8	0	INF
ATP-dependent RNA helicase DDX54 isoform 1	gi|164419743	8	0	INF
ribosomal RNA-processing protein 8	gi|12758125 (+1)	9	0	INF
60S ribosomal protein L15 isoform 1	gi|15431293 (+5)	4	0	INF
elongation factor 2	gi|4503483	4	0	INF
zinc finger protein 512 isoform a	gi|40217790 (+1)	8	0	INF
high mobility group protein HMGI-C isoform a	gi|4504431	6	0	INF
nucleolar complex protein 3 homolog	gi|20806097	5	0	INF
PREDICTED: chromodomain-helicase-DNA-binding protein 4 isoform X6	gi|578822562	5	0	INF
YLP motif-containing protein 1	gi|146134388	6	0	INF
helicase SRCAP	gi|146219843	7	0	INF

inner centromere protein isoform 1	gi|102467235 (+6)	5	0	INF
SAFB-like transcription modulator isoform b	gi|62244004 (+3)	7	0	INF
guanine nucleotide-binding protein G(k) subunit alpha	gi|5729850	6	0	INF
nuclear pore complex protein Nup85 isoform 1	gi|13376259 (+2)	8	0	INF
aurora kinase B isoform 3	gi|548960892 (+1)	8	0	INF
nucleoporin NUP188 homolog	gi|62955803	6	0	INF
nuclear valosin-containing protein-like isoform 4	gi|341865581 (+3)	7	0	INF
plasminogen activator inhibitor 1 RNA-binding protein isoform 1	gi|66346679 (+3)	4	0	INF
probable ATP-dependent RNA helicase DDX47 isoform 1	gi|20149629 (+1)	5	0	INF
60S ribosomal protein L17 isoform a	gi|313569768 (+6)	4	0	INF
ribosome biogenesis protein NSA2 homolog isoform 1	gi|7662677 (+1)	4	0	INF
RNA-binding protein 12B	gi|118722349 (+5)	6	0	INF
ribosomal RNA processing protein 1 homolog A	gi|4503247 (+1)	5	0	INF
double-strand-break repair protein rad21 homolog	gi|5453994	6	0	INF
PREDICTED: PH-interacting protein isoform X3	gi|767943077	5	0	INF
60S ribosomal protein L27	gi|4506623	4	0	INF
ATP-dependent RNA helicase DDX24	gi|9966805	5	0	INF
CTD small phosphatase-like protein 2	gi|100815975 (+3)	4	0	INF
PREDICTED: serine/arginine repetitive matrix protein 2 isoform X2	gi|530407861	3	0	INF
PREDICTED: ribosomal RNA small subunit methyltransferase NEP1 isoform X1	gi|767971201	6	0	INF
surfeit locus protein 6 isoform 1	gi|19557702	5	0	INF
histone-lysine N-methyltransferase 2A isoform 1 precursor	gi|308199413 (+4)	4	0	INF
PREDICTED: nucleoporin SEH1 isoform X4	gi|530424957 (+5)	5	0	INF
ATP-dependent RNA helicase DDX50	gi|13129006 (+2)	4	0	INF
PREDICTED: p21-activated protein kinase-interacting protein 1 isoform X3	gi|530382198 (+4)	6	0	INF
replication protein A 70 kDa DNA-binding subunit	gi|4506583	6	0	INF
nucleolar protein 10 isoform 1	gi|171460958	6	0	INF
transcription activator BRG1 isoform B	gi|192807312 (+17)	4	0	INF
nucleoporin Nup37	gi|34222121 (+1)	4	0	INF

eukaryotic translation initiation factor 6 isoform a	gi|31563378 (+2)	4	0	INF
nucleoporin NUP53 isoform a	gi|31982904 (+5)	6	0	INF
serine/arginine-rich splicing factor 10 isoform 2	gi|16905517 (+7)	4	0	INF
60S ribosomal protein L24	gi|4506619	3	0	INF
cleavage stimulation factor subunit 3 isoform 1	gi|4557495	5	0	INF
cell cycle and apoptosis regulator protein 2	gi|24432106 (+2)	3	0	INF
regulation of nuclear pre-mRNA domain-containing protein 1B	gi|11034845	5	0	INF
something about silencing protein 10	gi|9966799	5	0	INF
kinesin-like protein KIF22 isoform 1	gi|6453818	6	0	INF
U3 small nucleolar RNA-associated protein 6 homolog	gi|49574529	5	0	INF
nuclear pore complex protein Nup50 isoform a	gi|24497447 (+7)	6	0	INF
U4/U6.U5 tri-snRNP-associated protein 1	gi|10863889	4	0	INF
protein FAM208A isoform a	gi|163838631 (+3)	5	0	INF
chromobox protein homolog 5	gi|188035908 (+2)	3	0	INF
RNA-binding protein PNO1	gi|10047140	3	0	INF
glutamine--tRNA ligase isoform b	gi|441478305 (+1)	3	0	INF
coiled-coil domain-containing protein 86	gi|13129104	4	0	INF
keratin, type II cytoskeletal 5	gi|119395754	4	0	INF
far upstream element-binding protein 3	gi|100816392 (+3)	5	0	INF
FACT complex subunit SSRP1	gi|4507241 (+2)	3	0	INF
PREDICTED: DNA topoisomerase 2-beta isoform X1	gi|530373069 (+1)	3	0	INF
PREDICTED: cleavage and polyadenylation specificity factor subunit 7 isoform X5	gi|530397405 (+2)	3	0	INF
PREDICTED: polycomb protein EED isoform X1	gi|767968954 (+1)	3	0	INF
mRNA turnover protein 4 homolog	gi|18490987 (+1)	4	0	INF
SWI/SNF complex subunit SMARCC2 isoform c	gi|194363725 (+5)	4	0	INF
A-kinase anchor protein 8	gi|5031579 (+2)	4	0	INF
protein AATF	gi|7657013 (+2)	6	0	INF
PREDICTED: importin subunit alpha-5 isoform X2	gi|767926661	5	0	INF
cohesin subunit SA-2 isoform a	gi|112789526 (+13)	3	0	INF
DNA (cytosine-5)-methyltransferase 3A isoform a	gi|12751473 (+3)	5	0	INF
myelin expression factor 2 isoform a	gi|33620747	4	0	INF
60S ribosomal protein L18a	gi|11415026	3	0	INF
chromobox protein homolog 1	gi|187960037 (+1)	4	0	INF
cell growth-regulating nucleolar protein	gi|224591430 (+3)	5	0	INF
DNA replication licensing factor MCM5	gi|23510448	3	0	INF
histone H1x	gi|5174449	3	0	INF
nuclear pore complex protein Nup88	gi|24497453 (+1)	4	0	INF

SUN domain-containing protein 2 isoform a	gi|313760643 (+4)	4	0	INF
serine/arginine repetitive matrix protein 1 isoform 2	gi|42542379 (+13)	4	0	INF
insulin-like growth factor 2 mRNA-binding protein 2 isoform b	gi|56118219 (+2)	4	0	INF
nucleolar MIF4G domain-containing protein 1	gi|61097912	3	0	INF
polyadenylate-binding protein 2	gi|4758876	4	0	INF
H/ACA ribonucleoprotein complex subunit 1	gi|15011916 (+1)	3	0	INF
splicing factor 3B subunit 5	gi|13775200	3	0	INF
electron transfer flavoprotein subunit alpha, mitochondrial isoform b	gi|189181759 (+1)	4	0	INF
nucleolar GTP-binding protein 2	gi|7019419 (+1)	4	0	INF
regulation of nuclear pre-mRNA domain-containing protein 1A isoform 1	gi|21361709 (+1)	4	0	INF
protein mago nashi homolog	gi|4505087 (+1)	5	0	INF
spermatid perinuclear RNA-binding protein isoform 1	gi|21361745 (+3)	3	0	INF
neuroguidin isoform 1	gi|111038128 (+2)	6	0	INF
keratin, type I cytoskeletal 16	gi|24430192	6	0	INF
WD repeat-containing protein 18	gi|56243583	4	0	INF
DNA replication licensing factor MCM6	gi|7427519	3	0	INF
cold-inducible RNA-binding protein isoform 1	gi|4502847 (+1)	3	0	INF
PREDICTED: methionine--tRNA ligase, cytoplasmic isoform X2	gi|767974264	3	0	INF
small nuclear ribonucleoprotein E isoform 1	gi|4507129	3	0	INF
PREDICTED: double-stranded RNA-binding protein Staufen homolog 1 isoform X2	gi|530418339 (+9)	3	0	INF
protein KRI1 homolog	gi|145580615 (+1)	3	0	INF
60S ribosome subunit biogenesis protein NIP7 homolog isoform 2	gi|313661502 (+1)	3	0	INF
probable RNA-binding protein 19	gi|226497574 (+3)	3	0	INF
transcription elongation factor SPT5 isoform b	gi|195546902 (+1)	4	0	INF
cleavage and polyadenylation specificity factor subunit 5	gi|5901926	4	0	INF
PREDICTED: lysine-rich nucleolar protein 1 isoform X3	gi|767988568	4	0	INF
microfibrillar-associated protein 1	gi|50726968	4	0	INF
protein PML isoform 5	gi|109637788 (+4)	3	0	INF
zinc finger CCCH domain-containing protein 14 isoform 5	gi|231570121 (+5)	4	0	INF
DNA-directed RNA polymerase I subunit RPA1	gi|103471997 (+1)	4	0	INF
DNA methyltransferase 1-associated protein 1	gi|13123776 (+7)	4	0	INF
poly(A)-specific ribonuclease PARN isoform 2	gi|197333695 (+8)	4	0	INF
polycomb protein SUZ12	gi|197333809 (+1)	4	0	INF
transcription factor 20 isoform 2	gi|31652242 (+15)	5	0	INF

cleavage and polyadenylation specificity factor subunit 2	gi|34101288 (+1)	4	0	INF
RNA-binding protein 8A	gi|4826972	4	0	INF
serine/threonine-protein kinase PRP4 homolog	gi|89276756	4	0	INF
5'-3' exoribonuclease 2	gi|18860916 (+1)	3	0	INF
methyl-CpG-binding protein 2 isoform 2	gi|160707950 (+6)	3	0	INF
polynucleotide 5'-hydroxyl-kinase NOL9	gi|40217805 (+3)	3	0	INF
torsin-1A-interacting protein 1 isoform 1	gi|389886539 (+1)	3	0	INF
nuclear cap-binding protein subunit 1	gi|4505343 (+5)	3	0	INF
pre-mRNA 3'-end-processing factor FIP1 isoform 2	gi|201023339 (+17)	3	0	INF
DNA-directed RNA polymerases I, II, and III subunit RPABC1	gi|14589951 (+1)	3	0	INF
E3 ubiquitin-protein ligase UHRF1 isoform 2	gi|115430233 (+5)	4	0	INF
DNA replication licensing factor MCM2	gi|33356547	3	0	INF
germinal-center associated nuclear protein	gi|19923191 (+5)	3	0	INF
RNA-binding protein 10 isoform 1	gi|20127479 (+3)	3	0	INF
DNA-directed RNA polymerase I subunit RPA2 isoform 2	gi|212286172 (+2)	3	0	INF
digestive organ expansion factor homolog	gi|75677335	3	0	INF
RNA exonuclease 4 isoform 1	gi|76781492	3	0	INF
splicing factor 3B subunit 6	gi|7706326	3	0	INF
importin subunit alpha-3	gi|4504901	3	0	INF
AT-rich interactive domain-containing protein 2	gi|56549668 (+1)	3	0	INF
RNA binding protein fox-1 homolog 2 isoform 5	gi|133925803 (+12)	3	0	INF
DNA replication licensing factor MCM4	gi|33469917 (+2)	3	0	INF

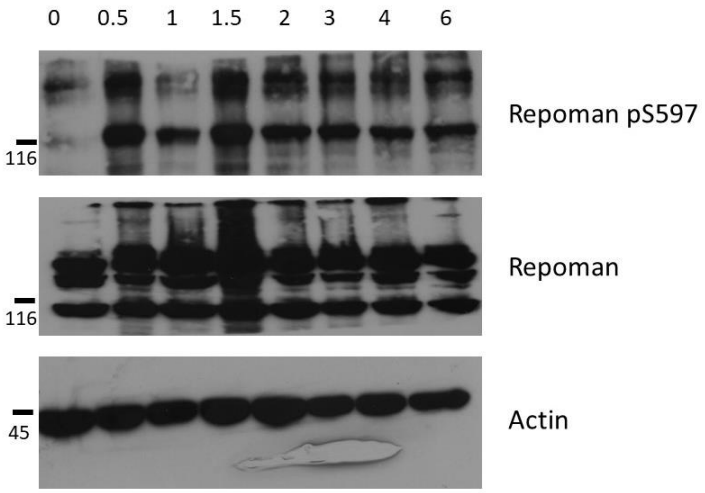

Figure AB.1: Repoman is phosphorylated on pS597 in HEK293T cells under asynchronous and mitotic conditions. HEK293T cells were synchronized using a thymidine/nocodazole block. Cells were collected at various time points after release from the block as indicated by the numbers above the western blot. Cell lysate was as previously described, quantified using Bradford assay and equal amounts of cell lysate were resolved on SDS PAGE and transferred to nitrocellulose membrane. Western blotting was performed with anti actin antibody to shows equal loading of samples. Western blotting was also performed with anti Repoman and anti Repoman pS597 antibodies. Time point 0 indicates asynchronous samples.

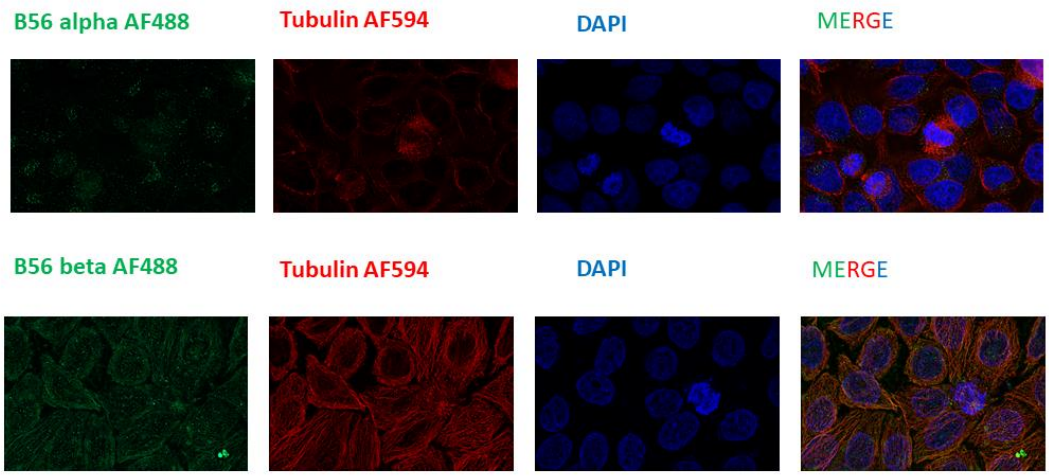

Figure AB.2: Localization of B56 alpha and B56 beta in HeLa cells. Hela cells were grown on coverslips and fixed in 2% paraformaldehyde. Cells were permeabilized then stained for B56 alpha or B56 beta (AF488 or green) and tubulin (AF594 or red). Nuclei were stained with DAPI (blue). Cells were imaged using oil immersion 100X objective on a Zeiss Axio Imager Z2 microscope.

References:

1 Krebs, E. G., Kent, A. B. & Fischer, E. H. The muscle phosphorylase b kinase reaction. *The Journal of biological chemistry* **231**, 73-83 (1958).

2 Fischer, E. H. & Krebs, E. G. Conversion of phosphorylase b to phosphorylase a in muscle extracts. *The Journal of biological chemistry* **216**, 121-132 (1955).

3 Krebs, E. G. & Fischer, E. H. Phosphorylase activity of skeletal muscle extracts. *The Journal of biological chemistry* **216**, 113-120 (1955).

4 Engin, A. Human Protein Kinases and Obesity. *Advances in experimental medicine and biology* **960**, 111-134, doi:10.1007/978-3-319-48382-5_5 (2017).

5 Mustelin, T., Vang, T. & Bottini, N. Protein tyrosine phosphatases and the immune response. *Nature reviews. Immunology* **5**, 43-57, doi:10.1038/nri1530 (2005).

6 Dolton, G. M., Sathish, J. G. & Matthews, R. J. Protein tyrosine phosphatases as negative regulators of the immune response. *Biochemical Society transactions* **34**, 1041-1045, doi:10.1042/BST0341041 (2006).

7 Mansuy, I. M. & Shenolikar, S. Protein serine/threonine phosphatases in neuronal plasticity and disorders of learning and memory. *Trends in neurosciences* **29**, 679-686, doi:10.1016/j.tins.2006.10.004 (2006).

8 Sharma, K. *et al.* Ultradeep human phosphoproteome reveals a distinct regulatory nature of Tyr and Ser/Thr-based signaling. *Cell reports* **8**, 1583-1594, doi:10.1016/j.celrep.2014.07.036 (2014).

9 Moorhead, G. B., Trinkle-Mulcahy, L. & Ulke-Lemee, A. Emerging roles of nuclear protein phosphatases. *Nature reviews. Molecular cell biology* **8**, 234-244, doi:10.1038/nrm2126 (2007).

10 Cohen, P. The role of protein phosphorylation in human health and disease. The Sir Hans Krebs Medal Lecture. *European journal of biochemistry* **268**, 5001-5010 (2001).

11 Cohen, P. Protein kinases--the major drug targets of the twenty-first century? *Nature reviews. Drug discovery* **1**, 309-315, doi:10.1038/nrd773 (2002).

12 Li, B., Liu, Y., Uno, T. & Gray, N. Creating chemical diversity to target protein kinases. *Combinatorial chemistry & high throughput screening* **7**, 453-472 (2004).

13 Lazo, J. S., McQueeney, K. E. & Sharlow, E. R. New Approaches to Difficult Drug Targets: The Phosphatase Story. *SLAS discovery : advancing life sciences R & D*, 2472555217721142, doi:10.1177/2472555217721142 (2017).

14 Manning, G., Plowman, G. D., Hunter, T. & Sudarsanam, S. Evolution of protein kinase signaling from yeast to man. *Trends in biochemical sciences* **27**, 514-520 (2002).

15 Knighton, D. R. *et al.* Crystal structure of the catalytic subunit of cyclic adenosine monophosphate-dependent protein kinase. *Science* **253**, 407-414 (1991).

16 Taylor, S. S. & Kornev, A. P. Protein kinases: evolution of dynamic regulatory proteins. *Trends in biochemical sciences* **36**, 65-77, doi:10.1016/j.tibs.2010.09.006 (2011).
17 Zheng, J. *et al.* Crystal structure of the catalytic subunit of cAMP-dependent protein kinase complexed with MgATP and peptide inhibitor. *Biochemistry* **32**, 2154-2161 (1993).
18 Johnson, L. N., Noble, M. E. & Owen, D. J. Active and inactive protein kinases: structural basis for regulation. *Cell* **85**, 149-158 (1996).
19 Chen, M. J., Dixon, J. E. & Manning, G. Genomics and evolution of protein phosphatases. *Science signaling* **10**, doi:10.1126/scisignal.aag1796 (2017).
20 Manning, G., Whyte, D. B., Martinez, R., Hunter, T. & Sudarsanam, S. The protein kinase complement of the human genome. *Science* **298**, 1912-1934, doi:10.1126/science.1075762 (2002).
21 Alonso, A. *et al.* Protein tyrosine phosphatases in the human genome. *Cell* **117**, 699-711, doi:10.1016/j.cell.2004.05.018 (2004).
22 Cohen, P. T. Protein phosphatase 1--targeted in many directions. *Journal of cell science* **115**, 241-256 (2002).
23 Lam, P. K., Yang, M. & Lam, M. H. Toxicology and evaluation of microcystins. *Therapeutic drug monitoring* **22**, 69-72 (2000).
24 Bialojan, C. & Takai, A. Inhibitory effect of a marine-sponge toxin, okadaic acid, on protein phosphatases. Specificity and kinetics. *The Biochemical journal* **256**, 283-290 (1988).
25 Li, X., Wilmanns, M., Thornton, J. & Kohn, M. Elucidating human phosphatase-substrate networks. *Science signaling* **6**, rs10, doi:10.1126/scisignal.2003203 (2013).
26 Cohen, P. The structure and regulation of protein phosphatases. *Annual review of biochemistry* **58**, 453-508, doi:10.1146/annurev.bi.58.070189.002321 (1989).
27 Swingle, M. R., Honkanen, R. E. & Ciszak, E. M. Structural basis for the catalytic activity of human serine/threonine protein phosphatase-5. *The Journal of biological chemistry* **279**, 33992-33999, doi:10.1074/jbc.M402855200 (2004).
28 Egloff, M. P., Cohen, P. T., Reinemer, P. & Barford, D. Crystal structure of the catalytic subunit of human protein phosphatase 1 and its complex with tungstate. *Journal of molecular biology* **254**, 942-959, doi:10.1006/jmbi.1995.0667 (1995).
29 Goldberg, J. *et al.* Three-dimensional structure of the catalytic subunit of protein serine/threonine phosphatase-1. *Nature* **376**, 745-753, doi:10.1038/376745a0 (1995).
30 Kresge, N., Simoni, R. D. & Hill, R. L. The process of reversible phosphorylation: the work of Edmond H. Fischer. *The Journal of biological chemistry* **286**, e1-2 (2011).
31 Roy, J. & Cyert, M. S. Cracking the phosphatase code: docking interactions determine substrate specificity. *Science signaling* **2**, re9, doi:10.1126/scisignal.2100re9 (2009).

32 Hendrickx, A. *et al.* Docking motif-guided mapping of the interactome of protein phosphatase-1. *Chemistry & biology* **16**, 365-371, doi:10.1016/j.chembiol.2009.02.012 (2009).
33 Bollen, M., Peti, W., Ragusa, M. J. & Beullens, M. The extended PP1 toolkit: designed to create specificity. *Trends in biochemical sciences* **35**, 450-458, doi:10.1016/j.tibs.2010.03.002 (2010).
34 Heroes, E. *et al.* The PP1 binding code: a molecular-lego strategy that governs specificity. *The FEBS journal* **280**, 584-595, doi:10.1111/j.1742-4658.2012.08547.x (2013).
35 Cannon, J. F. How phosphorylation activates the protein phosphatase-1 * inhibitor-2 complex. *Biochimica et biophysica acta* **1834**, 71-86, doi:10.1016/j.bbapap.2012.09.003 (2013).
36 Hertz, E. P. T. *et al.* A Conserved Motif Provides Binding Specificity to the PP2A-B56 Phosphatase. *Molecular cell* **63**, 686-695, doi:10.1016/j.molcel.2016.06.024 (2016).
37 Tonks, N. K. Protein tyrosine phosphatases: from genes, to function, to disease. *Nature reviews. Molecular cell biology* **7**, 833-846, doi:10.1038/nrm2039 (2006).
38 Ruvolo, P. P. Role of protein phosphatases in the cancer microenvironment. *Biochimica et biophysica acta. Molecular cell research*, doi:10.1016/j.bbamcr.2018.07.006 (2018).
39 He, R. J., Yu, Z. H., Zhang, R. Y. & Zhang, Z. Y. Protein tyrosine phosphatases as potential therapeutic targets. *Acta pharmacologica Sinica* **35**, 1227-1246, doi:10.1038/aps.2014.80 (2014).
40 Janssens, V. & Goris, J. Protein phosphatase 2A: a highly regulated family of serine/threonine phosphatases implicated in cell growth and signalling. *The Biochemical journal* **353**, 417-439 (2001).
41 Xu, Y., Chen, Y., Zhang, P., Jeffrey, P. D. & Shi, Y. Structure of a protein phosphatase 2A holoenzyme: insights into B55-mediated Tau dephosphorylation. *Molecular cell* **31**, 873-885, doi:10.1016/j.molcel.2008.08.006 (2008).
42 Xu, Y. *et al.* Structure of the protein phosphatase 2A holoenzyme. *Cell* **127**, 1239-1251, doi:10.1016/j.cell.2006.11.033 (2006).
43 Arino, J., Woon, C. W., Brautigan, D. L., Miller, T. B., Jr. & Johnson, G. L. Human liver phosphatase 2A: cDNA and amino acid sequence of two catalytic subunit isotypes. *Proceedings of the National Academy of Sciences of the United States of America* **85**, 4252-4256 (1988).
44 Gotz, J., Probst, A., Ehler, E., Hemmings, B. & Kues, W. Delayed embryonic lethality in mice lacking protein phosphatase 2A catalytic subunit Calpha. *Proceedings of the National Academy of Sciences of the United States of America* **95**, 12370-12375 (1998).
45 Baharians, Z. & Schonthal, A. H. Autoregulation of protein phosphatase type 2A expression. *The Journal of biological chemistry* **273**, 19019-19024 (1998).
46 Longin, S. *et al.* Selection of protein phosphatase 2A regulatory subunits is mediated by the C terminus of the catalytic Subunit. *The Journal of biological chemistry* **282**, 26971-26980, doi:10.1074/jbc.M704059200 (2007).

47 Xie, H. & Clarke, S. Protein phosphatase 2A is reversibly modified by methyl esterification at its C-terminal leucine residue in bovine brain. *The Journal of biological chemistry* **269**, 1981-1984 (1994).
48 Xing, Y. *et al.* Structural mechanism of demethylation and inactivation of protein phosphatase 2A. *Cell* **133**, 154-163, doi:10.1016/j.cell.2008.02.041 (2008).
49 Ogris, E., Sontag, E., Wadzinski, B. & Narla, G. Specificity of research antibodies: "trust is good, validation is better". *Human pathology* **72**, 199-201, doi:10.1016/j.humpath.2017.12.003 (2018).
50 Hemmings, B. A. *et al.* alpha- and beta-forms of the 65-kDa subunit of protein phosphatase 2A have a similar 39 amino acid repeating structure. *Biochemistry* **29**, 3166-3173 (1990).
51 Seshacharyulu, P., Pandey, P., Datta, K. & Batra, S. K. Phosphatase: PP2A structural importance, regulation and its aberrant expression in cancer. *Cancer letters* **335**, 9-18, doi:10.1016/j.canlet.2013.02.036 (2013).
52 Wang, F. *et al.* Protein interactomes of protein phosphatase 2A B55 regulatory subunits reveal B55-mediated regulation of replication protein A under replication stress. *Scientific reports* **8**, 2683, doi:10.1038/s41598-018-21040-6 (2018).
53 Eichhorn, P. J., Creyghton, M. P. & Bernards, R. Protein phosphatase 2A regulatory subunits and cancer. *Biochimica et biophysica acta* **1795**, 1-15, doi:10.1016/j.bbcan.2008.05.005 (2009).
54 Corpet, F. Multiple sequence alignment with hierarchical clustering. *Nucleic acids research* **16**, 10881-10890, doi:10.1093/nar/16.22.10881 (1988).
55 Walter, E. & Scott, M. The life and work of Rudolf Virchow 1821-1902: "Cell theory, thrombosis and the sausage duel". *Journal of the Intensive Care Society* **18**, 234-235, doi:10.1177/1751143716663967 (2017).
56 Orlowski, C. C. & Furlanetto, R. W. The mammalian cell cycle in normal and abnormal growth. *Endocrinology and metabolism clinics of North America* **25**, 491-502 (1996).
57 Vermeulen, K., Van Bockstaele, D. R. & Berneman, Z. N. The cell cycle: a review of regulation, deregulation and therapeutic targets in cancer. *Cell proliferation* **36**, 131-149 (2003).
58 Furukawa, Y. Cell cycle regulation of hematopoietic stem cells. *Human cell* **11**, 81-92 (1998).
59 Dunphy, W. G. & Newport, J. W. Unraveling of mitotic control mechanisms. *Cell* **55**, 925-928 (1988).
60 Fukagawa, T. & Earnshaw, W. C. The centromere: chromatin foundation for the kinetochore machinery. *Developmental cell* **30**, 496-508, doi:10.1016/j.devcel.2014.08.016 (2014).
61 Joglekar, A. P. & Kukreja, A. A. How Kinetochore Architecture Shapes the Mechanisms of Its Function. *Current biology : CB* **27**, R816-R824, doi:10.1016/j.cub.2017.06.012 (2017).
62 Etemad, B. & Kops, G. J. Attachment issues: kinetochore transformations and spindle checkpoint silencing. *Current opinion in cell biology* **39**, 101-108, doi:10.1016/j.ceb.2016.02.016 (2016).

63 Rieder, C. L., Cole, R. W., Khodjakov, A. & Sluder, G. The checkpoint delaying anaphase in response to chromosome monoorientation is mediated by an inhibitory signal produced by unattached kinetochores. *The Journal of cell biology* **130**, 941-948 (1995).
64 Musacchio, A. & Salmon, E. D. The spindle-assembly checkpoint in space and time. *Nature reviews. Molecular cell biology* **8**, 379-393, doi:10.1038/nrm2163 (2007).
65 Musacchio, A. The Molecular Biology of Spindle Assembly Checkpoint Signaling Dynamics. *Current biology : CB* **25**, R1002-1018, doi:10.1016/j.cub.2015.08.051 (2015).
66 Sarangapani, K. K. & Asbury, C. L. Catch and release: how do kinetochores hook the right microtubules during mitosis? *Trends in genetics : TIG* **30**, 150-159, doi:10.1016/j.tig.2014.02.004 (2014).
67 Lampson, M. A. & Grishchuk, E. L. Mechanisms to Avoid and Correct Erroneous Kinetochore-Microtubule Attachments. *Biology* **6**, doi:10.3390/biology6010001 (2017).
68 Izawa, D. & Pines, J. Mad2 and the APC/C compete for the same site on Cdc20 to ensure proper chromosome segregation. *The Journal of cell biology* **199**, 27-37, doi:10.1083/jcb.201205170 (2012).
69 Fang, G. Checkpoint protein BubR1 acts synergistically with Mad2 to inhibit anaphase-promoting complex. *Molecular biology of the cell* **13**, 755-766, doi:10.1091/mbc.01-09-0437 (2002).
70 Lara-Gonzalez, P., Scott, M. I., Diez, M., Sen, O. & Taylor, S. S. BubR1 blocks substrate recruitment to the APC/C in a KEN-box-dependent manner. *Journal of cell science* **124**, 4332-4345, doi:10.1242/jcs.094763 (2011).
71 Makrantoni, V. & Marston, A. L. Cohesin and chromosome segregation. *Current biology : CB* **28**, R688-R693, doi:10.1016/j.cub.2018.05.019 (2018).
72 Peters, J. M., Tedeschi, A. & Schmitz, J. The cohesin complex and its roles in chromosome biology. *Genes & development* **22**, 3089-3114, doi:10.1101/gad.1724308 (2008).
73 Kueng, S. *et al.* Wapl controls the dynamic association of cohesin with chromatin. *Cell* **127**, 955-967, doi:10.1016/j.cell.2006.09.040 (2006).
74 Haarhuis, J. H., Elbatsh, A. M. & Rowland, B. D. Cohesin and its regulation: on the logic of X-shaped chromosomes. *Developmental cell* **31**, 7-18, doi:10.1016/j.devcel.2014.09.010 (2014).
75 Mendez, R. & Richter, J. D. Translational control by CPEB: a means to the end. *Nature reviews. Molecular cell biology* **2**, 521-529, doi:10.1038/35080081 (2001).
76 Groisman, I., Jung, M. Y., Sarkissian, M., Cao, Q. & Richter, J. D. Translational control of the embryonic cell cycle. *Cell* **109**, 473-483 (2002).
77 Stonyte, V., Boye, E. & Grallert, B. Regulation of global translation during the cell cycle. *Journal of cell science* **131**, doi:10.1242/jcs.220327 (2018).
78 Afonso, O., Figueiredo, A. C. & Maiato, H. Late mitotic functions of Aurora kinases. *Chromosoma* **126**, 93-103, doi:10.1007/s00412-016-0594-5 (2017).

79 Joukov, V. & De Nicolo, A. Aurora-PLK1 cascades as key signaling modules in the regulation of mitosis. *Science signaling* **11**, doi:10.1126/scisignal.aar4195 (2018).
80 Saurin, A. T. Kinase and Phosphatase Cross-Talk at the Kinetochore. *Frontiers in cell and developmental biology* **6**, 62, doi:10.3389/fcell.2018.00062 (2018).
81 Nasa, I. & Kettenbach, A. N. Coordination of Protein Kinase and Phosphoprotein Phosphatase Activities in Mitosis. *Frontiers in cell and developmental biology* **6**, 30, doi:10.3389/fcell.2018.00030 (2018).
82 Pines, J. & Hunter, T. Human cyclin A is adenovirus E1A-associated protein p60 and behaves differently from cyclin B. *Nature* **346**, 760-763, doi:10.1038/346760a0 (1990).
83 Timofeev, O., Cizmecioglu, O., Settele, F., Kempf, T. & Hoffmann, I. Cdc25 phosphatases are required for timely assembly of CDK1-cyclin B at the G2/M transition. *The Journal of biological chemistry* **285**, 16978-16990, doi:10.1074/jbc.M109.096552 (2010).
84 Strausfeld, U. *et al.* Dephosphorylation and activation of a p34cdc2/cyclin B complex in vitro by human CDC25 protein. *Nature* **351**, 242-245, doi:10.1038/351242a0 (1991).
85 Liu, F., Stanton, J. J., Wu, Z. & Piwnica-Worms, H. The human Myt1 kinase preferentially phosphorylates Cdc2 on threonine 14 and localizes to the endoplasmic reticulum and Golgi complex. *Molecular and cellular biology* **17**, 571-583 (1997).
86 Parker, L. L., Atherton-Fessler, S. & Piwnica-Worms, H. p107wee1 is a dual-specificity kinase that phosphorylates p34cdc2 on tyrosine 15. *Proceedings of the National Academy of Sciences of the United States of America* **89**, 2917-2921 (1992).
87 Ducommun, B. *et al.* cdc2 phosphorylation is required for its interaction with cyclin. *The EMBO journal* **10**, 3311-3319 (1991).
88 Enserink, J. M. & Kolodner, R. D. An overview of Cdk1-controlled targets and processes. *Cell division* **5**, 11, doi:10.1186/1747-1028-5-11 (2010).
89 Holt, L. J. *et al.* Global analysis of Cdk1 substrate phosphorylation sites provides insights into evolution. *Science* **325**, 1682-1686, doi:10.1126/science.1172867 (2009).
90 Ubersax, J. A. *et al.* Targets of the cyclin-dependent kinase Cdk1. *Nature* **425**, 859-864, doi:10.1038/nature02062 (2003).
91 Nigg, E. A. Mitotic kinases as regulators of cell division and its checkpoints. *Nature reviews. Molecular cell biology* **2**, 21-32, doi:10.1038/35048096 (2001).
92 Borisa, A. C. & Bhatt, H. G. A comprehensive review on Aurora kinase: Small molecule inhibitors and clinical trial studies. *European journal of medicinal chemistry* **140**, 1-19, doi:10.1016/j.ejmech.2017.08.045 (2017).
93 Hochegger, H., Hegarat, N. & Pereira-Leal, J. B. Aurora at the pole and equator: overlapping functions of Aurora kinases in the mitotic spindle. *Open biology* **3**, 120185, doi:10.1098/rsob.120185 (2013).

94 Walter, A. O., Seghezzi, W., Korver, W., Sheung, J. & Lees, E. The mitotic serine/threonine kinase Aurora2/AIK is regulated by phosphorylation and degradation. *Oncogene* **19**, 4906-4916, doi:10.1038/sj.onc.1203847 (2000).
95 Hutterer, A. *et al.* Mitotic activation of the kinase Aurora-A requires its binding partner Bora. *Developmental cell* **11**, 147-157, doi:10.1016/j.devcel.2006.06.002 (2006).
96 Thomas, Y. *et al.* Cdk1 Phosphorylates SPAT-1/Bora to Promote Plk1 Activation in C. elegans and Human Cells. *Cell reports* **15**, 510-518, doi:10.1016/j.celrep.2016.03.049 (2016).
97 Vigneron, S. *et al.* Cyclin A-cdk1-Dependent Phosphorylation of Bora Is the Triggering Factor Promoting Mitotic Entry. *Developmental cell* **45**, 637-650 e637, doi:10.1016/j.devcel.2018.05.005 (2018).
98 Macurek, L. *et al.* Polo-like kinase-1 is activated by aurora A to promote checkpoint recovery. *Nature* **455**, 119-123, doi:10.1038/nature07185 (2008).
99 Chan, E. H., Santamaria, A., Sillje, H. H. & Nigg, E. A. Plk1 regulates mitotic Aurora A function through betaTrCP-dependent degradation of hBora. *Chromosoma* **117**, 457-469, doi:10.1007/s00412-008-0165-5 (2008).
100 Bruinsma, W., Macurek, L., Freire, R., Lindqvist, A. & Medema, R. H. Bora and Aurora-A continue to activate Plk1 in mitosis. *Journal of cell science* **127**, 801-811, doi:10.1242/jcs.137216 (2014).
101 Carmena, M. & Earnshaw, W. C. The cellular geography of aurora kinases. *Nature reviews. Molecular cell biology* **4**, 842-854, doi:10.1038/nrm1245 (2003).
102 Honda, R., Korner, R. & Nigg, E. A. Exploring the functional interactions between Aurora B, INCENP, and survivin in mitosis. *Molecular biology of the cell* **14**, 3325-3341, doi:10.1091/mbc.e02-11-0769 (2003).
103 Kelly, A. E. *et al.* Chromosomal enrichment and activation of the aurora B pathway are coupled to spatially regulate spindle assembly. *Developmental cell* **12**, 31-43, doi:10.1016/j.devcel.2006.11.001 (2007).
104 Petsalaki, E., Akoumianaki, T., Black, E. J., Gillespie, D. A. & Zachos, G. Phosphorylation at serine 331 is required for Aurora B activation. *The Journal of cell biology* **195**, 449-466, doi:10.1083/jcb.201104023 (2011).
105 Hewitt, L. *et al.* Sustained Mps1 activity is required in mitosis to recruit O-Mad2 to the Mad1-C-Mad2 core complex. *The Journal of cell biology* **190**, 25-34, doi:10.1083/jcb.201002133 (2010).
106 Jelluma, N. *et al.* Mps1 phosphorylates Borealin to control Aurora B activity and chromosome alignment. *Cell* **132**, 233-246, doi:10.1016/j.cell.2007.11.046 (2008).
107 Rosasco-Nitcher, S. E., Lan, W., Khorasanizadeh, S. & Stukenberg, P. T. Centromeric Aurora-B activation requires TD-60, microtubules, and substrate priming phosphorylation. *Science* **319**, 469-472, doi:10.1126/science.1148980 (2008).
108 Crosio, C. *et al.* Mitotic phosphorylation of histone H3: spatio-temporal regulation by mammalian Aurora kinases. *Molecular and cellular biology* **22**, 874-885 (2002).

109 Gimenez-Abian, J. F. *et al.* Regulation of sister chromatid cohesion between chromosome arms. *Current biology : CB* **14**, 1187-1193, doi:10.1016/j.cub.2004.06.052 (2004).
110 Hauf, S. *et al.* The small molecule Hesperadin reveals a role for Aurora B in correcting kinetochore-microtubule attachment and in maintaining the spindle assembly checkpoint. *The Journal of cell biology* **161**, 281-294, doi:10.1083/jcb.200208092 (2003).
111 Kallio, M. J., McCleland, M. L., Stukenberg, P. T. & Gorbsky, G. J. Inhibition of aurora B kinase blocks chromosome segregation, overrides the spindle checkpoint, and perturbs microtubule dynamics in mitosis. *Current biology : CB* **12**, 900-905 (2002).
112 Guimaraes, G. J., Dong, Y., McEwen, B. F. & Deluca, J. G. Kinetochore-microtubule attachment relies on the disordered N-terminal tail domain of Hec1. *Current biology : CB* **18**, 1778-1784, doi:10.1016/j.cub.2008.08.012 (2008).
113 Welburn, J. P. *et al.* Aurora B phosphorylates spatially distinct targets to differentially regulate the kinetochore-microtubule interface. *Molecular cell* **38**, 383-392, doi:10.1016/j.molcel.2010.02.034 (2010).
114 Kraft, C. *et al.* Mitotic regulation of the human anaphase-promoting complex by phosphorylation. *The EMBO journal* **22**, 6598-6609, doi:10.1093/emboj/cdg627 (2003).
115 Kernan, J., Bonacci, T. & Emanuele, M. J. Who guards the guardian? Mechanisms that restrain APC/C during the cell cycle. *Biochimica et biophysica acta. Molecular cell research* **1865**, 1924-1933, doi:10.1016/j.bbamcr.2018.09.011 (2018).
116 Chang, L. F., Zhang, Z., Yang, J., McLaughlin, S. H. & Barford, D. Molecular architecture and mechanism of the anaphase-promoting complex. *Nature* **513**, 388-393, doi:10.1038/nature13543 (2014).
117 Chang, L., Zhang, Z., Yang, J., McLaughlin, S. H. & Barford, D. Atomic structure of the APC/C and its mechanism of protein ubiquitination. *Nature* **522**, 450-454, doi:10.1038/nature14471 (2015).
118 Yamashiro, S. *et al.* Myosin phosphatase-targeting subunit 1 regulates mitosis by antagonizing polo-like kinase 1. *Developmental cell* **14**, 787-797, doi:10.1016/j.devcel.2008.02.013 (2008).
119 Posch, M. *et al.* Sds22 regulates aurora B activity and microtubule-kinetochore interactions at mitosis. *The Journal of cell biology* **191**, 61-74, doi:10.1083/jcb.200912046 (2010).
120 Moura, M. *et al.* Protein Phosphatase 1 inactivates Mps1 to ensure efficient Spindle Assembly Checkpoint silencing. *eLife* **6**, doi:10.7554/eLife.25366 (2017).
121 Ren, D. *et al.* Cell cycle-dependent regulation of Greatwall kinase by protein phosphatase 1 and regulatory subunit 3B. *The Journal of biological chemistry* **292**, 10026-10034, doi:10.1074/jbc.M117.778233 (2017).
122 Zeng, K., Bastos, R. N., Barr, F. A. & Gruneberg, U. Protein phosphatase 6 regulates mitotic spindle formation by controlling the T-loop phosphorylation

state of Aurora A bound to its activator TPX2. *The Journal of cell biology* **191**, 1315-1332, doi:10.1083/jcb.201008106 (2010).
123 Yamashita, K. *et al.* Okadaic acid, a potent inhibitor of type 1 and type 2A protein phosphatases, activates cdc2/H1 kinase and transiently induces a premature mitosis-like state in BHK21 cells. *The EMBO journal* **9**, 4331-4338 (1990).
124 Gowdy, P. M., Anderson, H. J. & Roberge, M. Entry into mitosis without Cdc2 kinase activation. *Journal of cell science* **111 (Pt 22)**, 3401-3410 (1998).
125 Peti, W., Nairn, A. C. & Page, R. Structural basis for protein phosphatase 1 regulation and specificity. *The FEBS journal* **280**, 596-611, doi:10.1111/j.1742-4658.2012.08509.x (2013).
126 Vagnarelli, P. & Earnshaw, W. C. Repo-Man-PP1: a link between chromatin remodelling and nuclear envelope reassembly. *Nucleus* **3**, 138-142, doi:10.4161/nucl.19267 (2012).
127 Trinkle-Mulcahy, L. *et al.* Repo-Man recruits PP1 gamma to chromatin and is essential for cell viability. *The Journal of cell biology* **172**, 679-692, doi:10.1083/jcb.200508154 (2006).
128 Nilsson, J. Protein phosphatases in the regulation of mitosis. *The Journal of cell biology*, doi:10.1083/jcb.201809138 (2018).
129 Nasa, I., Rusin, S. F., Kettenbach, A. N. & Moorhead, G. B. Aurora B opposes PP1 function in mitosis by phosphorylating the conserved PP1-binding RVxF motif in PP1 regulatory proteins. *Science signaling* **11**, doi:10.1126/scisignal.aai8669 (2018).
130 Bajaj, R., Bollen, M., Peti, W. & Page, R. KNL1 Binding to PP1 and Microtubules Is Mutually Exclusive. *Structure* **26**, 1327-1336 e1324, doi:10.1016/j.str.2018.06.013 (2018).
131 Duan, H. *et al.* Phosphorylation of PP1 Regulator Sds22 by PLK1 Ensures Accurate Chromosome Segregation. *The Journal of biological chemistry* **291**, 21123-21136, doi:10.1074/jbc.M116.745372 (2016).
132 Emanuele, M. J. *et al.* Aurora B kinase and protein phosphatase 1 have opposing roles in modulating kinetochore assembly. *The Journal of cell biology* **181**, 241-254, doi:10.1083/jcb.200710019 (2008).
133 Wang, F. *et al.* Phosphatase 1 Nuclear Targeting Subunit (PNUTS) Regulates Aurora Kinases and Mitotic Progression. *Molecular cancer research : MCR*, doi:10.1158/1541-7786.MCR-17-0670 (2018).
134 Liu, D. *et al.* Regulated targeting of protein phosphatase 1 to the outer kinetochore by KNL1 opposes Aurora B kinase. *The Journal of cell biology* **188**, 809-820, doi:10.1083/jcb.201001006 (2010).
135 Dohadwala, M. *et al.* Phosphorylation and inactivation of protein phosphatase 1 by cyclin-dependent kinases. *Proceedings of the National Academy of Sciences of the United States of America* **91**, 6408-6412 (1994).
136 Kwon, Y. G., Lee, S. Y., Choi, Y., Greengard, P. & Nairn, A. C. Cell cycle-dependent phosphorylation of mammalian protein phosphatase 1 by cdc2 kinase. *Proceedings of the National Academy of Sciences of the United States of America* **94**, 2168-2173 (1997).

137 Wu, J. Q. *et al.* PP1-mediated dephosphorylation of phosphoproteins at mitotic exit is controlled by inhibitor-1 and PP1 phosphorylation. *Nature cell biology* **11**, 644-651, doi:10.1038/ncb1871 (2009).
138 Olsen, J. V. *et al.* Quantitative phosphoproteomics reveals widespread full phosphorylation site occupancy during mitosis. *Science signaling* **3**, ra3, doi:10.1126/scisignal.2000475 (2010).
139 Vagnarelli, P. *et al.* Repo-Man coordinates chromosomal reorganization with nuclear envelope reassembly during mitotic exit. *Developmental cell* **21**, 328-342, doi:10.1016/j.devcel.2011.06.020 (2011).
140 Castro, A. & Lorca, T. Greatwall kinase at a glance. *Journal of cell science* **131**, doi:10.1242/jcs.222364 (2018).
141 Labandera, A. M., Vahab, A. R., Chaudhuri, S., Kerk, D. & Moorhead, G. B. The mitotic PP2A regulator ENSA/ARPP-19 is remarkably conserved across plants and most eukaryotes. *Biochemical and biophysical research communications* **458**, 739-744, doi:10.1016/j.bbrc.2015.01.123 (2015).
142 Mochida, S., Maslen, S. L., Skehel, M. & Hunt, T. Greatwall phosphorylates an inhibitor of protein phosphatase 2A that is essential for mitosis. *Science* **330**, 1670-1673, doi:10.1126/science.1195689 (2010).
143 Gharbi-Ayachi, A. *et al.* The substrate of Greatwall kinase, Arpp19, controls mitosis by inhibiting protein phosphatase 2A. *Science* **330**, 1673-1677, doi:10.1126/science.1197048 (2010).
144 Mochida, S. Regulation of alpha-endosulfine, an inhibitor of protein phosphatase 2A, by multisite phosphorylation. *The FEBS journal* **281**, 1159-1169, doi:10.1111/febs.12685 (2014).
145 Williams, B. C. *et al.* Greatwall-phosphorylated Endosulfine is both an inhibitor and a substrate of PP2A-B55 heterotrimers. *eLife* **3**, e01695, doi:10.7554/eLife.01695 (2014).
146 Heim, A., Konietzny, A. & Mayer, T. U. Protein phosphatase 1 is essential for Greatwall inactivation at mitotic exit. *EMBO reports* **16**, 1501-1510, doi:10.15252/embr.201540876 (2015).
147 Rogers, S. *et al.* PP1 initiates the dephosphorylation of MASTL, triggering mitotic exit and bistability in human cells. *Journal of cell science* **129**, 1340-1354, doi:10.1242/jcs.179754 (2016).
148 Cundell, M. J. *et al.* A PP2A-B55 recognition signal controls substrate dephosphorylation kinetics during mitotic exit. *The Journal of cell biology* **214**, 539-554, doi:10.1083/jcb.201606033 (2016).
149 Schmitz, M. H. *et al.* Live-cell imaging RNAi screen identifies PP2A-B55alpha and importin-beta1 as key mitotic exit regulators in human cells. *Nature cell biology* **12**, 886-893, doi:10.1038/ncb2092 (2010).
150 Porter, I. M., Schleicher, K., Porter, M. & Swedlow, J. R. Bod1 regulates protein phosphatase 2A at mitotic kinetochores. *Nature communications* **4**, 2677, doi:10.1038/ncomms3677 (2013).

151 Foley, E. A., Maldonado, M. & Kapoor, T. M. Formation of stable attachments between kinetochores and microtubules depends on the B56-PP2A phosphatase. *Nature cell biology* **13**, 1265-1271, doi:10.1038/ncb2327 (2011).
152 Wang, J. *et al.* Crystal structure of a PP2A B56-BubR1 complex and its implications for PP2A substrate recruitment and localization. *Protein & cell* **7**, 516-526, doi:10.1007/s13238-016-0283-4 (2016).
153 Xu, P., Raetz, E. A., Kitagawa, M., Virshup, D. M. & Lee, S. H. BUBR1 recruits PP2A via the B56 family of targeting subunits to promote chromosome congression. *Biology open* **2**, 479-486, doi:10.1242/bio.20134051 (2013).
154 Prevost, M. *et al.* Quantitative fragmentome mapping reveals novel, domain-specific partners for the modular protein RepoMan (recruits PP1 onto mitotic chromatin at anaphase). *Molecular & cellular proteomics : MCP* **12**, 1468-1486, doi:10.1074/mcp.M112.023291 (2013).
155 Watanabe, Y. & Kitajima, T. S. Shugoshin protects cohesin complexes at centromeres. *Philosophical transactions of the Royal Society of London. Series B, Biological sciences* **360**, 515-521, discussion 521, doi:10.1098/rstb.2004.1607 (2005).
156 Xu, Z. *et al.* Structure and function of the PP2A-shugoshin interaction. *Molecular cell* **35**, 426-441, doi:10.1016/j.molcel.2009.06.031 (2009).
157 Jones, H. W., Jr., McKusick, V. A., Harper, P. S. & Wuu, K. D. George Otto Gey. (1899-1970). The HeLa cell and a reappraisal of its origin. *Obstetrics and gynecology* **38**, 945-949 (1971).
158 Macville, M. *et al.* Comprehensive and definitive molecular cytogenetic characterization of HeLa cells by spectral karyotyping. *Cancer research* **59**, 141-150 (1999).
159 Pear, W. S., Nolan, G. P., Scott, M. L. & Baltimore, D. Production of high-titer helper-free retroviruses by transient transfection. *Proceedings of the National Academy of Sciences of the United States of America* **90**, 8392-8396 (1993).
160 Arur, S. & Schedl, T. Generation and purification of highly specific antibodies for detecting post-translationally modified proteins in vivo. *Nature protocols* **9**, 375-395, doi:10.1038/nprot.2014.017 (2014).
161 Seeling, J. M. *et al.* Regulation of beta-catenin signaling by the B56 subunit of protein phosphatase 2A. *Science* **283**, 2089-2091, doi:10.1126/science.283.5410.2089 (1999).
162 Lin, Y. N. *et al.* CEP120 interacts with CPAP and positively regulates centriole elongation. *The Journal of cell biology* **202**, 211-219, doi:10.1083/jcb.201212060 (2013).
163 Ma, H. T. & Poon, R. Y. Synchronization of HeLa cells. *Methods Mol Biol* **761**, 151-161, doi:10.1007/978-1-61779-182-6_10 (2011).
164 Trinkle-Mulcahy, L., Sleeman, J. E. & Lamond, A. I. Dynamic targeting of protein phosphatase 1 within the nuclei of living mammalian cells. *Journal of cell science* **114**, 4219-4228 (2001).

165 Krystkowiak, I. & Davey, N. E. SLiMSearch: a framework for proteome-wide discovery and annotation of functional modules in intrinsically disordered regions. *Nucleic acids research* **45**, W464-W469, doi:10.1093/nar/gkx238 (2017).
166 Shannon, P. *et al.* Cytoscape: a software environment for integrated models of biomolecular interaction networks. *Genome research* **13**, 2498-2504, doi:10.1101/gr.1239303 (2003).
167 Bindea, G. *et al.* ClueGO: a Cytoscape plug-in to decipher functionally grouped gene ontology and pathway annotation networks. *Bioinformatics* **25**, 1091-1093, doi:10.1093/bioinformatics/btp101 (2009).
168 Davey, N. E., Haslam, N. J., Shields, D. C. & Edwards, R. J. SLiMSearch 2.0: biological context for short linear motifs in proteins. *Nucleic acids research* **39**, W56-60, doi:10.1093/nar/gkr402 (2011).
169 Tompa, P. Intrinsically disordered proteins: a 10-year recap. *Trends in biochemical sciences* **37**, 509-516, doi:10.1016/j.tibs.2012.08.004 (2012).
170 Tompa, P., Davey, N. E., Gibson, T. J. & Babu, M. M. A million peptide motifs for the molecular biologist. *Molecular cell* **55**, 161-169, doi:10.1016/j.molcel.2014.05.032 (2014).
171 Dosztanyi, Z. Prediction of protein disorder based on IUPred. *Protein science : a publication of the Protein Society* **27**, 331-340, doi:10.1002/pro.3334 (2018).
172 Meszaros, B., Erdos, G. & Dosztanyi, Z. IUPred2A: context-dependent prediction of protein disorder as a function of redox state and protein binding. *Nucleic acids research* **46**, W329-W337, doi:10.1093/nar/gky384 (2018).
173 Punta, M., Simon, I. & Dosztanyi, Z. Prediction and analysis of intrinsically disordered proteins. *Methods Mol Biol* **1261**, 35-59, doi:10.1007/978-1-4939-2230-7_3 (2015).
174 Dosztanyi, Z., Meszaros, B. & Simon, I. ANCHOR: web server for predicting protein binding regions in disordered proteins. *Bioinformatics* **25**, 2745-2746, doi:10.1093/bioinformatics/btp518 (2009).
175 Pathan, M. *et al.* FunRich: An open access standalone functional enrichment and interaction network analysis tool. *Proteomics* **15**, 2597-2601, doi:10.1002/pmic.201400515 (2015).
176 Sommer, L. M., Cho, H., Choudhary, M. & Seeling, J. M. Evolutionary Analysis of the B56 Gene Family of PP2A Regulatory Subunits. *International journal of molecular sciences* **16**, 10134-10157, doi:10.3390/ijms160510134 (2015).
177 Betts, M. J. *et al.* Systematic identification of phosphorylation-mediated protein interaction switches. *PLoS computational biology* **13**, e1005462, doi:10.1371/journal.pcbi.1005462 (2017).
178 Nishi, H., Fong, J. H., Chang, C., Teichmann, S. A. & Panchenko, A. R. Regulation of protein-protein binding by coupling between phosphorylation and intrinsic disorder: analysis of human protein complexes. *Molecular bioSystems* **9**, 1620-1626, doi:10.1039/c3mb25514j (2013).
179 Nishi, H., Hashimoto, K. & Panchenko, A. R. Phosphorylation in protein-protein binding: effect on stability and function. *Structure* **19**, 1807-1815, doi:10.1016/j.str.2011.09.021 (2011).

180 Hornbeck, P. V. *et al.* PhosphoSitePlus, 2014: mutations, PTMs and recalibrations. *Nucleic acids research* **43**, D512-520, doi:10.1093/nar/gku1267 (2015).
181 Ranieri, A., Kemp, E., Burgoyne, J. R. & Avkiran, M. beta-Adrenergic regulation of cardiac type 2A protein phosphatase through phosphorylation of regulatory subunit B56delta at S573. *Journal of molecular and cellular cardiology* **115**, 20-31, doi:10.1016/j.yjmcc.2017.12.016 (2018).
182 Boeing, S. *et al.* Multiomic Analysis of the UV-Induced DNA Damage Response. *Cell reports* **15**, 1597-1610, doi:10.1016/j.celrep.2016.04.047 (2016).
183 Matsuoka, S. *et al.* ATM and ATR substrate analysis reveals extensive protein networks responsive to DNA damage. *Science* **316**, 1160-1166, doi:10.1126/science.1140321 (2007).
184 Bolanos-Garcia, V. M. & Davies, O. R. Structural analysis and classification of native proteins from E. coli commonly co-purified by immobilised metal affinity chromatography. *Biochimica et biophysica acta* **1760**, 1304-1313, doi:10.1016/j.bbagen.2006.03.027 (2006).
185 Chhetri, G., Kalita, P. & Tripathi, T. An efficient protocol to enhance recombinant protein expression using ethanol in Escherichia coli. *MethodsX* **2**, 385-391, doi:10.1016/j.mex.2015.09.005 (2015).
186 Francis, D. M. & Page, R. Strategies to optimize protein expression in E. coli. *Current protocols in protein science* **Chapter 5**, Unit 5 24 21-29, doi:10.1002/0471140864.ps0524s61 (2010).
187 Jackson, M. P. & Hewitt, E. W. Cellular proteostasis: degradation of misfolded proteins by lysosomes. *Essays in biochemistry* **60**, 173-180, doi:10.1042/EBC20160005 (2016).
188 Hershko, A. Mechanisms and regulation of the degradation of cyclin B. *Philosophical transactions of the Royal Society of London. Series B, Biological sciences* **354**, 1571-1575; discussion 1575-1576, doi:10.1098/rstb.1999.0500 (1999).
189 Kruse, T. *et al.* Direct binding between BubR1 and B56-PP2A phosphatase complexes regulate mitotic progression. *Journal of cell science* **126**, 1086-1092, doi:10.1242/jcs.122481 (2013).
190 Bastos, R. N., Cundell, M. J. & Barr, F. A. KIF4A and PP2A-B56 form a spatially restricted feedback loop opposing Aurora B at the anaphase central spindle. *The Journal of cell biology* **207**, 683-693, doi:10.1083/jcb.201409129 (2014).
191 Vallardi, G., Allan, L. A., Crozier, L. & Saurin, A. T. Division of labour between PP2A-B56 isoforms at the centromere and kinetochore. *eLife* **8**, doi:10.7554/eLife.42619 (2019).
192 Hwang, I. *et al.* FOXO protects against age-progressive axonal degeneration. *Aging cell* **17**, doi:10.1111/acel.12701 (2018).
193 Heller, F. A., Xue, C., Fisher, A. & Everett, A. D. Expression and mapping of protein phosphatase 2A alpha in the developing rat heart. *Pediatric research* **43**, 68-76, doi:10.1203/00006450-199804001-00406 (1998).

194 Fujita, H., Yoshino, Y. & Chiba, N. Regulation of the centrosome cycle. *Molecular & cellular oncology* **3**, e1075643, doi:10.1080/23723556.2015.1075643 (2016).
195 Fu, J., Hagan, I. M. & Glover, D. M. The centrosome and its duplication cycle. *Cold Spring Harbor perspectives in biology* **7**, a015800, doi:10.1101/cshperspect.a015800 (2015).
196 Nasa, I. *et al.* Recruitment of PP1 to the centrosomal scaffold protein CEP192. *Biochemical and biophysical research communications* **484**, 864-870, doi:10.1016/j.bbrc.2017.02.004 (2017).